

## **6. Stochastic Finite Element Formulation**

A key objective of this study has been to assess the effects of errors in the formulation, solution procedures and input data on the predictions of the CALGRID model. Even with the superior sampling efficiency of the new Hammersley-Wozniakowsky method, introduced in the previous chapter, the processing time and storage requirements needed to assess the effects of data errors on the predictions of complete airshed model are prohibitive. Despite the difficulties the information is critically important in air quality management studies and there is great demand for some answers. Given the weaknesses of most previous attempts a totally new approach is needed. This chapter introduces a first step towards realizing the goal of directly quantifying the effects of error propagation. The key idea is to start at the point at which the numerical form of the model is formulated and build the uncertainty directly into the solution process. The approach is analogous to the sensitivity analysis technique used by Milford et al. (1992) where both the solution and its derivatives are calculated. The technique proposed in this chapter has its origins in structural analysis where the goal was to determine how errors propagate through a complex analysis.

At the outset the reader is encouraged to persevere with the mathematical derivations to be presented in the following sections. Despite their apparent complexity the final algorithm is in fact quite easy to implement and should be a part of the formulation of any new airshed model. For additional background on the statistical concepts and mathematical methodology the reader is referred to Spanos and Ghanem (1991) and Papoulis (1991)

### **6.1 The Decomposition Method**

The heart of the proposed approach is the decomposition method developed by Adomian and co-workers (Adomian, 1983). Originally, this method was proposed as a substitute for the perturbation techniques where the idea was to make the parameter variations small enough so that the response of the model could be considered locally linear. The problem with this technique is that even a linear differential equation with random coefficients will have solution which depend nonlinearly upon the coefficients. One example of this phenomenon can be observed in Figure 5.9. The key contribution of Adomian (1990), was not to manipulate the problem into a form where linear perturbation theory applied but to address the difficulty directly.

In the following paragraphs, the basic ideas behind the decomposition method will be given. As a starting point consider a linear partial differential equation of the form likely to be encountered in airshed modeling. The presence of uncertainties or errors in the data produces a situation where the governing system of equations must be treated as a stochastic systems. A linear stochastic partial differential equations may be written in the form,

$$L_{t,x} u = g \quad (6.1)$$

where  $g$  may be stochastic, and the operator  $L$  can be decomposed into the time and space operators. As an illustration the operator form of the CALGRID model is:

$$L_{x,t} = \frac{\partial(\ )}{\partial t} + \nabla \cdot \mathbf{u}(\ ) - \nabla \cdot \mathbf{K} \nabla(\ )$$

and

$$g = R[c;T;t]$$

where  $\mathbf{u}$  is the flow field,  $\mathbf{K}$  the eddy diffusivity tensor and  $R$  the chemical reaction rate. Because of the uncertainties in the data the system (6.1) can be further decomposed into the deterministic ( $L$ ) and zero-mean random ( $R$ ) parts,

$$\begin{aligned} L_{t,x} &= L_t + L_x \\ L_t &= L_t + R_t \\ L_x &= L_x + R_x \end{aligned} \quad (6.2)$$

For example the diffusion coefficient might be written in the form  $\mathbf{K} = \langle \mathbf{K} \rangle + \mathbf{K}(\omega)$ , where  $\langle \mathbf{K} \rangle$  is the deterministic or expected value and  $\mathbf{K}(\omega)$  is the stochastic fluctuation. Now, if we assume that  $L_{t,x}^{-1}$ ,  $L_t^{-1}$ , and  $L_x^{-1}$  exist, then one can determine the solution of (6.1) in the form

$$\begin{aligned} u &= L_t^{-1} g - L_t^{-1} R_t u - L_t^{-1} L_x u - L_t^{-1} R_x u, \\ u &= L_x^{-1} g - L_x^{-1} R_x u - L_x^{-1} L_t u - L_x^{-1} R_t u \end{aligned} \quad (6.3)$$

For convenience the the initial and boundary conditions have been included in the inverse operators. Since  $u = L_{t,x}^{-1} g$ , then equation (6.3) may have an equivalent form,

$$\begin{aligned} L_{t,x}^{-1} g &= L_t^{-1} g - L_t^{-1} R_t L_{t,x}^{-1} g - L_t^{-1} L_x L_{t,x}^{-1} g - L_t^{-1} R_x L_{t,x}^{-1} g, \\ L_{t,x}^{-1} g &= L_x^{-1} g - L_x^{-1} R_x L_{t,x}^{-1} g - L_x^{-1} L_t L_{t,x}^{-1} g - L_x^{-1} R_t L_{t,x}^{-1} g \end{aligned} \quad (6.4)$$

After adding the two equations above and dividing the result by 2, an operator equation of  $L_{t,x}^{-1}$  is obtained,

$$L_{t,x}^{-1} = \frac{1}{2} \left[ (L_t^{-1} + L_x^{-1}) - L_t^{-1} (R_t + L_x + R_x) L_{t,x}^{-1} - L_t^{-1} (R_x + L_t + R_t) L_{t,x}^{-1} \right] \quad (6.5)$$

The next step is representing  $L_{t,x}^{-1}$  as infinite summation of operators multiplied by the power of parameter,  $\lambda$ . Thus, equation (6.5) becomes

$$\sum \lambda^n H_n = \frac{1}{2} \left[ \begin{array}{c} (L_t^{-1} + L_x^{-1}) - L_t^{-1} (R_t + L_x + R_x) \\ \sum \lambda^n H_n - L_t^{-1} (R_x + L_t + R_t) \sum \lambda^n H_n \end{array} \right] \quad (6.6)$$

Equating comparable powers of  $\lambda$ , then

$$\begin{aligned} H_0 &= \frac{1}{2} (L_t^{-1} + L_x^{-1}), \\ H_1 &= -\left(\frac{1}{2}\right)^2 [L_t^{-1} (R_t + L_x + R_x) + L_t^{-1} (R_x + L_t + R_t)] (L_t^{-1} + L_x^{-1}), \\ &\vdots \\ H_n &= (-1)^n \left(\frac{1}{2}\right)^{n+1} [L_t^{-1} (R_t + L_x + R_x) + L_t^{-1} (R_x + L_t + R_t)]^n (L_t^{-1} + L_x^{-1}) \end{aligned} \quad (6.7)$$

Therefore, the inverse operator is given by

$$L_{t,x}^{-1} = \sum_{n=0}^{\infty} (-1)^n \left(\frac{1}{2}\right)^{n+1} [L_t^{-1} (R_t + L_x + R_x) + L_t^{-1} (R_x + L_t + R_t)]^n (L_t^{-1} + L_x^{-1}) \quad (6.8)$$

Adomian and Malakian (1980) also proposed an alternative approach. Instead of decomposing the stochastic linear partial differential operator into ordinary differential operators, they suggested a decomposition it into a deterministic partial differential operator and a zero-mean random partial differential operator. After using a similar procedure, the decomposed inverse operator can be written as,

$$L_{t,x}^{-1} = \sum_{n=0}^{\infty} (-1)^n (L_{t,x}^{-1} R_{t,x}^{-1})^n L_{t,x}^{-1} \quad (6.9)$$

This latter approach does not use the averaging method, however it is more difficult to compute the series of operators. Both approaches must satisfy conditions inherited from

the binomial expansion scheme condition. The necessary and sufficient conditions are given in equation (6.10) and (6.11).

$$\|L_t^{-1} (R_t + L_x + R_x) + L_t^{-1} (R_x + L_t + R_t)\| < 1 \quad \text{a.s.} \quad (6.10)$$

$$\|L_{t,x}^{-1} R_{t,x}^{-1}\| < 1 \quad \text{a.s.} \quad (6.11)$$

The extension of the above procedure to the the non-linear case is presented in Adomian and Rach (1983). The main idea is to make analytic expansions in the parameter  $\lambda$  for the nonlinear deterministic term  $N u$  and the nonlinear stochastic term  $M u$ . These analytic expansions are called the Adomian polynomials (Riganti, 1987). In general the inversion of the stochastic operator may always be determined by the decomposition method, regardless the non-linearity .

A knowledge of the decomposition method is clearly not enough for solving the stochastic model problem, because what is needed are the moments of the predicted air quality distributions. For a Gaussian process, one can describe the solution completely by calculating the first and the second moment of solution. However, one may need more than the second moment for other processes. The issues then become how to handle more general forms of the parameter distributions directly in the decomposition process. As obtained from the decomposition method, the solution vector,  $u$ , may be represented by the series,

$$\begin{aligned} u &= a_0 + a_{\lambda_1} \Pi_{\lambda_1}(\xi) + a_{\lambda_1 \lambda_2} \Pi_{\lambda_1 \lambda_2}(\xi) + \dots \\ &= \sum_{k=0}^{\infty} a_{\lambda_0 \dots \lambda_k} \Pi_{\lambda_0 \dots \lambda_k}(\xi) \end{aligned} \quad (6.12)$$

where the coefficients  $a$  are deterministic vectors and the polynomials  $\Pi$  are simply the homogeneous polynomials given by the equation

$$\Pi_{\lambda_0 \dots \lambda_k}(\xi) = \prod_{i=1}^k \xi_{\lambda_i} \quad (6.13)$$

In the probability theory, the logarithm of a characteristic function is defined as the cumulant generating function (Ochi, 1986) and it can be expressed in the form of a series where the coefficient of each term is the cumulant. That is,

$$\psi(t) = \ln \phi(t) = \sum_{j=1}^{\infty} \frac{(it)^j}{j!} k_j \quad (6.14)$$

where  $\phi(t)$  = characteristic function, and  $k_j$  = cumulant.

Using equation (6.13), the r-th component of  $\mathbf{u}$ ,  $u_r$  can be written as

$$u_r = P^{(r)} \xi \quad (6.15)$$

where  $P^{(r)}$  is the operator indicated by equation (6.12) as applicable to  $u_r$ . Thus, the cumulant generating function for  $u_r$  is given by equation,

$$K_u(\chi) = e^{\chi P^{(r)}} \kappa_\xi \quad (6.16)$$

where  $\kappa_\xi$  represents cumulants of vector  $\xi$ . The exponential operator can be expanding into a series,

$$e^{\chi P^{(r)}} = \left[ I + \chi_r P^{(r)} + \frac{1}{2} \chi_r \chi_s P^{(r)} P^{(s)} + \dots \right] \quad (6.17)$$

Thus, the result of equation (6.16) may be obtained by considering each term of operators in equation (6.17). Because of the complexity of the algebra it is better to use symbolic manipulation packages, such as Mathematica or Maple for carrying out the calculations on equations (6.16) and (6.17), to obtain the cumulants of  $\mathbf{u}$ .

Once the cumulants of solution are available, it is easy obtain the central moments of the solution as,

$$\begin{aligned} E[(x - \mu)^2] &= k_2 = \text{variance} \\ E[(x - \mu)^3] &= k_3 \\ E[(x - \mu)^4] &= k_4 + 3 k_2^2 \\ E[(x - \mu)^5] &= k_5 + 10 k_3 k_2 \\ E[(x - \mu)^6] &= k_6 + 15 k_4 k_2 + 10 k_3^2 + 15 k_2^3, \text{ etc.} \end{aligned} \quad (6.18)$$

There is another important aspect of the cumulants and the moments of the solution. Those moments and cumulants can be employed to derive approximations of the probability density function of the solution. Several series distributions have been suggested for estimating the probability density functions (Ochi (1986)). They are Gram-Charlier, Edgeworth, and Longuet-Higgins series distribution. A brief derivation for those series will be given below following Ochi (1986).

Each of the three series distributions are actually functions of Hermite polynomials. The Hermite polynomial of degree  $n$ , denoted by  $H_n(z)$ , is defined as a function which satisfies the relationship given by,

$$\frac{d^n}{dz^n} e^{-z^2/2} = (-1)^n H_n(z) e^{-z^2/2} \quad n = 0,1,2,\dots \quad (6.19)$$

It can be shown (Ochi, 1986) that the polynomials,

$$\frac{1}{\sqrt{n!}} H_n(z) \quad (6.20)$$

are orthogonal with respect to the standardized normal probability density function,  $\alpha(z)$ .

The Gram-Charlier probability density function is developed by applying the concept of polynomials orthogonal with respect to the probability density function, and also by assuming that an arbitrarily given standardized probability density function,  $f(z)$ , may be expressed in the following form,

$$f(z) = a_0 \alpha(z) + a_1 \alpha^{(1)}(z) + a_2 \alpha^{(2)}(z) + \dots \quad (6.21)$$

where

$a_n =$  unknown constants

$$\alpha^{(n)}(z) = \frac{d^n}{dz^n} \alpha(z)$$

Equation (6.21) is somewhat similar to the Taylor series, because it approximates an arbitrary probability density function by expanding it into the Gaussian probability density function. Consequently, if one use equation (6.21) to express a Gaussian probability

density function, then only the first term will be retained. The Gram-Charlier series distribution is clearly not the best choice.

Using the orthogonal property of the Hermite polynomials with respect to the standardized normal probability density function, the unknown coefficients in equation (6.21) can be determined. Thus, the probability density function of a standardized random variable can be expressed as,

$$f(z) = \frac{1}{\sqrt{2\pi}} e^{-z^2/2} \left[ 1 + \frac{m_3}{3!} H_3(z) + \frac{m_4 - 3}{4!} H_4(z) + \frac{m_5 - 10m_3}{5!} H_5(z) + \frac{m_6 - 15m_4 + 30}{6!} H_6(z) + \dots \right] \quad (6.22)$$

where  $m_j = j$ -th moment of the standardized random variable. This equation is called the Gram-Charlier series of type A probability density function (Ochi (1986)).

In several instances it is useful to express equation (6.22) in terms of the cumulants rather than the moments. Equation (6.18) gives a tool for transforming the moments in equation (6.22) into the cumulants. Thus, for a random variable with zero mean and variance  $\sigma^2$ , it becomes

$$f(z) = \frac{1}{\sigma\sqrt{2\pi}} e^{-z^2/2\sigma^2} \left[ 1 + \frac{\lambda_3}{3!} H_3(z/\sigma) + \frac{\lambda_4}{4!} H_4(z/\sigma) + \frac{\lambda_5}{5!} H_5(z/\sigma) + \left( \frac{\lambda_6}{6!} + \frac{\lambda_3^2}{72} \right) H_6(z/\sigma) + \dots \right] \quad (6.23)$$

where

$$\lambda_j = \frac{k_j}{(k_2)^{j/2}} = \frac{k_j}{\sigma^j} \quad (6.24)$$

Another approach to the expansion is the Edgeworth series distribution. The primary difference between Gram-Charlier and the Edgeworth asymptotic expansions of an arbitrary univariate probability density function is that the terms are taken in different order (Trim, 1989). Edgeworth developed an asymptotic series probability density function of distribution for the sum of random variables in connection with the probability law of errors (Ochi, 1986). Thus, the assumption in deriving the Edgeworth probability density

function is that an arbitrary random variable,  $x$ , can be decomposed into the sum of independent identical distributed functions (not necessarily normal distributions). Furthermore, the variable  $x$  can be transformed into a standardized random variable,  $z$ ,

$$z = \frac{(x - n \mu_r)}{\sqrt{n} \sigma_r} \quad (6.25)$$

From the definition of characteristic function

$$e^{t^2/2} \phi(t) = \int_{-\infty}^{\infty} e^{t^2/2 + itz} f(z) dz \quad (6.26)$$

and also from equation (6.19), the following Hermite polynomial formula can be stated,

$$\sum_{n=0}^{\infty} \frac{H_n(z)}{n!} t^n = e^{(t^2/2) + tz} \quad (6.27)$$

Thus, equation (6.26) can be written as,

$$e^{t^2/2} \phi(t) = \sum_{n=0}^{\infty} \frac{c_n}{\sqrt{n!}} (-it)^n \quad (6.28)$$

where

$$c_n = (-1)^n \frac{1}{\sqrt{n!}} \int_{-\infty}^{\infty} H_n(z) f(z) dz \quad (6.29)$$

Next, by considering equation (6.14), one may get

$$e^{t^2/2} \phi(t) = \sum_{s=0}^{\infty} \frac{(it)^{2s}}{s!} \left( \sum_{j=1}^{\infty} \frac{\lambda_{j+2}}{(j+2)!} (it)^j \right)^s \quad (6.30)$$

then, from comparison of equation (6.28) and (6.30), the unknown coefficients,  $c_n$ , can be determined, for example

$$c_0 = 1, c_1 = c_2 = 1, c_3 = -\frac{\lambda_3}{\sqrt{3!}} \quad (6.31)$$

$$c_4 = \frac{\lambda_4}{\sqrt{4!}}, c_5 = -\frac{\lambda_5}{\sqrt{5!}}, c_6 = \frac{\lambda_6}{\sqrt{6!}} + \frac{\sqrt{6!}}{2!3!3!} \lambda_3^2, \text{ etc.}$$

If one use equation (6.21) for expressing an arbitrary probability density function, then the Edgeworth series distribution will have the same form with the Gram-Charlier. Thus, in the case of zero mean random variable with variance  $\sigma^2$ , the probability density function can be expressed in the terms of the parameter  $c_n$ . That is,

$$f(z) = \frac{1}{\sigma\sqrt{2\pi}} e^{-z^2/2\sigma^2} \sum_{n=0}^{\infty} (-1)^n \frac{c_n}{n!} H_n(z/\sigma) \quad (6.32)$$

The Longuet-Higgins series distribution is derived by considering the moments or the cumulants generating function and expanding the exponential of the cumulant series into a power series of the cumulants (Ochi, 1986). For a random variable with zero mean and variance  $\sigma^2$ , the probability density function is given by the same formula as derived through the other two approaches, equation (6.23) and (6.32). Those three probability density function estimation methods retain only the first term in the case of Gaussian process.

## 6.2 Algorithm and Implementation

By implementing the finite element method for generating the numerical approximation of the functions in space, the partial differential operators in the decomposition method become the matrix operators or the ordinary differential operators. The stochastic differential model, after time discretization becomes,

$$\left[ K_m + \sum_{n=1}^M \xi_n K_f^{(n)} \right] \mathbf{u}_{t+\Delta t} = \mathbf{g}(\mathbf{u}_t, \mathbf{f}) \quad (6.33)$$

where  $K_m$  is the mean matrix operator,  $K_f$  is the fluctuation matrix operator, and  $\mathbf{f}$  is the forcing vector. At this stage, the boundary conditions may be imposed on  $K_m$  and each of the  $K_f$  matrices individually. Then, equation (6.33) can be normalized by multiplying throughout by  $K_m^{-1}$  to obtain,

$$\left[ I + \sum_{n=1}^M \xi_n Q^{(n)} \right] \mathbf{u} = \mathbf{h} \quad (6.34)$$

where

$$Q^{(n)} = K_m^{-1} K_f^{(n)}, \quad (6.35)$$

$$\mathbf{h} = K_m^{-1} \mathbf{g}$$

Obviously, the response vector  $\mathbf{u}$  is a nonlinearly filtered version of  $\xi_n$ . A straightforward scheme for obtaining the response vector from equation (6.34) relies on performing the decomposition method for those matrices operators to derive

$$\mathbf{u} = \sum_{i=0}^{\infty} (-1)^i \left[ \sum_{n=1}^M \xi_n Q^{(n)} \right]^i \mathbf{h} \quad (6.36)$$

Equation (6.36) gives the response vector in its probabilistic form and one may deduce from it the moments or statistical analysis of that response vector. The moment generating function and the orthonormal property of the basis random variables in the series expansion are the basic methods for performing such statistical analysis of the response vector (see Figure 6.1.b and figure 6.2). Figure 6.1 presents a comparison between the stochastic finite element algorithm and the Monte Carlo method. Each step of both methods is equivalent, but the time required for performing such calculations is obviously different.

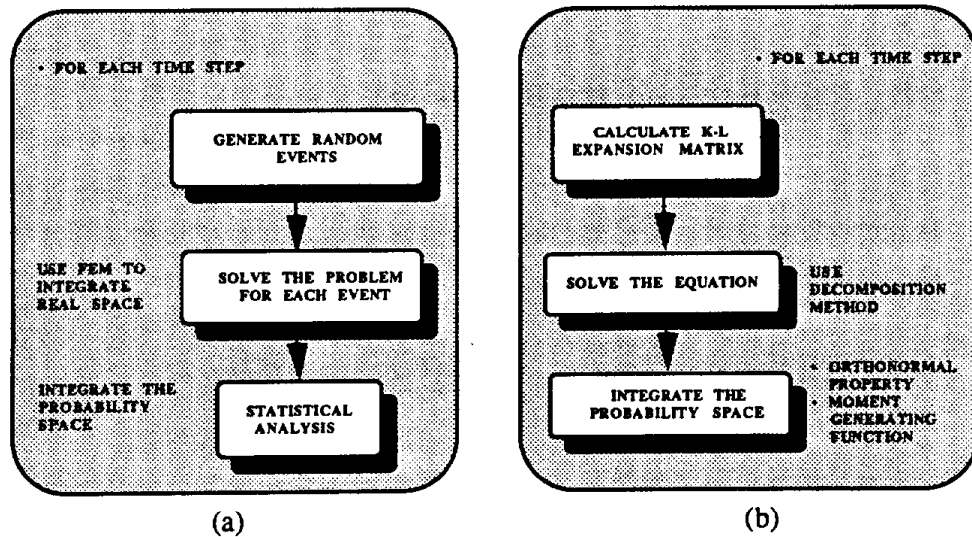


**Figure 6.1** Flowchart of the main steps of (a) Monte Carlo-based method and the Stochastic Finite Element algorithm.

A general outline of the SFEM method can be seen in Figure 6.2.

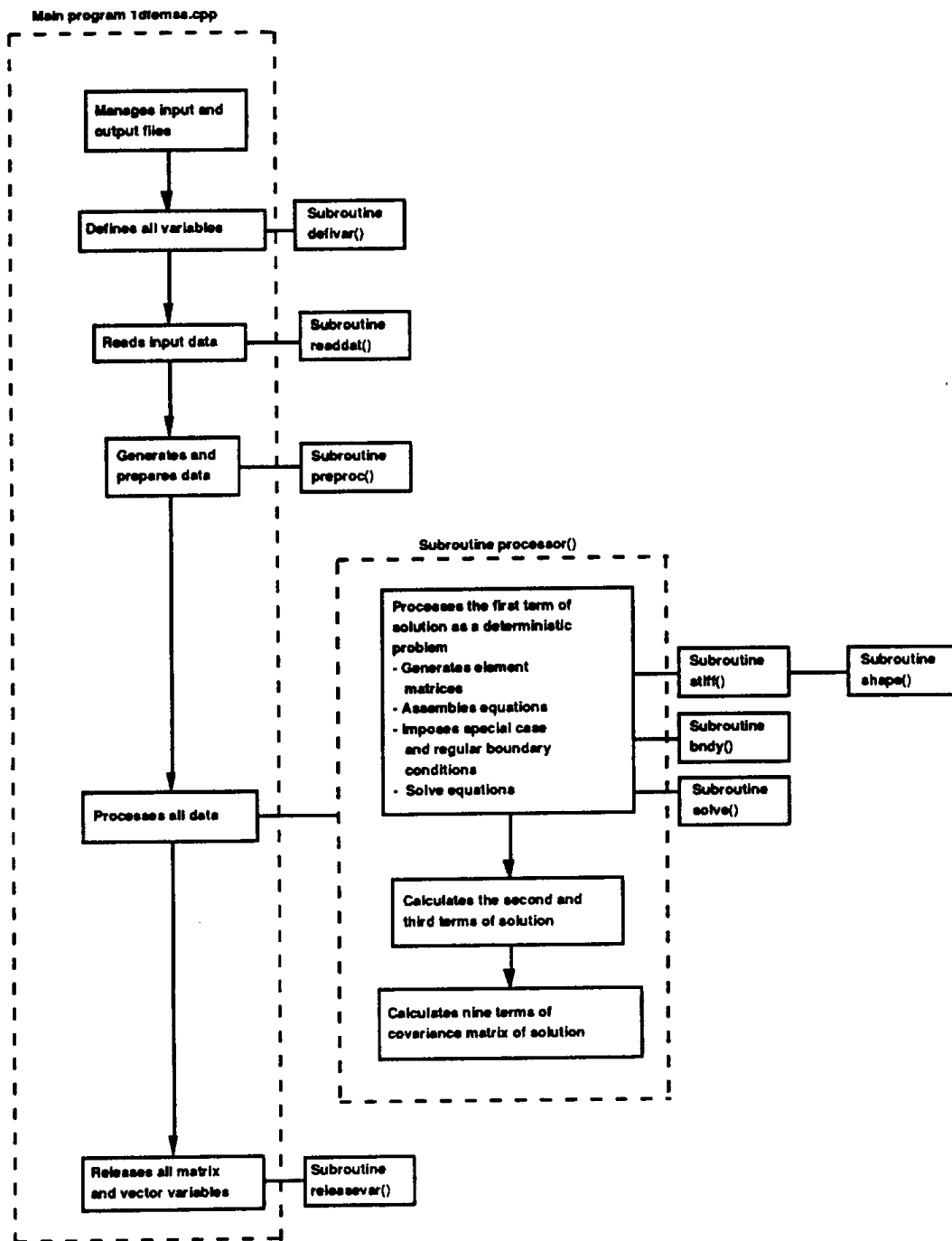
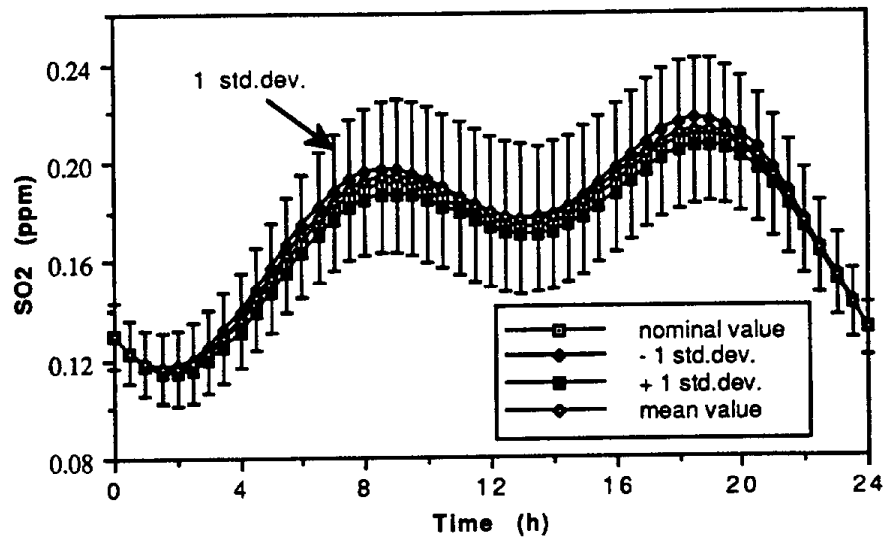


Figure 6.2 Flowchart of the Stochastic Finite Element Method (SFEM)

### 6.3 Application of the Stochastic Finite Element Method to Vertical Transport Module of CALGRID

The same example problem stated in section 5 will be solved by the SFEM. The variation in the predicted ground level concentration as a function of time are given in Figures 6.3, 6.4, and 6.5 respectively. For comparison purposes the large error bars correspond to the systematic high and low bias in the turbulent diffusivity. The smaller error bars indicate one standard deviation of the concentration from stochastic analysis. Again as in the case of the Monte Carlo analysis the systematic bias severely overestimates the variance in the predictions.



**Figure 6.3** Ground level concentration of SO<sub>2</sub> as a function of time for the case of errors in the vertical turbulent diffusivity  $\sigma(D) = 20 \%$ ,  $\sigma(k) = 0 \%$ ,  $\sigma(v_g) = 0 \%$ . The  $\pm$  standard deviation bars correspond to the solution when the diffusivity is set at  $\pm 1\sigma$ .

Similarly, Figures 6.6, 6.7, and 6.8 show the concentration profiles of SO<sub>2</sub> with respect to the height, and all these figures support the discussion in chapter 5 on the relative effects of systematics and random errors. If we compare the results against those shown in chapter 5 we can see that the Monte Carlo and SFEM yield equivalent trends and numerical values. The key difference is however that the SFEM procedure obtains the statistics of the predicted concentration values with only one solution of the model.

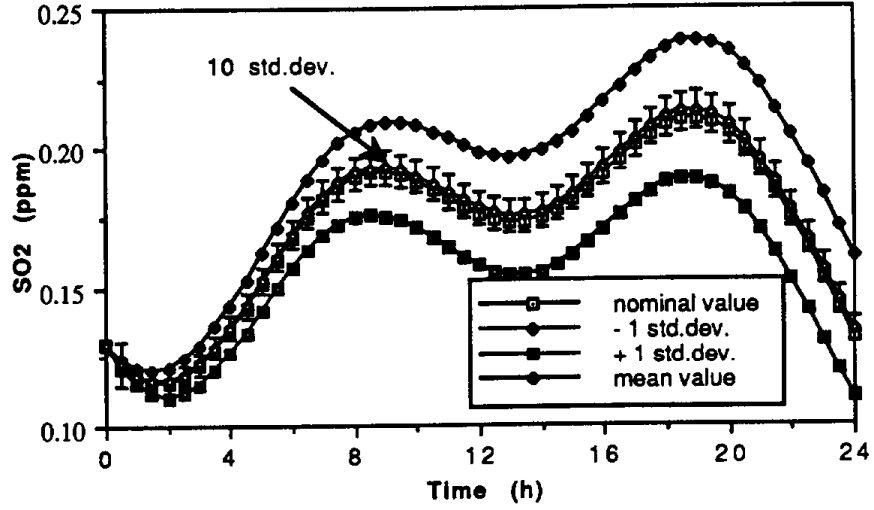


**Figure 6.4** Ground level concentration of SO<sub>2</sub> as a function of time for the case of errors in the reaction constant i.e.  $\sigma(D) = 0\%$ ,  $\sigma(k) = 20\%$ ,  $\sigma(vg) = 0\%$ .

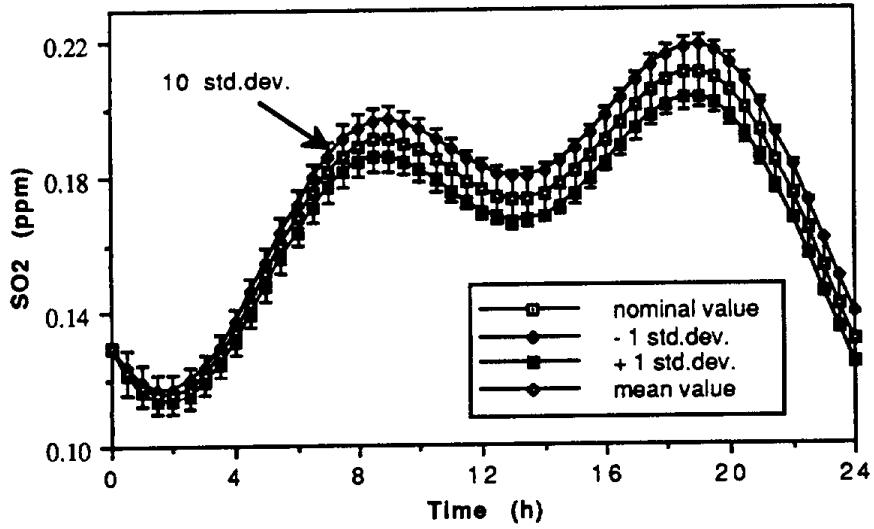


**Figure 6.5** Ground level concentration of SO<sub>2</sub> as a function of time for the case of errors in the deposition velocity i.e.  $\sigma(D) = 0\%$ ,  $\sigma(k) = 0\%$ ,  $\sigma(vg) = 20\%$ .

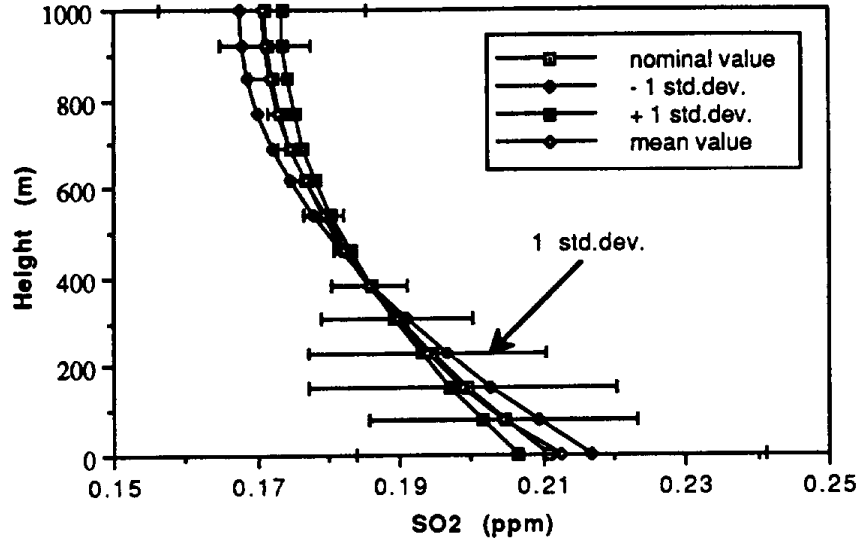


**Figure 6.6** Concentration profile of SO<sub>2</sub> at time = 19 hours for  $\sigma(D) = 20\%$ ,  $\sigma(k) = 0\%$ ,  $\sigma(vg) = 0\%$ .

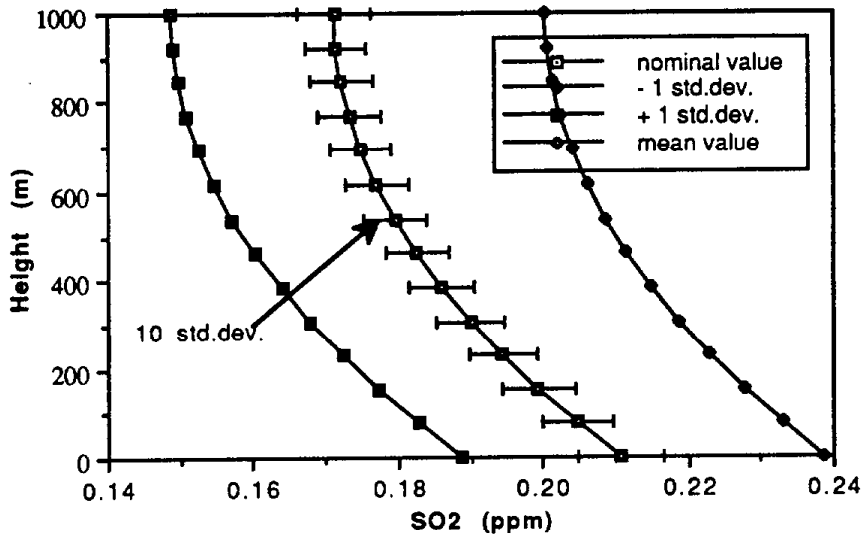


**Figure 6.7** Concentration profile of SO<sub>2</sub> at time = 19 hours for  $\sigma(D) = 0\%$ ,  $\sigma(k) = 20\%$ ,  $\sigma(vg) = 0\%$ .

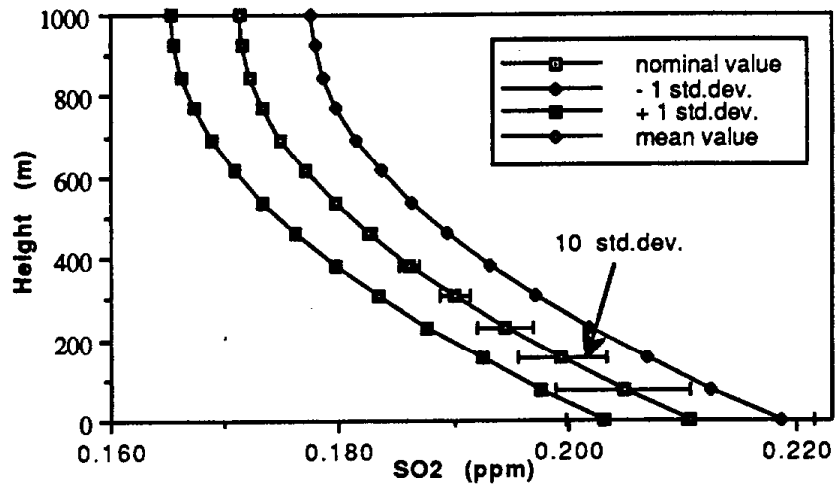


**Figure 6.8** Concentration profile of SO<sub>2</sub> at time = 19 hours for  $\sigma(D) = 0 \%$ ,  $\sigma(k) = 0 \%$ ,  $\sigma(vg) = 20 \%$ .

## 6.4 Conclusions

Without a doubt the most important conclusion to be drawn from this chapter is that the stochastic finite element method is approximately two orders of magnitude faster than the Monte Carlo analysis procedures discussed in section 5. In addition there is also a considerable savings in storage. The practical implications of the result is that the effects of data errors can be built directly into the solution process at small additional computational cost. Given the new algorithm a key observation is that there is now no reason why error propagation cannot be treated directly. While the procedure would be difficult to apply to the complete CALGRID model because of the design of the data structures future models could easily incorporate the concepts introduced in the chapter.

## **7. Application of CALGRID and Component Testing Using SCAQS Data**

### **7.1 Introduction**

The report, up to this point, has dealt with evaluating CALGRID and its individual modules using idealized problems. This is necessary because it is presently impossible to calculate the exact solution to the governing set of equations in an actual setting. First, the values of the variables used by CALGRID (or any other air quality model) are not exactly known. For example, the available data does not allow us to know exactly the wind velocities at all points, particularly above the surface layer. The effective vertical diffusivities are not well established. (Furthermore, K-theory is an approximation to a much more complicated process.) Deposition resistances are still only approximate. Emissions estimates are questionable (NAS, 1991). In short, there are significant uncertainties in the inputs.

Compounding the problem further is that, even if the inputs and equation parameters were accurately and precisely known, the analytical solution to the governing equations is not known. Thus, the usual procedure, and a powerful one as demonstrated above, to estimate error propagation and uncertainty is to develop idealized cases where an analytical solution is known (or more readily approximated). These cases can then be utilized to find which parts of a model, such as CALGRID, are responsible for the greatest uncertainty or likely to generate and propagate errors. In the tests described above, horizontal transport was found to develop the greatest error (particularly after the modifications to the QSSA solver to utilize a predictor corrector scheme). At question, however, is, "What are the magnitudes of those errors when applied to an actual simulation?" To this end, the data from the Southern California Air Quality Study (SCAQS; Lawson, 1990) provides an unparalleled evaluation set.

In this study, the SCAQS data has been used for evaluating CALGRID in two ways. First, the CB-IV version of CALGRID was applied to the August 26-28, 1987 SCAQS intensive measurement period. (Funding for the bulk of the model conversion to CB-IV and the initial application to SCAQS was provided under separate contract by the California Air Resources Board. This support is gratefully acknowledged. The module testing is done as part of this project.) This application was used to test how well CALGRID could reproduce the observations using the available input, and to test the sensitivity of the modified QSSA solver to the choice of time steps (see Chapter 4 above). However, it is recognized that the emissions data for that application likely understates the ROG and CO

emissions, so it is not appropriate to determine model validity using that evaluation. In essence, this application was primarily motivated to testing the modified QSSA solver.

A second question, and more relevant given the findings above, is, "How does the horizontal transport scheme impact predictions?" In the previous tests, this one element was found to produce the greatest error, and that other errors (e.g. from the chemical ODE solver) were not exacerbated. To this end, a test case was designed to estimate how the choice of horizontal transport algorithm might impact model predictions in an actual simulation, again using the August SCAQS episode. The tests described above showed that the Streamwise Upwind Petrov Galerkin (SUPG) method (Odman and Russell, 1990), when applied to an identical grid as the Chapeau method, gave superior results, so it was decided to compare predictions using these two methods, with no other changes. This would isolate the uncertainties associated with the transport algorithm. (Note, while the SUPG algorithm performed in a superior fashion in the tests above against known solutions, and as will be seen below, also provides better predictions when applied to SCAQS, it should not be taken that the SUPG results are correct. In fact, it is likely that the SUPG method is still more diffusive than desired.) While it has been the intent of the Error Propagation study to test the CALGRID model components as part of the CALGRID system whenever feasible, it was not in this case. After studying the code structure, it was determined that this test could be more readily conducted using the CMU modeling system applied to SCAQS. Thus, the SUPG (Odman and Russell, 1990) and Chapeau function (i.e. as used in CALGRID, STEM II, etc.) algorithms were both implemented in the CMU modeling system using the SAPRC/ERT chemistry. (Note, the CIT model refers to the particular formulation of the CMU modeling system as described in Harley et al. 1992, The CMU modeling system is an extension to include other modules, e.g. for testing their properties as described in this chapter.) For interest, the Smolarkiewicz (1984) method (which is currently used in UAM and RADM) was also tested.

The two applications to test CALGRID model components are a unique way to test error development and propagation in an airshed modeling system. Results of these tests, outlined below, are indicative of where, and to what degree uncertainties and model-based errors (as opposed to input errors) arise in actual model applications. First the test of the ODE solver is briefly presented, followed by the test of the transport algorithms.

## 7.2 Application of the CB-IV-based version of CALGRID and ODE Solver Evaluation

A project currently being conducted (and near completion) by our group is to incorporate the CB-IV chemistry into the CALGRID model (which was previously based on the SAPRC chemistry). As part of that study, it was applied to the August 26-28, 1987 SCAQS episode. The results of that model application are found in Kumar et al. (1992), and are briefly summarized below. Model performance for ozone predictions as compared to observations was not good. However, the severe tendency to underpredict ozone is likely caused by an underestimation of ROG and CO emissions believed to exist in the inventory. During the conduct of that study (as well as this one) an updated version of the CALGRID code was provided by CARB. One of the more major revisions was to the QSSA ODE solver. As pointed out in Chapter 3 of this report, the original QSSA solver could generate significant errors under certain circumstances. This problem was fixed by modifying the QSSA algorithm to be a predictor-corrector method with automatic time step determination. However, that modification led to a significant increase in computer time consumption. As part of this study, the modified, predictor-corrector QSSA was further analyzed for error propagation, and to decrease computer time requirements.

Tests of the modified QSSA solver incorporated in the CALGRID code showed that the feature that automatically chose a time step could lead to an initial time step on the order of 0.0001 minutes or less. Typically, the time step was on the order of 0.1 minute. This led to the large increase in CPU time. However, the previous tests (see Chapter 3.2) indicated that with a predictor-corrector, acceptable accuracy could be achieved with much larger time steps. It was decided to modify the QSSA solver to remove the automatic choice of time step. Instead, a fixed time step was used. As before, however, the modified QSSA retained the predictor-corrector feature (as opposed to just the predicting time marching as originally incorporated). Next, the CALGRID code was tested to quantify how the choice of time step affected predictions. This was done by applying CALGRID to the SCAQS episode several times, with exactly the same inputs. The only difference was the choice of fixed time step to be used by QSSA. This is a measure of how well the ODE solver works in an actual application.

The results of this test are shown graphically in Figure 7.1. With the predictor-corrector feature, the choice of time step between 0.1 and 0.5 minutes had little effect on the ozone predictions. Thus, it was decided to adopt 0.5 minutes to minimize computer time. This

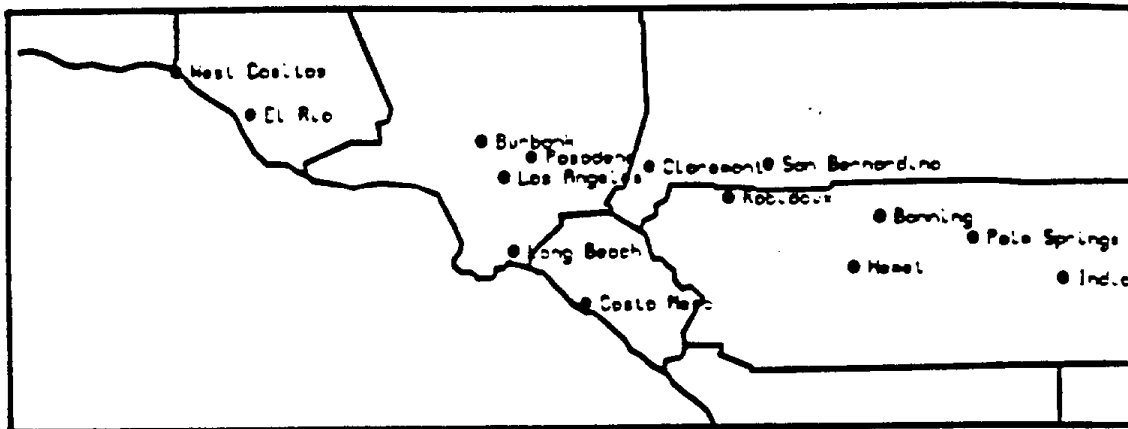


**Figure 7.1.** Domain definition: the SCAQS modeling region covers a 400 x 150 km area over southern California divided into 5km by 5km grids.

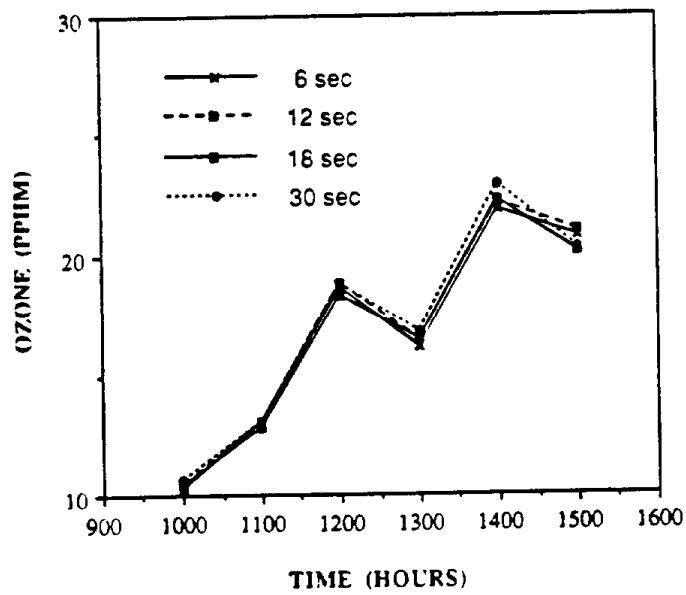
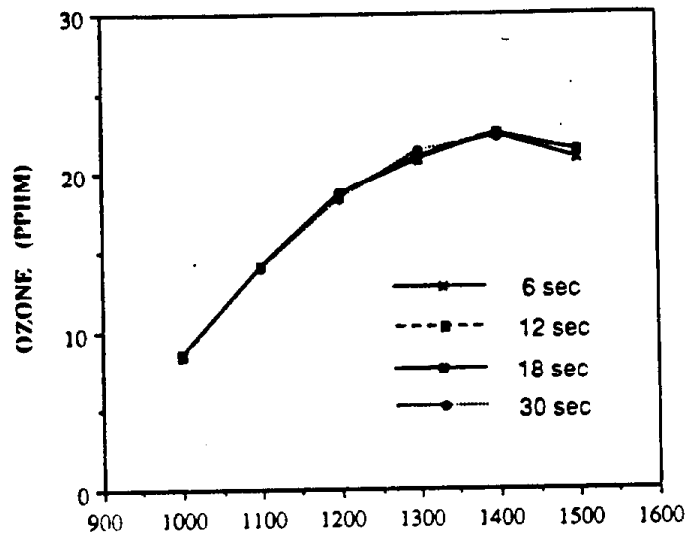


**Figure 7.2.** Effect of using various time steps in the CALGRID QSSA solver as applied to SCAQS.

cut the required computational time significantly from before, but it is still considerably more than if the predictor-only QSSA solver is used (about a factor of two greater).

This test along with the tests described in Chapter 3 indicate that the modified QSSA solver is not adding as much error as the transport algorithm (as is further demonstrated below). Again, this study is relatively unique in that the test is performed in the CALGRID modeling system, as applied to an actual episode simulation.

### **7.3 Error and Uncertainty Propagation from the Horizontal Transport Algorithm**

In the previous test, it was found that the horizontal transport algorithm used by CALGRID (i.e. the Chapeau function scheme with non-linear filtering) could lead to significant errors due to both dispersion and diffusion. Of note, it was found in the parabolic rotating puff test that the algorithm could lead to both overpredictions and diffusive diminishing of the peak. Non-linear chemistry did not significantly change this behavior. In those tests, the SUPG method did not have such large errors. Thus, an interesting comparison is between the two methods in an actual episode simulation.

In this project, we have attempted to test the model components in the CALGRID system. However, the SUPG scheme is not fully split, i.e. it does not split the horizontal transport into x- and y-linear operators. Instead, the algorithm does x- and y- direction transport simultaneously, and allows for multiple scales. Inclusion of SUPG in CALGRID would have required significant modification, and given the code structure, would have led, in essence, into a new-generation model. This was determined to be prohibitive, and also would not be the original test desired (i.e. no longer a test within the original CALGRID modeling system). Instead, the chapeau-function based finite element method adopted by CALGRID (and others) was compared against the SUPG using the CMU-modeling system structure that readily accepted either algorithm. CALGRID is largely based on many of the same principles as the CMU formulation (Yamartino et al. 1992), so this is a very applicable test. Also, the Smolarkiewicz method was similarly tested because it is also used by a number of air quality models. Again, the model was applied to the August 27-29, 1987 SCAQS period. Thus, this is an evaluation of the the CALGRID transport algorithm in an actual simulation. This test, a further description of the application of the three algorithms, and the results, are described below.

In solving the atmospheric diffusion equation, the CMU modeling system uses the operator splitting method. As implemented, the Chapeau-function algorithm, as used in CALGRID, and the Smolarkiewicz method, as implemented in UAM and others, advances the solution in time as

$$c^{n+1} = L_x L_y L_{cz}(\Delta t) L_y L_x c^n \quad (7.3.1)$$

The horizontal transport is split into two one-dimensional operators,  $L_x$  and  $L_y$ . It should be noted that this type of splitting is not consistent with the most general boundary conditions, though this appears to have little effect in general air quality modeling practice. In the Chapeau function scheme, the positivity of the solution is assured by applying the Forester filter, followed by a second filter if necessary. The Smolarkiewicz scheme, on the other hand, is positive definite. The diffusion-dominated vertical transport has time scales very similar to the chemistry. Also, the solution of a diffusive process involves an exponential structure similar to the chemical decay. Therefore, chemistry and vertical transport are combined in a single operator,  $L_{cz}$ . The resulting system is solved using the hybrid scheme of Young and Boris (1977) for stiff systems of ordinary differential equations. The hybrid scheme is one of the two in CALGRID. The condensed, lumped-molecule mechanism of Lurmann et al. (1987) (also referred to as the LCC or SAPRC/ERT mechanism) is used to describe the chemical kinetics. Other details of the CMU modeling system as applied to this problem can be found in Odman and Russell (1991b) and Harley et al. (1992).

The SUPG algorithm differs from the CALGRID implementation of the chapeau function scheme (or the Smolarkiewicz scheme) in the way it treats the horizontal transport. The transport operator,  $L_{xy}$ , is two-dimensional and the solution is advanced in time as

$$c^{n+1} = L_{xy} L_{cz}(\Delta t) L_{xy} c^n \quad (7.3.2)$$

The elements are selected from the bilinear interpolation function space. To avoid negative concentrations, the linear SUPG solution is preceded by a non-linear streamline filter. This filter is a two-dimensional generalization of the Forester (1974) filter. The filter has been further advanced to filter dispersive waves in the streamline direction only (Odman and Russell (1992a)). Other components of the CMU-system are the same as the CIT model described by Harley et al. (1992).

## **7.4 Model Simulations**

The simulations focus on two applications: (i) transport of SO<sub>2</sub> without chemistry, and (ii) O<sub>3</sub> formation over the Southern California Basin for a 3-day summer period. The Southern California Air Quality Study (SCAQS) provides a comprehensive set of measurements for these simulations during the 27-29 August, 1987 period. The Chapeau function, Smolarkiewicz and SUPG algorithms are used in the simulations to compare their predictions. A uniform 5 km grid is used to evaluate their performance. Meteorological and air quality (O<sub>3</sub>) measurements for this period, and emission inventories for the region were obtained from the California Air Resources Board. In addition to the routine measurements, special measurements were taken during SCAQS (Lawson, 1990), which augmented the data base significantly. Detailed information about these measurements and input data processing can be found in Harley et al. (1992).

### **7.4.1 Modeling domain and grid systems**

The modeling domain covers a 400 x 150 km region over Southern California (Figure 7.2). The lower-left corner of the domain is located at 210 km Easting and 3680 km Northing Universal Transverse Mercator (UTM) coordinates. The domain was divided into 80 x 30 cells of 5 x 5 km size for Chapeau and Smolarkiewicz tests, and 79 x 29 finite elements of the same size for CMU model (this is because the SUPC calculates the concentrations at the cell centers, as opposed to the nodes). Since the cells or finite elements are of the same size everywhere, these grid systems will be called uniform hereafter. The height of the domain is fixed at 1100 m. The heights of individual layers are, from the ground up, 38.5 m, 115.5 m, 154 m, 363 m and 429 m, respectively.

### **7.4.2 Comparison of the SO<sub>2</sub> transport simulations**

In these simulations, the chemistry modules of both models are disabled to more readily identify the differences in the solutions of horizontal transport. The initial SO<sub>2</sub> concentrations (August 27, 0:00 hrs) are magnified by a factor of 10 in a region centered at a coastal location (Long Beach), such that the SO<sub>2</sub> puff has a conical shape with a base radius of 20 km (4 Δx). The peak concentration is 50 ppb. The emission inventories contain a point source at 510 km Easting and 3810 km Northing UTM coordinates, emitting approximately  $5.133 \times 10^{-3}$  ppm-m/min of SO<sub>2</sub>.

The transport of the elevated peak, as well as the emissions, is followed for the 24 hours of August 27, 1987. During this period, winds are primarily northeasterly. Figure 7.3

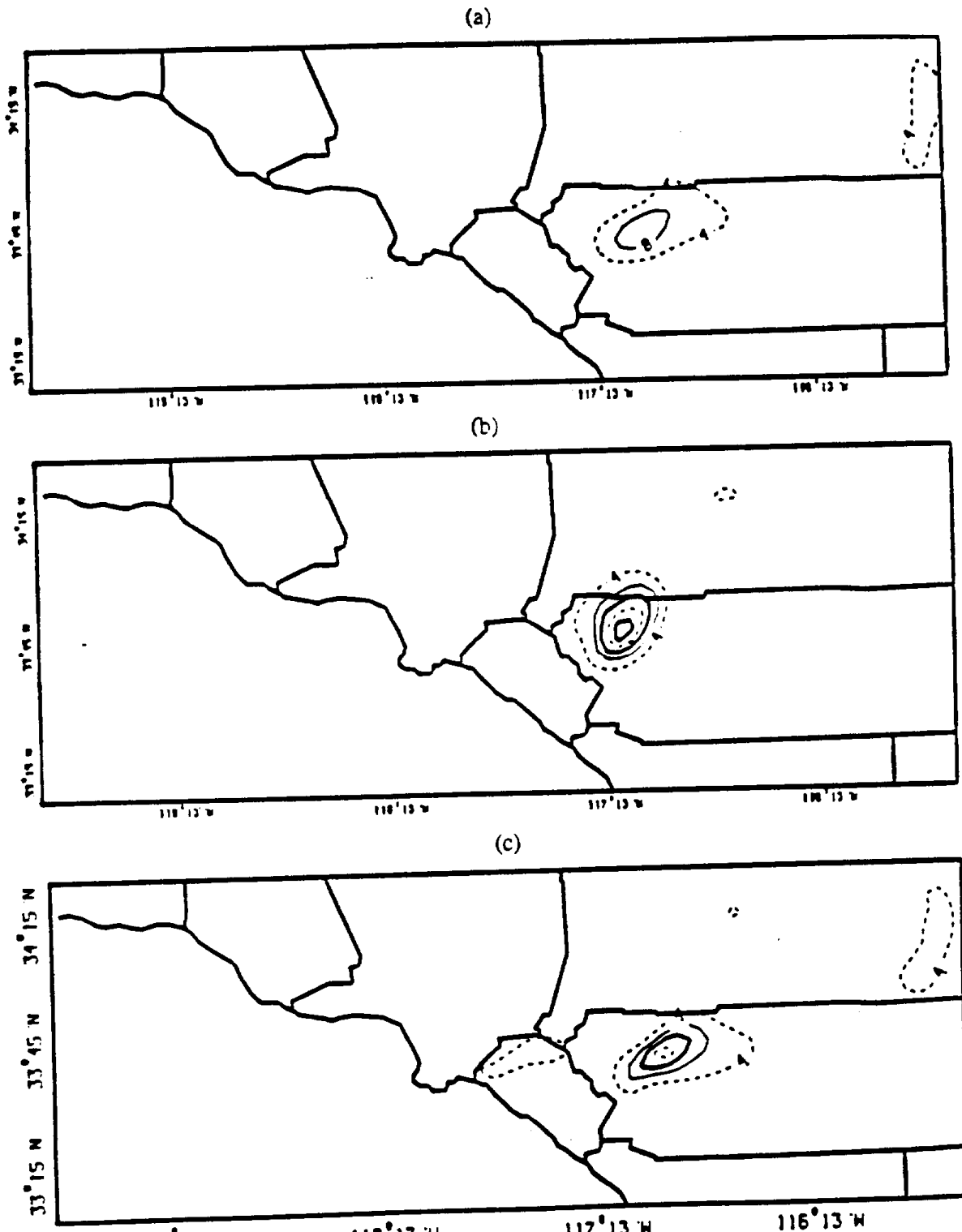


Figure 7.3 Contour plots of the predicted SO<sub>2</sub> concentrations (ppb) in a transport simulation with no chemistry on August 27, 1987 at 24:00 hrs: a) chapeau, b) SUPG, c) Smolarkiewicz.

shows the contour plots of the predicted SO<sub>2</sub> concentrations averaged for hour 24:00 of August 27 (1-hr average). The Chapeau algorithm predicts that the puff would expand as far as Perris to the south and Banning to the east. The shape of the puff is elongated in the southwest-northeast direction. Its peak concentration is 8 ppb. On the other hand, the SUPG algorithm locates the peak in Riverside and maintains a more conical shape. The puff covers a much smaller area and has a peak concentration of 20 ppb. When the Smolarkiewicz scheme is used, the peak concentration is 16 ppb, and is located in approximately the same location. This indicates that the Chapeau function and the Smolarkiewicz schemes are more diffusive, and that the one-dimensional splitting may be biasing the solution. The use of a two dimensional horizontal operator is computationally effective, and removes this bias.

What happens to the puffs generated by the point source is also of interest. The Chapeau function-based solution does not show the second puff that builds after the stagnant night conditions prevail. The SUPG solution shows this puff with 4 ppb contour. The first puff that built up during early morning moves out of the domain through the northeast boundary in the simulation with the SUPG algorithm. The chapeau function scheme shows this same puff with a peak of 4 ppb to the far northeast corner of the domain. One other result is of significant interest here. There is a large SO<sub>2</sub> source near the original location of the elevated puff. Both the SUPG and Chapeau schemes rapidly diffused these emissions because the non-linear filters identified the emissions from this source as a dispersive wave. This indicates that the use of a non-linear filter, while preserving positivity, can over-diffuse a concentrated source. This would tend to make the schemes less useful for determining the impact from single sources, such as a power plant. The use of such filters must be scrutinized in situations where this effect is important, and would indicate that the actual resolution of the model in those cases is limited to no better than  $3\Delta x$ .

This test showed a southeasterly bias in the movement of the puff in Chapeau function-based predictions with significant diffusion of the peak height. The SUPG scheme predicted higher peak concentrations.

### **7.4.3 Comparison of the Ozone Formation**

The formation and transport of O<sub>3</sub> was followed over the 3-day SCAQS period. The predicted O<sub>3</sub> fields are displayed with contour plots of averaged concentrations for hour 14:00 in Figures 7.4 - 7.6. This hour corresponds approximately to the highest measured (and predicted) concentrations.

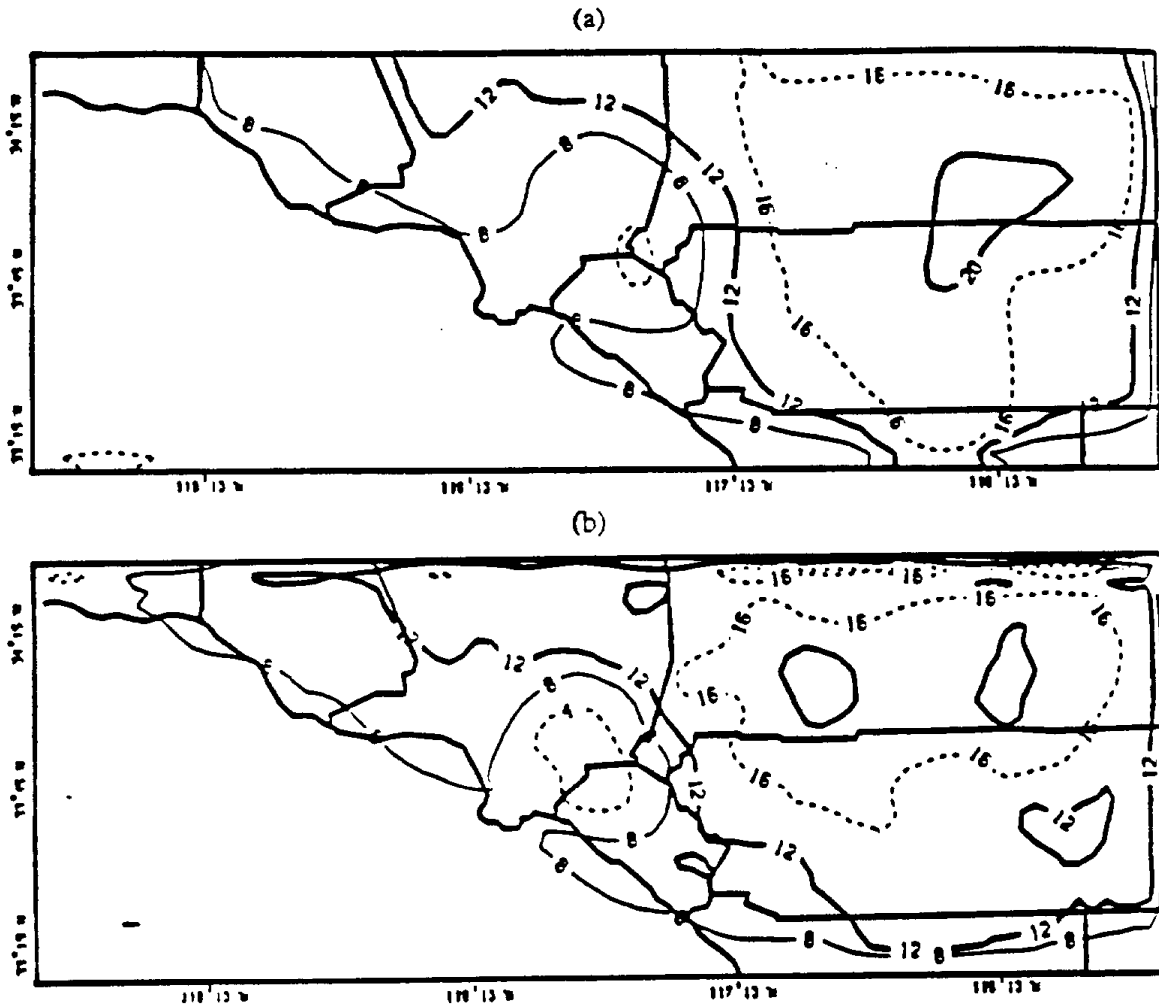


Figure 7.4 Contour plots of the predicted O<sub>3</sub> concentrations (pphm) on August 27, 1987 at 14:00 hrs: a) chapeau, b) SUPG

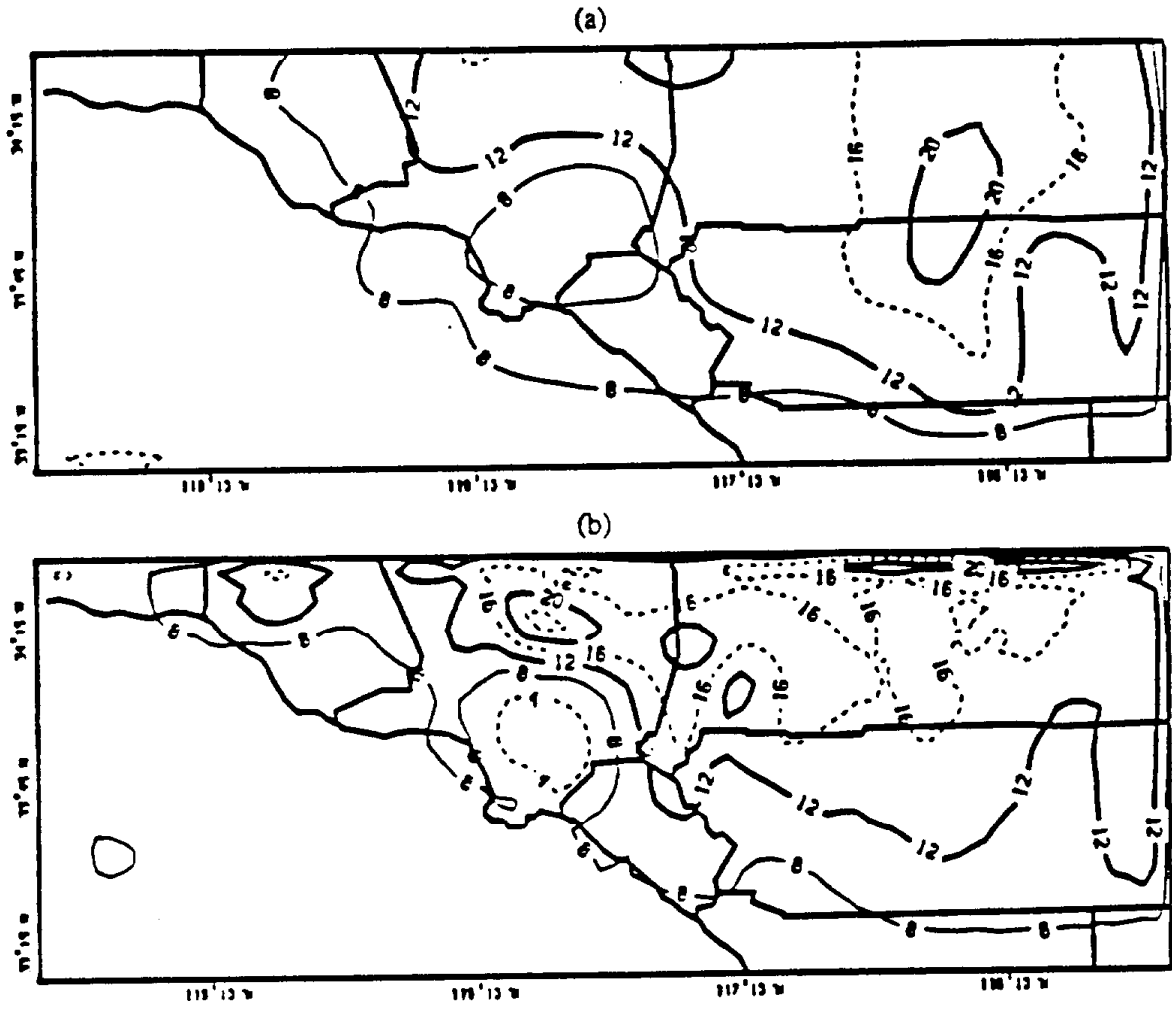


Figure 7.5 Contour plots of the predicted O<sub>3</sub> concentrations (pphm) on August 28, 1987 at 14:00 hrs: a) chapeau, b) SUPG

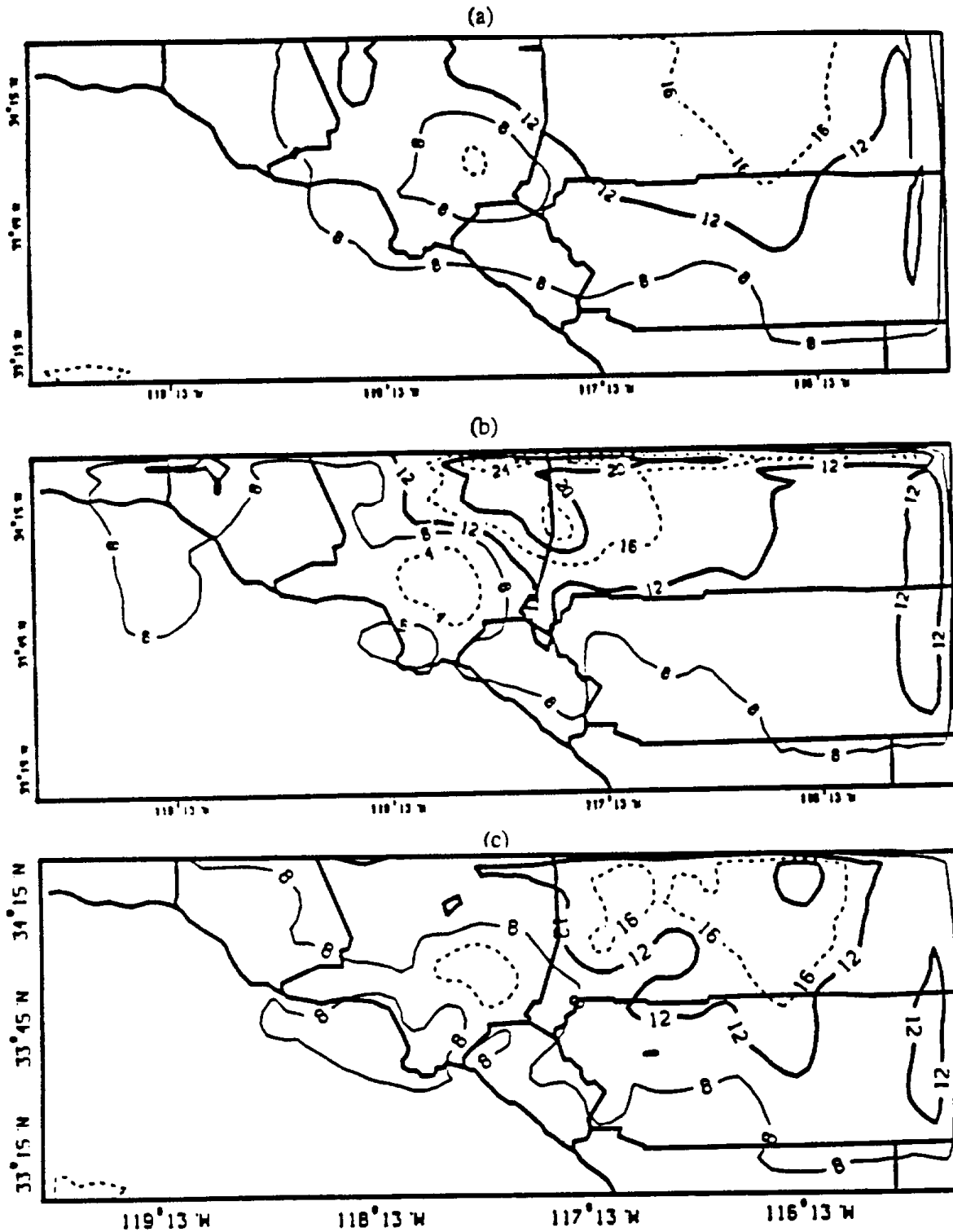


Figure 7.6 Contour plots of the predicted  $O_3$  concentrations (pphm) on August 29, 1987 at 14:00 hrs: a) chapeau, b) SUPG, c) Smolarkiewicz.

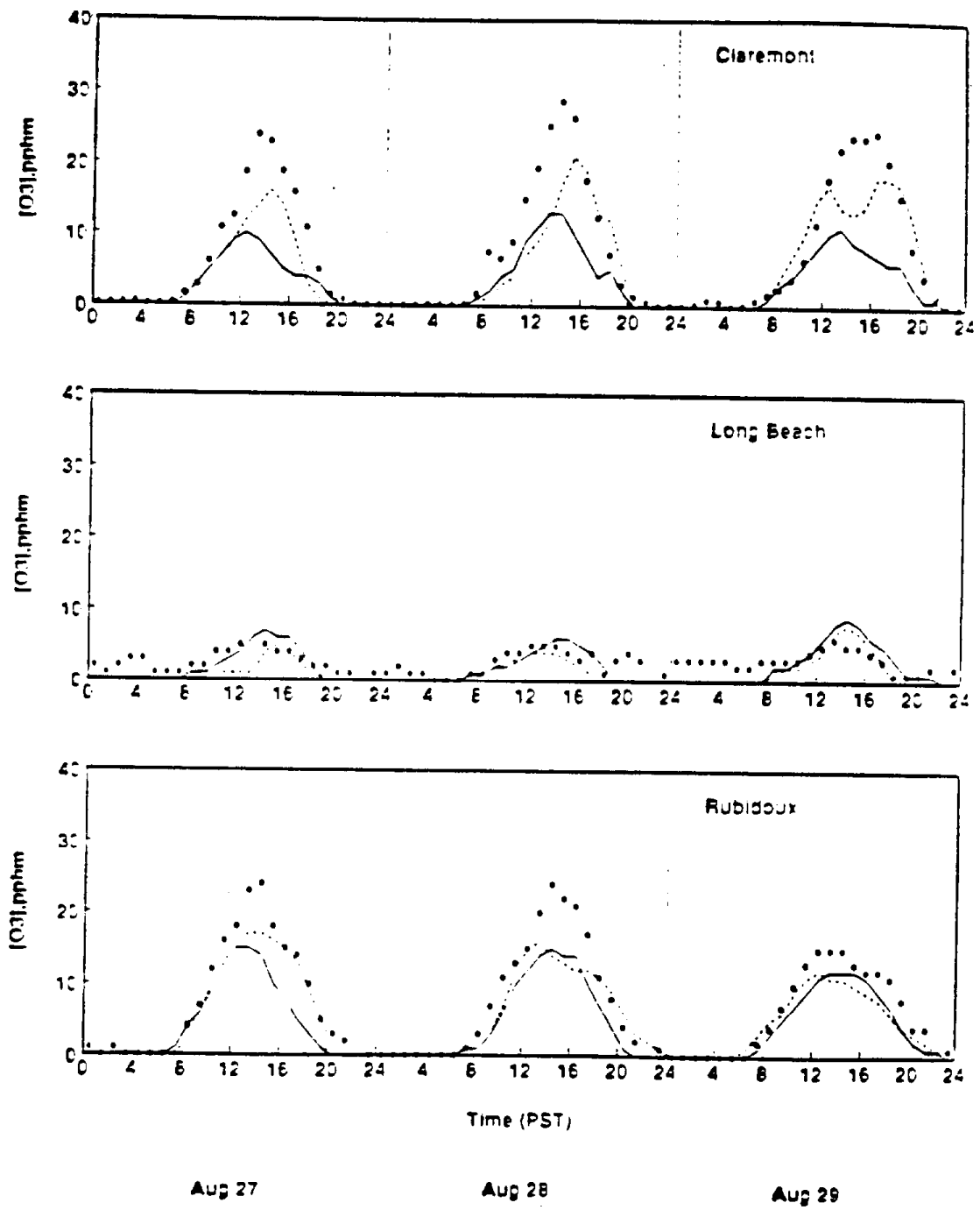


Figure 7.7 Time series plots of the O<sub>3</sub> concentrations at Claremont, Long Beach and Rubidoux: observed (•••), predicted by chapeau (—), and SUPG (---) algorithms

On August 27, the chapeau algorithm predicts an O<sub>3</sub> level of 8 pphm around Los Angeles with a low of 4 pphm northeast of Anaheim (Figure 7.4). The region to the east of the domain displays high O<sub>3</sub> concentrations (~ 16 pphm) with a peak of 20 pphm northeast of Banning. The SUPG scheme, on the other hand, predicts lower O<sub>3</sub> (4 pphm) around Los Angeles. O<sub>3</sub> is higher to the northwest, along the coastline up to Ventura. Also, the concentrations to the north are mostly higher. There is a distinct O<sub>3</sub> contour of 12 pphm over Mt. Wilson. Usually, O<sub>3</sub> concentrations in the northeast are at the same level (16 pphm). The concentrations to the east and southeast of the domain are significantly different. The single local peak of 20 pphm to the east of Banning in chapeau-based predictions is split into two in the SUPG-based fields. One of these distinct peaks is now in San Bernardino. Also, O<sub>3</sub> in the southeast of the domain (Perris and Hemet) are considerably lower. There is a distinct local peak (12 pphm) west of Indio. The Smolarkiewicz algorithm produced fields similar to the chapeau algorithm, though slightly more diffused.

In summary, when compared to the chapeau scheme, the SUPG algorithm predicts lower O<sub>3</sub> concentrations in the vicinity of Los Angeles, east and southeast of the domain on August 27. On the other hand the O<sub>3</sub> concentrations are higher in the northwest, north and northeast. In these regions, there are distinct peaks that the chapeau algorithm and Smolarkiewicz method did not resolve.

On August 28, the differences between the simulations becomes more noticeable (Figure 7.5). The chapeau algorithm predicts an O<sub>3</sub> concentration of 8 pphm over most of the Los Angeles basin (e.g., Anaheim, Burbank, downtown Los Angeles, Long Beach and Pasadena). The SUPG algorithm predicts concentrations of 4 pphm for this region. There is considerably higher O<sub>3</sub> to the north (20 pphm in Mt. Wilson), to the northwest (16 pphm north of Ventura) and northeast in the SUPG predictions. On the other hand chapeau-based predictions are usually higher to the south and to the east. The 20 pphm-peak to the east (Banning) in the CIT predictions is moved further up to the northeastern corner of the domain in SUPG-based simulations. There is considerably more O<sub>3</sub> directly to the northeast of Los Angeles (Claremont) in the SUPG predictions.

On August 29, the O<sub>3</sub> concentrations predicted by the algorithms are completely different in the northern half of the domain (Figure 7.6). The chapeau-based algorithm predicts high O<sub>3</sub> (16 pphm) to the northeast while the SUPG algorithm predicts only 12 pphm for most

of the San Bernardino County. There is high  $O_3$  (24 pphm) to the north of Azusa, in the mountains, according to the SUPG predictions while the chapeau algorithm does not predict these peaks. Also, the SUPG predicts higher  $O_3$  in the Northwestern sites (e.g., El Rio, Ventura and West Casitas). On the other hand, the chapeau algorithm predicts higher  $O_3$  (8 pphm) in downtown Los Angeles compared to the SUPG method (4 pphm). Peak ozone prediction differences in some regions differ by up to a factor of 50% (with the chapeau function having lower ozone predictions where the observations are high). Most of the south and southeastern parts of the domain look similar in both algorithm simulations, as well as the Smolarkiewicz scheme. The major differences in the predictions for all three schemes are in the regions with the greatest concentration changes and detail, i.e., where the second derivatives are greatest.

The trends observed for the 3-day period may be generalized as follows. The  $O_3$  fields predicted by the SUPG show more spatial variability and a wider range than the Chapeau function-based model. The SUPG predicts higher  $O_3$  to the north and lower  $O_3$  to the east and south compared to the chapeau scheme. Harley et al. (1992) reported low predictions compared to the observed concentrations in the northern measurement stations (Azusa, Burbank, Claremont, Glendora and Pasadena) when using the CIT model. The SUPG gives either the same or higher  $O_3$  levels in all these northern sites. It was also reported that the chapeau function gives high  $O_3$  concentrations in the eastern (e.g., Banning, Hemet and Palm Springs) and southern sites (Costa Mesa). SUPG predicts lower  $O_3$  concentrations in all of these sites. Figure 7.7 shows the time series plots of the observed and predicted  $O_3$  concentrations in Claremont, Long Beach and Rubidoux. Comparisons of the chapeau function and Smolarkiewicz algorithm-based predictions are given in Figure 7.8 for selected stations. The predictions of the SUPG are in better agreement with the observations. Figure 7.9 shows the observed and predicted concentrations for Banning, Hemet and Palm Springs. The SUPG predictions are lower, thus closer to the observations.

All the above results suggest that the SUPG model improves the overall accuracy of the predictions. For further insight, hourly predictions at all measuring stations (at 53 sites), for the 3-day simulation are analyzed using scatter plots. In Figure 7.10, the predictions of the CMU model with the SUPG using uniform grid are compared to the observed  $O_3$  concentrations. Figure 7.11 compares the predictions of the SUPG to the predictions of the chapeau algorithm. The  $O_3$  concentrations are plotted only if there is a measurement for

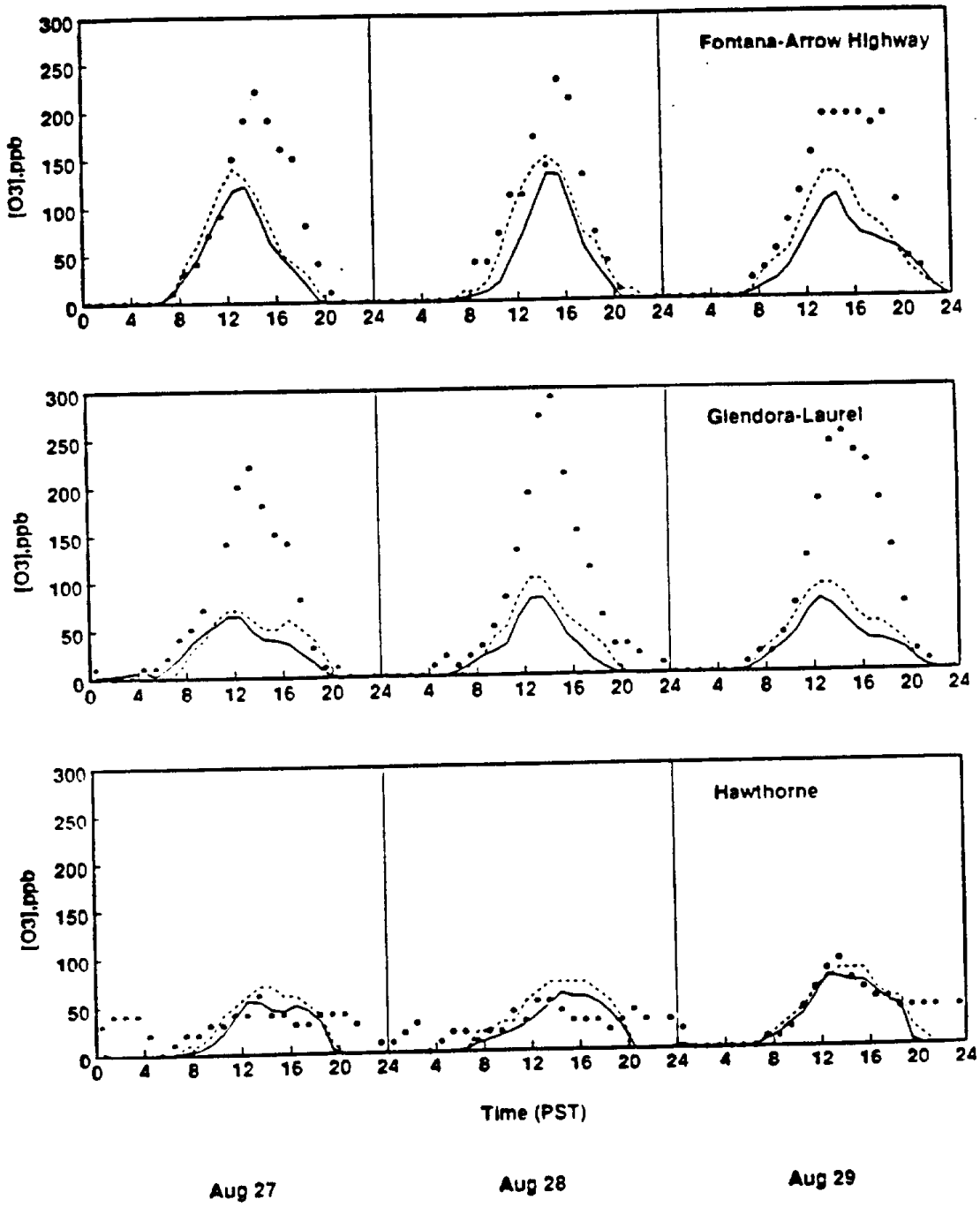


Figure 7.8 Time series plots of the  $O_3$  concentrations: observed (•••), predicted by chapeau (---), and Smolarkiewicz (—) algorithms

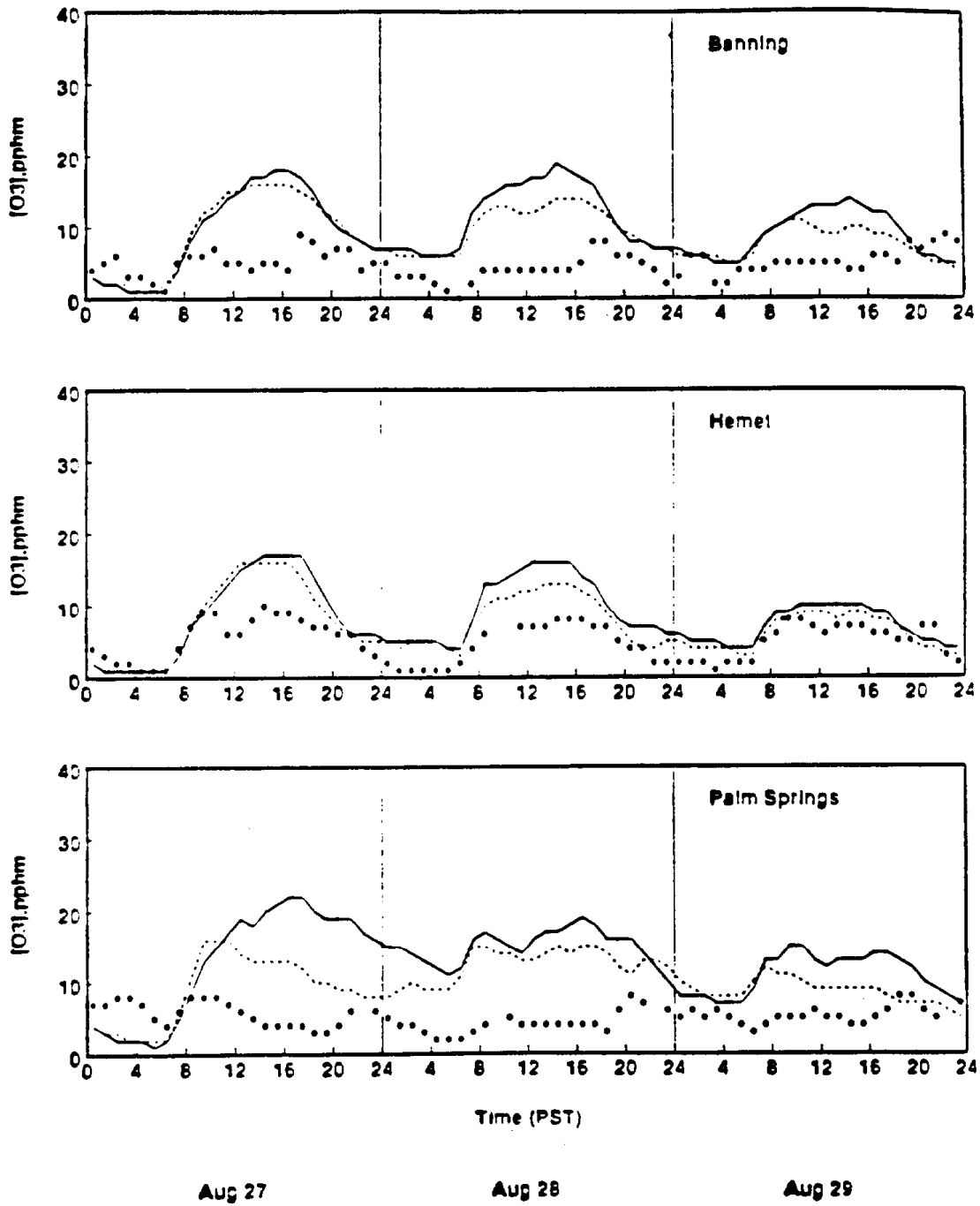
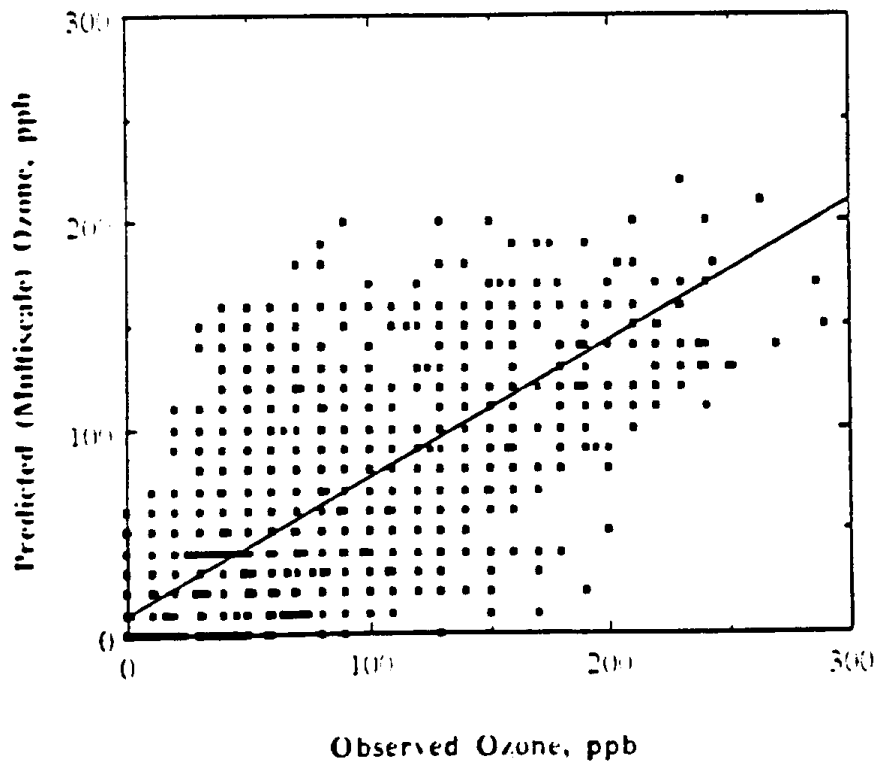
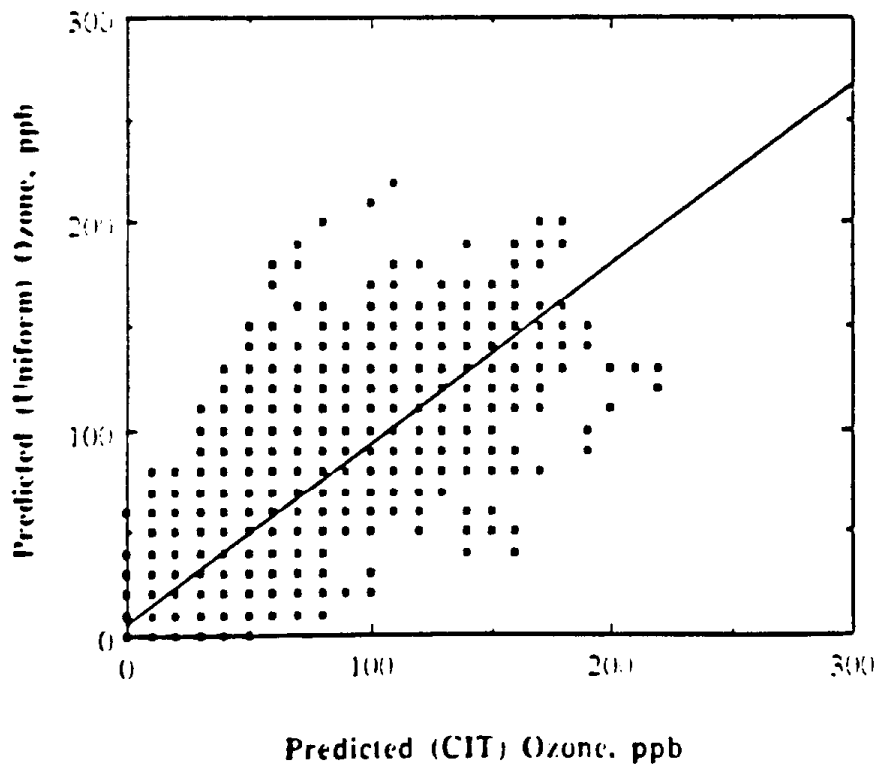


Figure 7.9 Time series plots of the O<sub>3</sub> concentrations at Banning, Hemet and Palm Springs: observed (•••), predicted by chapeau (—), and SUPG (---) algorithms



**Figure 7.10** Scatter plots of the SUPG algorithm predictions versus observed  $O_3$  concentrations.



**Figure 7.11** Scatter plots of the SUPG-based horizontal transport scheme predictions versus  $O_3$  concentrations predicted by the chapeau-based scheme at measurement stations.

that hour at the specific location. The correlation between the two model's predictions is not very strong.

## **7.5 Summary and Conclusions**

The SUPG, Chapeau and Smolarkiewicz algorithms were applied to the August 27-29 SCAQS period using the CMU modeling system. The grid was a uniform 5 x 5 km everywhere. The SUPG algorithm followed a puff, initially located at Long Beach, with considerably less diffusion than the chapeau or Smolarkiewicz schemes.

When following O<sub>3</sub> dynamics, there were significant differences between the predictions of the three schemes. The differences became more obvious in the second and third days of the simulation. The SUPG predicted higher O<sub>3</sub> concentrations to the north of Los Angeles, and lower to the east and southeast. Some of the systematic errors in CALGRID-based routine may be due to the numerically diffused solution of the one-dimensional Chapeau function scheme. Surprisingly, in rotating puff tests, the Chapeau function scheme is usually able maintain peak heights (Chock, 1991). However, as discussed in Section 3, the accuracy of the scheme drops sharply when a parabolic angular velocity field is used. This result is important because schemes that are more diffusive than the Chapeau function scheme in rotating puff tests are currently used in many air quality models (e.g., the Smolarkiewicz scheme also tested here). In the applications to SCAQS data, the chapeau function and SUPG schemes led to more diffused ozone fields, and the magnitude and location of the peak ozone levels differed considerably. Differences in peak ozone of 50% were found in some locations, particularly where the highest ozone levels were observed. In these cases, the SUPG scheme proved to provide closer predictions. These tests indicate that the more diffusive schemes may lead to less acceptable O<sub>3</sub> concentration predictions when numerical diffusion becomes much larger under the variable conditions of actual flow fields.

## 8. Summary and Conclusions

An extensive series of tests have been performed to quantify the error and uncertainty propagation in the CALGRID model and its modules. Further tests have been performed on calculating the sensitivity of the model calculations to different formulation of some of the modules (e.g., chemical kinetics, horizontal transport). Also, coding checks have been conducted both with software pad and one-by-one by a programmer. Further, recommendations and specific changes have been made to improve and understand model performance (e.g., the chemical ODE solver, the use of a filter in the transport algorithm, vertical transport solvers, etc.). Because of the importance of this project, and the interesting results obtained as the project proceeded, the tests have gone well beyond those originally proposed.

CALGRID was found to have utilized state-of-the-science algorithms for the time period it was formulated (late 1980's), in a relatively modular framework. This made tests of the model system, and its modules viable. The coding was found to have some nonstandards-FORTRAN sections (e.g., mixed common blocks, tabs, etc.), but these slight irregularities should not inhibit portability significantly given the robustness of most modern compilers. Its structure, however, could require significant paging on systems with minimal memory, thus increasing the run time. It has been successfully implemented on a variety of computational platforms by this group and others. Computational requirements are similar to other current photochemical airshed models (e.g., UAM, CIT, and the CMU models). The formulation and implementation were, as intended, a significant improvement over UAM, although some improvements are needed. The use of binary files is cumbersome and inhibits portability of the files (not all systems, e.g. the CRAY YMP, adhere to IEEE standards). Other input files, and the formatted equivalents of the binary files, can be very bulky. Standards, across the air quality modeling discipline, should be developed to rectify some of these problems. The bulkiness of some of the files can be remedied by further consideration of the data accuracy, precision and size.

Initial analysis of CALGRID suggested that the ODE solver used to integrate the chemical dynamics, the horizontal transport algorithm, and the vertical transport scheme would be the most likely sources of error. Efforts concentrated on quantifying the error and uncertainty propagation from these routines. It should be mentioned, however, that

there are inherent, un-resolvable uncertainties involved in air quality modeling due to the stochastic nature of the processes being simulated. Also, some of the approximations used to make the computational implementation practical add uncertainty (e.g. the use of K-theory). This formulation uncertainty would add to the uncertainty and error evolving directly from the computational implementation of CALGRID, as evaluated here.

The intent of the project was to analyze the error propagation from different modules within the CALGRID system when possible. If that was not feasible, the algorithms were tested outside of the CALGRID system, e.g., by implementing the algorithm and routines against standardized problems for direct comparison with analytical solutions or one situation where the solution is well approximated. For example, the ODE solvers were tested against a classical stiff ODE technique. When possible, these problems were built up to identify how the various modules would exacerbate errors from other modules. For example, an investigation focused on whether errors in the horizontal transport algorithm changed after interaction with the chemical ODE solver in the presence of non-linear chemistry.

First, the stiff ODE solvers were tested, using a Gear routine (LSODE) as a basis. This test, using a standard problem using two currently popular chemical mechanisms, showed that the QSSA solver could generate significant errors under certain conditions (ROG rich emissions). The use of the nitrogen-conserving constraint implemented in CALGRID reduced those errors. The hybrid solver, also available in CALGRID (though the documentation (Yamartino, 1989) appears to prefer the QSSA solver) was more accurate and less prone to error propagation. Again, a nitrogen-conserving constraint that was developed as part of this project improved accuracy. However, the hybrid solver was slower (factor of 1.5 to 2) than the QSSA solver originally provided as part of CALGRID. During the course of this study, CALGRID was updated, including a modification of the QSSA solver to add a corrector step and automatic choice of time step. In the original implementation, the QSSA solver was purely a predictor method with fixed time steps. This change did make the routine much more accurate and robust, but increased computer time by a factor of about 5 (significantly more than the hybrid solver). Tests showed that in an actual simulation (i.e., application to SCAQS), that the automatic time step choice often led to very small steps, and that little predictive performance degradation was found by using a fixed time step (as used in the original implementation), along with the predictor-corrector feature. This modification reduced run-time appreciably. These tests suggested that in practice, the errors derived from the solution of the non-linear chemical

kinetics is on the order of 1 to 2% for ozone in the current implementation. Note, the percent errors in species that are rapidly being depleted and have low concentrations can be larger, though at those concentrations this level of error has little effect on the dynamics of the more abundant species, such as ozone. This is found in other airshed modeling systems, and the level of error is directly associated with machine precision.

Next, the vertical transport algorithm was tested and, for likely atmospheric conditions, the errors are less than 5% when mixing is rapid. In passing, it is important to note that at least 5 vertical cells, logarithmically spaced (versus constant spacing) are necessary to provide acceptable accuracy.

The choice of algorithm to follow horizontal transport was found to add, and propagate, the greatest error and uncertainty of any of the CALGRID components. Thus, maximum effort was expended in quantifying the level of error and uncertainty, as seen by the variety of tests utilized. The horizontal transport algorithm was evaluated using the standard rotating puff test, a modified rotating puff test, stochastic solution of the transport using finite elements, and testing of the algorithm and others against SCAQS data.

One standard test used to identify errors resulting from the horizontal transport algorithm is the rotating puff test. In this test, a puff is followed around a grid with a velocity field corresponding to solid body rotation. Usually two revolutions are followed. CALGRID uses a chapeau-function, finite element routine, with a Forrester filter to reduce dispersive waves. If negative concentrations are still found after filtering, a second filter is also used. In this study, the chapeau-function algorithm was analyzed using this test. Other transport algorithms were tested for comparison. Similar comparisons have been conducted by others, notably Chock (1991), with similar results. The result was that the chapeau function algorithm was somewhat diffusive in this test, but less so than the Smolarkiewicz routine used by other models (e.g. RADM and UAM). However, it was slightly more diffusive than the SUPG scheme. The peak was diffused by about 30% during the two revolutions. Note, that the implementation of the one-dimensional splitting in CALGRID is not consistent for general boundary conditions, though this test does not evaluate this problem (which should not be large).

As it turns out, the choice of a solid body rotation velocity field is very artificial, and the one-dimensional operators (as used by CALGRID and other air quality models) perform

particularly well in this test. Because of this, a modified rotating puff test was designed, using a parabolic angular velocity field, to more severely test the transport algorithms. In this test, the one-dimensional chapeau function algorithm (embedded in CALGRID and other airshed models) did not behave as well. First, the predictions were seriously aliased, resulting in a significant overshoot (17%). Then, the peak of the puff was rapidly diffused (by about 40% from the peak). Also, the shape of the puff was seriously distorted. The two-dimensional transport operator based on the SUPG method did not show the overshoot, nor nearly so rapid diffusion of the peak. The Forrester filter used in CALGRID led to significant artificial diffusion in this cross stream direction.

Another test combined the rotating puff with simultaneous solution of non-linear chemical kinetics. This is an important test because the propagation of errors in different species may interact, causing still greater errors, or oscillations in the field (as has been found for other algorithms). It also adds a rapid temporal variation in the structure and magnitude of the components of the puff. Thus, it adds a level of severity to the rotating puff test. In this case it was found that the chemistry did not add an appreciable error to the results, and that the diffusion and dispersion of the transport algorithm, independent of the chemistry, dominated.

A unique contribution of this research, described in Chapters 5 and 6, is the introduction of some new computational procedures for assessing error propagation. These methods, making use of stochastic finite elements, show considerable promise as a way to quantitatively follow the effects of parameter errors. Using the vertical transport code used in CALGRID, it was found that vertical diffusivity errors and uncertainties were more significant than dry deposition and chemical conversion errors.

A final set of tests of the horizontal transport algorithm and chemical ODE solver were conducted by application to simulating a SCAQS intensive measurement period. First the CALGRID model was applied to SCAQS, following an initial, base case, application supported by separate contract. Of interest here was the integrity of the modified QSSA ODE solver. In these tests, use of a fixed time step versus automatic choice, was analyzed, as well as the choice of fixed time step. A fixed time step of 0.5 minutes was sufficiently accurate and have acceptable computational efficiency. In this application, the level of error introduced was on the order of 1%. A more telling test was analysis of the horizontal transport algorithm. As suggested by the previous tests, this would be the area where the greatest error would arise.

In the rotating puff test, it was found that the two-dimensional SUPG algorithm proved to be significantly more accurate than the one-dimensional operator splitting method, using a chapeau-function, finite-element algorithm adopted by CALGRID, when a non-solid body rotating velocity field was used. While both were somewhat diffusive in those tests, the SUPG was less so and also did not have the aliasing problems. The chapeau function algorithm was tested alongside the SUPG scheme and the Smolarkiewicz method in an application to the August SCAQS episode. The results of that comparison support the findings of the rotating puff tests. The chapeau function scheme was found to be more diffusive than the SUPG scheme. The comparison of the chapeau scheme to the Smolarkiewicz scheme was mixed. Most notably, the peak predictions were significantly lower in the chapeau-function simulations, as compared to SUPG, due most likely to numerical diffusion. Also, some biasing, due to the use of one-dimensional operators in the operator splitting, was noticed. While the ozone predictions in most of the region compared well between the three schemes, peak predictions in the regions where the observations also peaked were significantly less (about 40% in peak locations) using the chapeau and Smolarkiewicz schemes in comparison to the SUPG method. This would be the origination of the most significant amount of model-specific error. (Note that the errors in the model inputs are likely to be at least as big.) The SUPG-derived solution should not be taken as exact, and likely also includes some numerical diffusion. Thus, the fields should likely have even greater horizontal structure.

In summary, CALGRID can be an effective air quality model, with errors typical of most of the photochemical models currently in use. The horizontal transport algorithm is likely the largest source of error and uncertainty propagation, and the use of the non-linear filter will likely over-diffuse the emissions from some point sources. On the other hand, the transport algorithm is less diffusive than others currently in use, e.g. SHASTA and the Smolarkiewicz schemes. The code itself is relatively portable, though some non-standard FORTRAN statements were found. CALGRID should provide acceptable performance on most computational platforms, in terms of algorithm accuracy and efficiency, for use in typical photochemical air quality model applications.

## References

- Adomian, G. (1983). *Stochastic Systems*. Academic Press.
- Adomian, G. (1990). A Review of the Decomposition Method and Some Recent Results for Nonlinear Equations. *Mathl. Comput. Modelling*, 13, 7, pp. 17-43.
- Adomian, G. and K. Malakian (1980). Inversion of Stochastic Partial Differential Operators - The Linear Case. *Journal of Mathematical Analysis and Applications*, 77, pp. 505-512.
- Adomian, G. and R. Rach (1983). Inversion of Nonlinear Stochastic Operators *Journal of Mathematical Analysis and Applications*, 91, pp. 39-46.
- Baker, C.T.H. (1977). *The Numerical Treatment of Integral Equations*. Clarendon Press.
- Bellomo, N., L.M. de Socio, R. Monaco (1988). Random Heat Equation: Solutions by the Stochastic Adaptive Interpolation Method. *Comput. Math. Applic.*, 16, 9, pp. 759-766.
- Benaroya, H. and M. Rehak (1987). The Neumann Series/Born Approximation Applied to Parametrically Excited Stochastic Systems. *Prob. Eng. Mech.*, 2, 2, pp. 74-81.
- Benaroya, H., and M. Rehak (1988). Finite Element Methods in Probabilistic Structural Analysis: A Selective Review. *App. Mech. Rev.*, 41, 5, pp. 201-213.
- Boland, W.R. (1972). Algorithm 436, 437, 438, 439 Product Type Integration. *Communication of the ACM*, 15, 12, pp. 1070-1072.
- Braham, H.S. and L.J. Skidmore (1962). Guidance-Error Analysis of Satellite Trajectories. *J. Aerosp. Sci.*, 29, pp. 1091-1097.
- Buslenko, N.P., D.I. Golenko, Yu. A. Shreider, I.M. Sobol, V.G. Sragovich (1967). *The Monte Carlo Method: The Method of Statistical Trials*. Pergamon Press.
- Canu, P. and W.H. Ray (1991). Discrete Weighted Residual Methods Applied to Polymerization Reactions. *Computers Chem. Engng*, 15, 8, pp. 549-564.
- Carslaw, H.S. and Jaeger, J.C. (1986), *Conduction of Heat in Solids*, Second Edition, Clarendon Press, Oxford.
- Chang, J.S., Binkowski, F.S., Seaman, N.L., McHenry, J.N., Samson, P.J., Stockwell, W.R., Walcek, C.J., Madronich, S., Middleton, P.B., Pleim, J.E., Lansford, H.H., "The Regional Acid Deposition Model and Engineering Model," State-of-Science/Technology Report 4, National Acid Precipitation Assessment Program, Washington, DC, 1989.
- Chock, D.P. (1991) "A comparison of numerical methods for solving the advection equation - III," *Atmospheric Environment*, 25A, 853-871.

- Choi, U.J. and D.Y. Kwak (1989). Almost Sure Convergence of Galerkin Approximations for A Heat Equation with a Random Initial Condition. *Computers Math. Applic.*, 18, 12, pp. 1057-1063.
- Cipra, B.A. (1991). The Breaking of a Mathematical Curse. *Science*, 251, p. 165.
- Crandall, S.H. (1956). *Engineering Analysis, A Survey of Numerical Procedures*. McGraw-Hill.
- Devroye, L. (1986). *Non-Uniform Random Variate Generation*. Springer-Verlag.
- Dick, E. (1983). Accurate Petrov-Galerkin Methods for Transient Convective Diffusion Problems. *International Journal for Numerical Methods in Engineering*, 19, pp. 1425-1433.
- Doll, J.D. and D.L. Freeman (1986). Randomly Exact Methods. *Science*, 234, pp. 1356-1360.
- Falls, A.H., McRae, G.J. and Seinfeld, J.H. (1979), Sensitivity and Uncertainty of Reaction Mechanism for Photochemical Air Pollution, *International J. Chemical Kinetics*, 11, 1137-1162.
- Fletcher, C.A.J. (1984). *Computational Galerkin Methods*. Springer-Verlag.
- Franklin, J.N. (1965). Numerical Simulation of Stationary and Non-Stationary Gaussian Random Processes. *SIAM Review*, 7, 1, pp. 68-80.
- Georgopoulos, P.G. and Seinfeld, J.H. (1986), Mathematical Modeling of Turbulent Reacting Plumes, Final Report to the California Air Resources Board under Contract A0-044-32, Sacramento, California. (495 pp.).
- Ghanem, R.G. and P.D. Spanos (1991). *Stochastic Finite Elements: A Spectral Approach*. Springer-Verlag.
- Gill, A.E. (1982), "Atmosphere-Ocean Dynamics", Academic Press, San Diego.
- Gery M.W., Whitten G.Z., Killus J.P. and Dodge M.C. (1989), "A photochemical kinetics mechanism for urban and regional scale computer modeling," *Journal of Geophysical Research*, Vol.94 No. D10, 12,925-12,956.
- Gutierrez, R. and M.J. Valderrama (1989). Discussion of Two Procedures for Expanding a Vector-Valued Stochastic Process in an Orthonormal Way. *Linear Algebra and its Applications*, 120, pp. 617-623.
- Halton, J.H. (1960). On the Efficiency of Certain Quasi-Random Sequences of Points in Evaluating Multi-Dimensional Integrals. *Numerische Mathematik*, 2, pp. 84-90.
- Halton, J.H. (1970). A Retrospective and Prospective Survey of the Monte Carlo Method. *SIAM Review*, 12, 1, pp. 1-63.
- Hammersley, J.M. (1960). Monte Carlo Methods for Solving Multivariable Problems. *Annals of the New York Academy of Sciences*, 86, Art. 3, pp. 844-874.

- Harley, R. A., Russell, A. G., McRae G. J., McNair L. A., Winner D. A., Odman M. T., Dabdub D., Cass G. R. and Seinfeld J. H. (1992) "Continued development of a photochemical model and application to the Southern California Air Quality Study (SCAQS) intensive monitoring periods: Phase I," Final report to the Coordinating Research Council.
- Hestveldt E., Hov Ø. and Isaksen I.S.A. (1978), "Quasi-steady-state approximations in air pollution modeling," *Comp. J. Chem. Kinetics*, Vol. 10, 971-994).
- Hindmarsh A.C. (1980), "LSODE and LSODI, Two new initial value ordinary differential equation solvers," *ACM-SIGNUM Newsletter*, Vol. 15, No. 4, 10-11.
- Hopf, E. (1952). *Statistical Hydrodynamics and Functional Calculus. J. Ratl. Mech. Anal.*, 1, pp. 87-123.
- Hov Ø., Zlatev Z., Berkowicz R., Eliassen A. and Prahm L.P. (1989), "Comparison of numerical techniques for use in air pollution models with nonlinear chemical reactions," *Atmospheric Environment* 23, 967-983.
- Jazwinski, A.H. (1970). *Stochastic Processes and Filtering Theory*. Academic Press.
- Kaufman, L. (1975). Algorithm 496 The LZ Algorithm To Solve the Generalized Eigenvalue Problem for Complex Matrices. *ACM Transactions on Mathematical Software*, 1, 3, pp. 271-281.
- Kotulski, Z. and K. Sobczyk (1984). Characteristic Functionals of Randomly Excited Systems. *Physica*, 123A, pp. 261-278.
- Kozin, F. (1986). Some Results on Stability of Stochastic Dynamical Systems. *Probabilistic Engineering Mechanics*, 1, 1, pp. 13-22.
- Kumar, N, Russell, A.G. and McRae et al. (1992) "A Project to Add the CB-IV Chemical Mechanism to CALGRID," Final Report to the California Air Resources Board, Sacramento, California, June (in preparation).
- Kushner, H.J. (1967). *Stochastic Stability and Control*. Academic Press.
- Lamb, R.G. (1983) "Regional Scale (1000km) Model of Photochemical Air Pollution, Part 1. Theoretical Formulation," EPA/600/3-83-085. U.S. Environmental Protection Agency, Research Triangle Park, N.C.
- Lawson, D. R. (1990) "The Southern California Air Quality Study," *J. Air Waste Manage. Assoc.* 40, 156-165.
- Lee. L.C. (1974). Wave Propagation in a Random Medium: a Complete Set of the Moment Equations with Different Wavenumbers. *J. Math. Phy.*, 15, 9.
- Ligon, J.R. and N.R. Amundson (1981). Modelling of Fluidized Bed Reactors - Vi(a); An Isothermal Bed with Stochastic Bubbles. *Chemical Engineering Science*, 36, pp. 653-660.
- Lin, Y.K., F. Kozin, Y.K. Wen, F. Casciati, G.I. Schueller, A. Der Kiureghian, O. Ditlevsen, E.H. Vanmarcke (1986). Methods of Stochastic Structural Dynamics. *Struc. Safety*, 3, pp. 167-194.

- Lin, Y.K. (1967). *Probabilistic Theory of Structural Dynamics*. McGraw-Hill.
- Liu, M-K., Whitney, D.C. and Roth, P.M. (1976), Effects of Atmospheric Parameters on the Concentration of Photochemical Air Pollutants, *J. Applied Meteorology*, 15, 829-835.
- Liu, W.K., T. Belytschko, Mani (1986). Random Field Finite Element. *Int. J. Num. Meth. Eng.*, 23, pp. 1831-1845.
- Lo Dato, V.A. (1973). Stochastic Processes in Heat and Mass Transport. *Probabilistic Methods in Applied Mechanics*. ed. A.T. Bharucha-Reid. Academic Press.
- Lurmann F.W., Carter W.P.L. and Coyner L.A. (1987), "A surrogate species chemical reaction mechanism for urban-scale air quality simulation models, Vol. II-Guidelines for using the mechanism," EPA No. 68-02-4104 Atmospheric Sciences Research Laboratory, Office of Research and Development, U.S. Environmental Protection Agency, Research Triangle Park, N.C.
- Lurmann, F. W., Carter, W. P. L. and Coyner, L. A., (1987) "A surrogate species chemical reaction mechanism for urban-scale air quality simulation models, Vol. II - Guidelines for using the mechanism," Report EPA 68-02-4104, U.S. EPA, Research Triangle Park, NC.
- Luskin, M. and R. Rannacher (1981). On the Smoothing Property of the Galerkin Method for Parabolic Equations. *SIAM J. Numer. Anal.*, 19, 1, pp. 93-113.
- McRae, G.J., Goodin, W.R. and Seinfeld, J.H. (1981) Mathematical Modeling of Photochemical Air Pollution, Final Report to the California Air Resources Board under Contract A5-046-87, Sacramento, California. (661 pp.).
- McRae, G.J., Tilden, J.W. and Seinfeld, J.H. (1982), Global Sensitivity Analysis - A Computational Implementation of the Fourier Amplitude Sensitivity Test (FAST), *Computers and Chemical Engineering*, 6, 15-25.
- McRae, G. J., Goodin, W. R. and Seinfeld, J. H. (1982) "Numerical solutions of the atmospheric diffusion equation for chemically reacting flows," *J. of Comput. Phys.* 45, 1-42.
- McRae, G. J., Goodin, W. R. and Seinfeld, J. H. (1982) "Development of a second generation mathematical model for urban air pollution I - Model formulation," *Atmospheric Environment* 16, 679-696.
- McRae, G. J. and Seinfeld, J. H. (1983) "Development of a second generation mathematical model for urban air pollution II - Model evaluation," *Atmospheric Environment* 17, 501-522.
- Mead, R. and D.J. Pike (1975). A Review of Response Surface Methodology from a Biometric Viewpoint. *Biometrics*, 31, pp. 803-851.
- Mihail, R., L. Ionita, S. Straja (1989). A Stochastic Approach to the Diffusion Equation. *Atmosph. Environ.*, 23, 1, pp. 123-125.

- Milford, J.B., Gao, D., Russell, A.G. and McRae, G.J. (1992), "Use of Sensitivity Analysis to Compare Chemical Mechanisms for Air Quality Modeling, (In press, Environmental Science and Technology).
- Nawrocki, P.J. and Papa, R. (1963), "Atmospheric Processes," Prentice Hall, Inc. Englewood Cliffs, New Jersey.
- Niederreiter, H. (1978). Quasi Monte Carlo Methods and Pseudo-Random Numbers. *Bulletin of the American Mathematical Society*, 84, 6, pp. 957-1041.
- Ochi, M.K. (1986). Non-Gaussian Random Processes in Ocean Engineering. *Probabilistic Engineering Mechanics*, 1, 1, pp. 28-39.
- Odman M.T. and Russell A.G. (1991a), "A multiscale finite element pollutant transport scheme for urban and regional modeling," *Atmospheric Environment*, in press.
- Odman M.T. and Russell A.G. (1991a), "Multiscale modeling of transport and chemistry," *J. Geophys. Research*, in press.
- Odman M.T. Kumar N. and Russell A.G. (1991b), "A comparison of fast chemical kinetic solvers," *Atmospheric Environment*, in press.
- Odman, M. T. and Russell A. G. (1991) "A multiscale finite element pollutant transport scheme for urban and regional modeling," *Atmospheric Environment* 25A, 2385-2394.
- Odman, M. T. and Russell A. G. (1991) "Multiscale modeling of pollutant transport and chemistry," *J. Geophys. Res.* 96, 7363-7370.
- Odman, M. T. and Russell A. G. (1992) "On local finite element refinements in multiscale air quality modeling," submitted.
- Odman, M. T. and Russell A. G. (1992) "A nonlinear filtering algorithm for multi-dimensional finite element pollutant advection schemes," *Atmospheric Environment*, in press.
- Papoulis, A. (1991). *Probability, Random Variables, and Stochastic Processes*. McGraw-Hill.
- Pleim, J. E., Chang, J. S. and Zhang, K. (1991) "A nested grid mesoscale atmospheric chemistry model," *J. Geophys. Res.* 96, 3065-3084.
- Press, W.H. et al. (1988). *Numerical Recipes in C: The Art of Scientific Computing*.
- Rao, S. T., Sistla, G., Ku, J. Y., Schere K., Scheffe, R. and Godowitch, J. (1989) "Nested grid modeling approach for assessing urban ozone air quality," Paper 89-42A.2 presented to Air and Waste Management Association, Pittsburgh, PA.
- J.R. Rice (1983). *Numerical Methods, Software, and Analysis*. McGraw-Hill.
- Riganti, R. (1987). On a Class of Nonlinear Dynamical Systems: The Structure of a Differential Operator in the Application of the Decomposition Method. *Journal of Mathematical Analysis and Applications*, 124, pp. 189-199.

- Roache, P.J. (1976), *Computational Fluid Dynamics*, Hermosa Publishers, Albuquerque, New Mexico.
- Rubinstein, R.Y. (1981). *Simulation and the Monte Carlo Method*. John Wiley and Sons.
- Russell, A. G. and Odman, M. T. (1992) "Future directions in photochemical air quality modeling," *Water, Air, and Soil Pollution*, in press.
- Scire J.S., Yamartino R.J., Carmichael G.R., Chang Y.S. (1989), "CALGRID: a mesoscale photochemical grid model," Volume II: User's Guide Appendices," Report No. A049-2 prepared for California Air Resources Board under contract Number A6-215-74.
- Segall, A. and T. Kailath (1976). Orthogonal Functionals of Independent-Increment Processes. *IEEE Transc. Info. Theo.* IT-22, 3, pp. 287-298.
- Serrano, S.E. (1989). A New Approach in Modelling Groundwater Pollution Under Uncertainty. *Prob. Eng. Mech.*, 4, 2, pp. 85-98.
- Serrano, S.E. (1990). Using the C Language To Approximate Non-Linear Stochastic Systems. *Adv. Eng. Software*, 12, 2, pp. 59-68.
- Soong, T.T. and C.G. Pfeiffer (1966). Unified Guidance Analysis in Design of Space Trajectories. *J. Spacecr. Rockets*, 3, pp. 98-103.
- Soong, T.T. (1973). *Random Differential Equations in Science and Engineering*. Academic Press.
- Strikwerda, J.C. (1989), *Finite Difference Schemes and Partial Differential Equations*, Wadsworth and Brooks/Cole, Pacid Grove, California.
- Takada, T. (1990). Weighted Integral Method in Stochastic Finite Element Analysis. *Prob. Eng. Mech.*, 5, 3, pp. 146-156.
- Takada, T. (1990). Weighted Integral Method in Multi-Dimensional Stochastic Finite Element Analysis. *Prob. Eng. Mech.*, 5, 4, pp. 158-166.
- Tasaka, S. (1981). Stability Analysis of a Finite Element Scheme for the Heat Equation with a Random Initial Condition. *Computer Methods in Applied Mechanics and Engineering*
- Tasaka, S. (1983). Convergence of Statistical Finite Element Solutions of the Heat Equation with a Random Initial Condition. *Computer Methods in Applied Mechanics and Engineering*, 39, pp. 131-136.
- Tennekes, H.A. and Lumley, J.L. (1972), *A First Course in Turbulence*, The MIT Press, Cambridge.
- Tilden, J.W., Costanza, V., McRae, G.J. and Seinfeld, J.H. (1981), Sensitivity Analysis of Chemically Reacting Systems, in Springer Series in Chemical Physics, 18, eds. Ebert, K.H., Deuflhard, P. and Jager, W., Springer Verlag, 389 pp.

- Traina, M.I., R.K. Miller, S.F. Masri (1986). Orthogonal Decomposition and Transmission of Nonstationary Random Processes. *Prob. Eng. Mech.*, 1, 3, pp. 136-149.
- Trim, A.D. (1989). Estimation of Density Functions and Upcrossing-Rates from Samples. *Probabilistic Engineering Mechanics*, 4, 4, pp. 191-202.
- Valderrama, M.J. (1991). Stochastic Signal Analysis: Numerical Representation and Applications to System Theory. *Applied Stochastic Model and Data Analysis*, 7, pp. 93-106.
- Villadsen, J. and M.L. Michelsen (1978). *Solution of Differential Equation Models by Polynomial Approximation*. Prentice-Hall.
- White, B. (1989), *Programming Techniques for Software Development*, Van Nostrand Reinhold, New York.
- Wozniakowsky, H. (1991). Average Case Complexity of Multivariate Integration. *Bull. Amer. Math. Soc.*, 24, 1, pp. 185-194.
- Yadrenko, M.I. (1983). *Spectral Theory of Random Fields*. Springer-Verlag.
- Yaglom, A.M. (1987). *Correlation Theory of Stationary and Related Random Functions Volume I: Basic Results*. Springer-Verlag.
- Yakowitz, S.J. (1977). *Computational Probability and Simulation*. Addison-Wesley.
- Yamartino R.J., Scire J.S., Hanna S.R., Carmichael G.R., Chang Y.S. (1989), "CALGRID: a mesoscale photochemical grid model," Report No. A049-1 prepared for California Air Resources Board under contract Number A6-215-74.
- Yamartino R.J., Scire J.S., Carmichael G.R., Chang Y.S. (1992), "The CALGRID Mesoscale Photochemical Grid Model - I. Model Formulation," *Atmospheric Environment*, 26A(8), 1493-1512.
- Yang, Y.K. and R.K. Kapania (1984). Finite Element Random Response Analysis of Cooling Tower. *J. Eng. Mech., ASCE*, 10, EM4, pp. 589-609.
- Young T.R. and Boris J.P. (1977), "A numerical technique for solving stiff ordinary differential equations associated with the chemical kinetics of reactive flow problems," *J. Phys. Chem.* 81, 2424-2427.
- Yourdon, E. (1989), *Structured Walkthroughs*, Yourdon Press, Prentice Hall, Englewood Cliffs, New Jersey.
- Zhuo, Z. et al. (1991). Polychotomous Multivariate Models for Coronary Heart Disease Simulations III. Model Sensitivities and Risk Factor Interventions. *Int. J. Biomed. Comput.*, 28, pp. 205-220.

## **Appendix A**

### **A Comparison of Fast Chemical Kinetics Solvers for Air Quality Modeling**

**Odman, M.T., Kumar, N. and Russell, A.G., (1992)  
*Atmospheric Environment*, 26A, 1783-1789**

# TECHNICAL NOTE

## A COMPARISON OF FAST CHEMICAL KINETIC SOLVERS FOR AIR QUALITY MODELING

MEHMET T. ODMAN, NARESH KUMAR AND ARMISTEAD G. RUSSELL

Department of Mechanical Engineering, Carnegie Mellon University, Pittsburgh, PA 15213, U.S.A.

**Abstract** - Two methods for solving stiff systems of ordinary differential equations describing nonlinear chemical kinetics in air quality models, namely the hybrid and the quasi-steady state approximation (QSSA) schemes, are compared with respect to their accuracy and computational speed. Their implementation for parallel and vector processing computers is discussed. Tests are conducted using two different photochemical mechanisms. Also, a new test problem is developed to represent various degrees of stiffness encountered in urban and regional air quality simulations. It is concluded that the hybrid scheme is more accurate than the QSSA scheme. Different techniques are considered to eliminate mass conservation errors and make the solutions more accurate. As for the computational efficiency, QSSA scheme is approximately two to four times faster than the hybrid scheme.

**Key word index:** chemical modeling, photochemical kinetics, photochemical mechanism, stiff ordinary differential equations.

### 1. INTRODUCTION

The photochemical reaction mechanisms used in urban and regional air quality models are usually designed to follow 20 to 100 pollutant species. The equations describing the interactions between these pollutants are coupled, nonlinear ordinary differential equations. The spatial dependence in air quality models requires the solution of this system of equations at thousands of points in space. Typical simulations spread over several days and the system may become extremely stiff depending on the time of the day. When solving stiff systems, temporal scales must be kept very small to avoid numerical instabilities. Even with condensed reaction mechanisms, the numerical treatment of chemical kinetics takes approximately 80 to 90% of the total computation time in current photochemical air quality models.

Given the computational intensity of solving the chemical dynamics, the numerical algorithms must be very efficient to ensure valid results in a reasonable amount of time, without sacrificing accuracy. Classical algorithms can be prohibitive to current computers. In this study, two of the most widely used fast photochemical kinetic solvers are compared for accuracy and speed to ascertain their reliability and effectiveness for use in air quality models.

### 2. DESCRIPTION OF FAST CHEMICAL KINETIC SOLVERS

Given a set of initial concentrations for  $N$  pollutants and a mechanism describing how these pollutants react chemically, the problem of following the photochemical kinetics can be cast into the following form

$$\frac{dc_i}{dt} = F_i(c_1, c_2, \dots, c_N) - L_i(c_1, c_2, \dots, c_N)c_i \quad (1)$$

where  $c_i$  is the concentration of species  $i$ , and  $F_i$  and  $L_i c_i$  are its production and loss rates respectively. Equation (1) is a set of coupled, nonlinear ordinary differential equations. This system displays numerical stiffness due to large differences in the reaction rates of different species in a typical photochemical mechanism.

Classical methods for solving stiff systems are subject to very small step size limits. Gear's method with automatic step and error control can provide solutions of high accuracy. However, in photochemical models where 20 to 100 pollutants are being followed inversion of large matrices or solution of large sets of nonlinear equations repeatedly at thousands of grid points may become restrictive. Therefore, Gear's method is not practical to use in air quality models.

Fast solvers are techniques that do not require time consuming matrix inversions to solve equation (1). Table 1 lists the solvers used in various urban and regional air quality models. Here, the hybrid [Young and Boris, 1977] and the Quasi Steady State Approximation (QSSA) schemes [Hesswede *et al.*, 1978] will be discussed. It should be noted that, if  $F_i$  and  $L_i$  were constants, Equation (1) could be solved analytically as

TABLE 1. Chemical Kinetic Solvers Used in Air Quality Models.

Air Quality Model	Chemical Solver	Reference
CALGRID	Hybrid & QSSA	Yamartino <i>et al.</i> , 1989
CIT	Hybrid	McRae <i>et al.</i> , 1982
RADM	QSSA	Chang <i>et al.</i> , 1987
ROM	QSSA	Lamb, 1983
Sillman&Logan	Conventional	Sillman <i>et al.</i> , 1990
STEM	QSSA	Carmichael <i>et al.</i> , 1986
UAM	Conventional	Morris & Myers, 1990

$$c_i(t) = F_i \tau_i + [c_i(0) - F_i \tau_i] e^{-t/\tau_i} \quad (2)$$

where  $\tau_i$ , the reciprocal of  $L_i$ , is the characteristic time for the decay of species  $i$ . Both methods use certain characteristics of the solution in Equation (2) for fast and accurate integration.

### 2.1 Hybrid Scheme

The hybrid scheme predetermines the time step such that none of the variables will change by more than a prescribed amount. Then, it classifies the equations as stiff or non-stiff based on the step size to characteristic time ratio. If the time step,  $\Delta t$ , is larger than the equilibration time,  $\tau_i$ , the equation is identified as stiff. The non-stiff equations are integrated with the following predictor-multi-corrector algorithm:

Predictor:

$$c_i^n = c_i^* + \Delta t (F_i^n - c_i^* / \tau_i^n), \quad (3a)$$

Corrector:

$$c_i^{n+1} = c_i^n + \Delta t (F_i^n - c_i^n / \tau_i^n + F_i^* - c_i^* / \tau_i^*) / 2, \quad (3b)$$

where superscript  $n$  refers to time  $t$ ,  $n+1$  to time  $t + \Delta t$  and  $*$  to the predicted solution. Stiff equations are integrated with the more accurate asymptotic formula:

Predictor:

$$c_i^n = \frac{c_i^* (2\tau_i^n - \Delta t) + 2F_i^n \tau_i^n \Delta t}{2\tau_i^n + \Delta t}, \quad (4a)$$

Corrector:

$$c_i^{n+1} = \frac{c_i^n (\tau_i^n + \tau_i^* - \Delta t) + \Delta t (F_i^n + F_i^*) (\tau_i^n + \tau_i^*) / 2}{\tau_i^n + \tau_i^* + \Delta t}, \quad (4b)$$

It is this formula that maintains high accuracy for stiff components without restrictive time step requirements, and damps out oscillations that may lead to instabilities. Convergence of each class of equations is ascertained by comparing the concentrations after successive iterations.

When a stiff equation is far from equilibrium, the time step should be less than or comparable to the equilibration time to ensure that the transition to equilibrium can be followed accurately. However, when it is close to equilibrium, the changes in  $c_i$  over the time step will be small though the adjustment rate toward equilibrium can be much shorter than the time step. After readjustment, much longer time steps can be taken. The method takes full advantage of this fact, which furthers efficiency, particularly for rapidly reacting species, because their readjustment takes place faster.

Some rapidly reacting components in the mechanism may be identified, before hand, as steady state species. Since the transients associated with these components decay almost instantaneously to their equilibrium values, they may be eliminated from the computations of the hybrid scheme above, leaving behind a less stiff system,

and their concentrations are calculated based on the assumption of equilibrium:

$$c_i = F_i \tau_i. \quad (5)$$

This treatment may considerably increase computational efficiency, especially, for photochemical mechanisms with large number of species.

### 2.2 Quasi-Steady State Approximation (QSSA) Scheme

In the QSSA method, depending on the time step to characteristic time ratio, the following explicit formulas are used for calculating the concentrations:

$$c_i^{n+1} = F_i^n \tau_i^n, \quad \Delta t / \tau_i^n > 10 \quad (6a)$$

$$c_i^{n+1} = F_i^n \tau_i^n + (c_i^n - F_i^n \tau_i^n) e^{-\Delta t / \tau_i^n}, \quad 0.01 < \Delta t / \tau_i^n < 10 \quad (6b)$$

$$c_i^{n+1} = c_i^n + \Delta t (F_i^n - c_i^n / \tau_i^n), \quad \Delta t / \tau_i^n < 0.01 \quad (6c)$$

The exponential solution of Equation (6b) is exact under the assumptions of constant  $F_i$  and  $L_i$ . Solutions of Equations (6a) and (6c) are used to improve efficiency. In parallel processing, or when microprocessors that can rapidly evaluate exponential functions are present, the accuracy of QSSA method may be improved by eliminating these less accurate, simple formulas.

For species with  $\Delta t / \tau_i > 10$ , calculating  $c_i$  based on the steady state assumption of Equation (6a) introduces an error less than  $4.5 \times 10^{-3}\%$  relative to the exponential formula in Equation (6b). The simple Euler integration formula in Equation (6c) introduces an error of  $(\Delta t / \tau_i)^2 / 2$ , i.e., less than  $5.0 \times 10^{-3}\%$  when  $\Delta t / \tau_i < 0.01$ . Here, to improve efficiency, the scheme was modified by introducing the asymptotic formula:

$$c_i^{n+1} = \frac{c_i^n (2\tau_i^n - \Delta t) + 2F_i^n \tau_i^n \Delta t}{2\tau_i^n + \Delta t}, \quad 0.01 < \frac{\Delta t}{\tau_i^n} < 0.085. \quad (7)$$

The error introduced by this asymptotic approximation is  $(\Delta t / \tau_i)^3 / 12$ , therefore, the same magnitude of error as in the equilibrium and Euler formulas ( $5.0 \times 10^{-3}\%$ ) is obtained by setting the upper limit for  $\Delta t / \tau_i$  to 0.085.

The QSSA method employs a predetermined time step that is kept constant throughout. There is no mechanism to adjust the time step using the convergence information as feedback. Therefore, accuracy and stability of the method are highly dependent on the choice of the time step. *Hesstvedt et al.* [1978], from experience, suggest that a 30 sec time step would be appropriate throughout most simulations of photochemical air pollution.

### 2.3 Mass Conservation Techniques

Conservation of chemical balance is a very important characteristic required from kinetic solvers, however, neither of the methods described above is strictly mass conservative. The hybrid scheme has a built in feature of reducing the step size if convergence cannot be achieved. This feature can be further exploited to keep the conservation errors within tolerable limits. With the QSSA scheme, the errors are more pronounced and may

even lead to instabilities. One way of dealing with this problem is to decrease the step size. However, this solution may not always be desirable, especially when efficiency is of primary concern.

Two techniques that maintain chemical balance without adjusting the time step will be considered here. The first one eliminates strong couplings between species by lumping them together in new variables. The conservation error during the time step from  $n$  to  $n+1$  is estimated as

$$\text{error} = \sum_{i=1}^M [c_i^{n+1} - c_i - \Delta t (F_i - c_i / \tau_i)] \quad (8)$$

where  $M$  denotes the number of species being lumped. *Hesswold et al.* [1978] suggest that conservation errors originate mainly from the prediction of  $\text{NO}_x$  ( $\text{NO}$  and  $\text{NO}_2$ ) concentrations. To maintain nitrogen balance, all the nitrogen oxides are lumped together and the estimated error is subtracted from  $\text{NO}_2$  concentration. When the system runs out of  $\text{NO}_2$ ,  $\text{NO}$  is used to maintain the balance.

The second technique, restores the balance by redistributing the conservation errors proportionally among various species in a mass-conserving manner. The concentrations at time  $n+1$  are corrected as:

$$[c_i^{n+1}]_{\text{corrected}} = c_i^{n+1} \frac{\sum_{k=1}^M c_k^{n+1}}{\sum_{k=1}^M c_k} \quad (9)$$

where  $M$  denotes the number of species whose concentrations are being corrected. The major fault with both techniques is that a portion of the errors is incorporated into concentrations from which the errors may not have arisen. Because they use linear operators, both techniques are computationally very efficient.

### 3. NUMERICAL TESTS AND RESULTS

The performance of fast solvers described above is evaluated using two common photochemical mechanisms for urban and regional modeling. The first mechanism, referred to as LCC here, is the SAPRC/ERT condensed chemical mechanism developed by *Lurmann et al.* [1987]. There are 95 reactions and 36 species in this mechanism. The second one is the carbon bond mechanism, CB4, as given by *Gery et al.* [1989]. It has 81 reactions and 32 species. These mechanisms differ in lumping procedures used to limit the number of species and reactions. The LCC mechanism groups similar organics in lumped molecules, while the CB4 uses grouping according to the number and type of carbon bonds. A comparison of the predictions from these two mechanisms can be found in *Milford et al.* [1991] and *Dodge* [1989]. It is also important to note that in hybrid scheme solutions here, some species were explicitly assumed to be in equilibrium with others. There are 9 such species in the LCC mechanism: OH, O(3P), O(1D), two general  $\text{RO}_2$ 's, alkyl nitrate  $\text{RO}_2$ , phenol  $\text{RO}_2$ , benzaldehyde N- $\text{RO}_2$  and the phenoxy radical. In the CB4 mechanism there are only 4 steady state species: OH, O(3P), O(1D) and the NO to nitrate

operation that eliminates most peroxy radicals by substituting the specific organic products they form during NO to nitrate formation.

The accuracy of predictions will be evaluated in comparisons to the solution from Gear's method. The Gear solver used here is the Livermore Solver for Ordinary Differential Equations (LSODE) with automatic method switching for stiff and non-stiff problems [*Hindmarsh*, 1980]. The estimated local error in concentration  $c_i$ , is controlled by two input parameters, relative (RTOL) and absolute (ATOL) tolerances, in the form

$$\text{error} = \text{RTOL} \cdot c_i + \text{ATOL} \quad (10)$$

In all problems here, the values of RTOL and ATOL are set to  $10^{-3}$  and  $10^{-9}$  respectively. Also, no explicit steady state assumptions are made in any of the LSODE solutions.

Efficiency comparisons are based on CPU times spent in scalar and vector processing modes of a CRAY YMP/832 computer. In scalar mode, both methods were tested in their original form: the code for hybrid scheme was obtained from *McRae et al.* [1982] and QSSA from *Yamartino et al.* [1989]. For testing in vector processing mode, significant effort was spent for code optimization [*Pacific-Sierra Research Corp.*, 1989]. The first two test problems are simple problems that give important accuracy information. A third test problem was designed to test the performance on a vector processing computer over a wide range of atmospheric conditions.

#### 3.1 Accuracy Test with LCC Mechanism

The sample problem given by *Lurmann et al.* [1987] was used as the test case with the LCC mechanism. In this problem, photolytic reaction rates are calculated at a constant solar zenith angle of  $0^\circ$  and the temperature is kept constant at 298 K. The initial concentrations of the species are given in Table 2. There are no emissions or deposition. All integrators, including LSODE, are called at 5 min intervals. The solution obtained from LSODE after 8 hrs of simulation and the relative percentage errors of hybrid and QSSA solutions are shown in Table 3.

TABLE 2. Initial Concentrations for LCC Test Case.

Species	Concentration (ppm)
NO	7.50E-02
NO <sub>2</sub>	2.50E-02
O <sub>3</sub>	1.00E-05
CO	1.00E+00
HCHO	3.00E-02
ALD2	1.00E-02
ALKA	8.27E-02
ETHE	1.50E-02
ALKE	2.94E-02
TOLU	2.29E-02
AROM	1.19E-02
H <sub>2</sub> O	2.00E+04

TABLE 3. LCC Test Case Solution and % Errors in Concentrations.

Species	LSODE (ppm)	Hybrid	QSSA	Hybrid NO <sub>x</sub>	QSSA NO <sub>x</sub>	Hybrid Prop.	QSSA Prop.
NO	9.43E-05	1.5	98.4	0.5	5.2	0.0	14.1
NO <sub>2</sub>	2.16E-03	2.7	104.9	0.0	0.9	0.1	14.7
O <sub>3</sub>	3.06E-01	1.5	11.6	0.6	6.6	0.2	2.7
N <sub>2</sub> O <sub>5</sub>	3.41E-06	8.0	338.3	0.9	9.3	0.8	37.3
ALKE	3.52E-10	14.1	3.8	15.3	365.0	1.5	49.8
OH	2.84E-07	2.5	41.0	0.6	4.4	0.5	11.4
Total N	1.00E-01	3.7	36.1	0.1	0.0	0.1	0.0

The hybrid scheme predicted the NO<sub>x</sub> and O<sub>3</sub> concentrations within 3%. The total nitrogen mass in the system increased by 4%. The largest error observed was 14% in predicted concentration of alkenes. When nitrogen balance is enforced, either with NO<sub>x</sub> lumping or proportional distribution operator, all errors dropped sharply. The technique of proportional distribution of errors among nitrogen containing species works better for the hybrid scheme. The non-conservative nature of the QSSA scheme led to very large errors. The total nitrogen in the system increased by 36%. This result shows that QSSA must be used with a mass conservative linear operator. NO<sub>x</sub> lumping proved more favorable than proportional distribution for the QSSA scheme.

The errors in the QSSA solution originate mostly from inaccuracies in predicting the NO<sub>x</sub> concentrations. Distribution of these errors to other species activates other error components. Since no convergence check is carried in the QSSA, these errors are free to grow. More accurate results are obtained if errors are eliminated where they are generated, thus with NO<sub>x</sub> lumping. On the other hand, the hybrid scheme, because of its ability to keep the errors under a preset value with its convergence

checks and its predictor-multi-corrector nature, does not allow components of the error to grow as rapidly. Distributing the errors has a better eliminative effect in the hybrid scheme. The NO<sub>x</sub> lumped QSSA predicted the concentrations of most species within 10% except alkene concentration that changed by 8 orders of magnitude during this test problem.

When compared for efficiency, QSSA ran approximately twice as fast as the hybrid scheme. It should be remembered that the solar zenith angle is held constant, therefore, the problem is free from excessive stiffness during the sunrise or sunset periods, where the hybrid scheme runs much slower. QSSA would run with the same speed during these periods because the time step is predetermined (30 sec). Both schemes ran much faster than LSODE, the hybrid scheme approximately 5 times and QSSA approximately 10 times. Mass conservation techniques increased the CPU time by only a small fraction.

Two more issues were investigated with the QSSA scheme. First, *Hesswedi et al.* [1978] suggest that no species be specified at steady state for improved accuracy. Figure 1 shows the NO<sub>x</sub> and O<sub>3</sub> concentrations

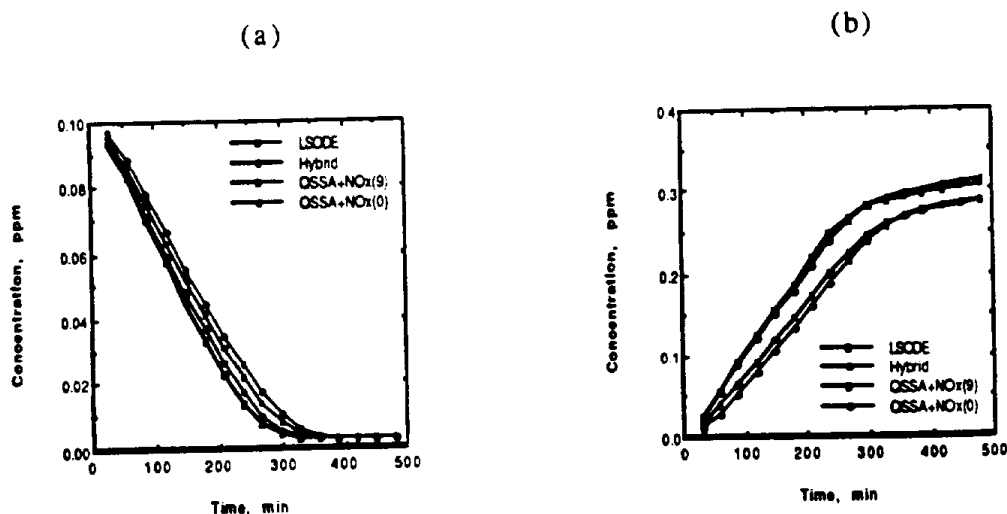


Fig. 1. Comparison of QSSA scheme predictions with and without pseudo-steady state approximations to LSODE and hybrid predictions: a) NO<sub>x</sub>, b) O<sub>3</sub>.

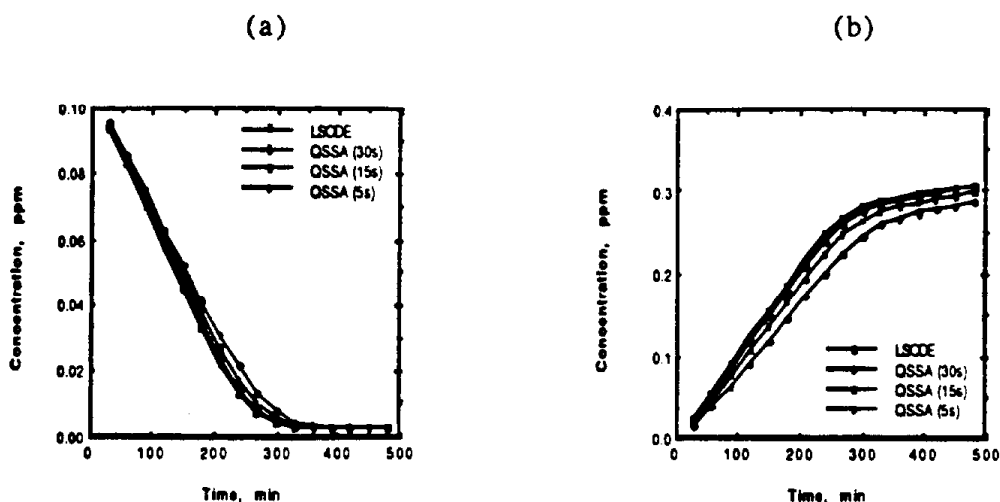


Fig. 2. Comparison of QSSA scheme with different time steps to LSODE predictions: a) NO<sub>x</sub>, b) O<sub>3</sub>.

predicted by the QSSA schemes with and without explicit steady state assumption. In contrast to their suggestion, the solution that assumed 9 species were in equilibrium with the others is more accurate. Also, the pseudo-steady state assumption makes the scheme faster because 9 species are eliminated from the process of selecting the formula to use in Equation (6). The second issue is the sensitivity of the QSSA solution to the predetermined time step. The time step was changed to 15 sec and 5 sec respectively and the results are shown in Figure 2. The effect of decreasing the time step is an increase in accuracy. The 5 sec time step solution is as accurate as the hybrid scheme solution in Figure 1, however, with this time step, QSSA scheme consumes 50% more time than the hybrid scheme.

Though the non-conservation of the nitrogen mass is, possibly, important, the accuracy of the hybrid scheme with no mass conserving operators is better than the QSSA and sufficient for use in current air quality models. On the other hand, the QSSA scheme with 30 sec predetermined time step is faster than the hybrid scheme. But, if the accuracy of the QSSA scheme is increased by decreasing the time step, it becomes less efficient than the hybrid scheme.

### 3.2 Accuracy Test with CB4 Mechanism

This test case uses varying photolysis rates for a location at 32° N and 80° W starting on June 4, at 8 pm and updates them every 15 minutes. The input parameters are depicted in Table 4. The temperature is held constant at 300 K. Since this problem is not a standard test case, the solutions were first compared to the solutions from OZIPR model [Hogo and Gery., 1988] for code validation. All integrators are called at 15 min intervals. The solution from LSODE after 10 hrs of simulation and relative errors of the hybrid and QSSA schemes are shown in Table 5.

The results are similar to the previous test. The hybrid scheme is more accurate even without any linear conservative operators. NO<sub>x</sub>-lumping performs better with QSSA scheme than the proportional distribution of errors among all nitrogen containing species. The carbon balance was also monitored in this problem.

Both schemes conserved the total mass of carbon within 1%. LSODE for this test is extremely slow: QSSA and hybrid schemes are respectively 20 and 40 times faster. This is due to the added stiffness by changing photolysis rates. However, since there is no sunset or sunrise periods in the problem, the speed difference between the hybrid and QSSA schemes is still the same.

### 3.3 Air Pollution Scenario for Efficiency Tests on Vector Processors

A 3-day episode, with photolysis values reflecting a start on March 21 at 12:00 am in Los Angeles, was designed as a test case to evaluate the efficiency of fast solvers on vector processing computers. The LCC mechanism was used in this test case with initial parameters as given in Table 2. The temperature was held constant at 298 K. ROG emissions of 14.4 ppm carbon per day were introduced in the problem. The base case ROG emissions distribution given by Russell *et al.*

TABLE 4. Initial Concentrations for CB4 Test Case.

Species	Concentration (ppm)
NO	5.00E-02
NO <sub>2</sub>	2.00E-02
HONO	1.00E-03
CO	3.00E-01
FORM	1.00E-02
ALD2	1.00E-02
MGLY	1.00E-02
PAR	5.00E-01
ETH	5.00E-02
OLE	5.00E-02
TOL	2.00E-02
XYL	2.00E-02
ISOP	5.00E-02
H <sub>2</sub> O	1.70E+04

TABLE 5. CB4 Test Case Solution and % Errors in Concentrations.

Species	LSODE (ppm)	Hybrid	QSSA	Hybrid NO <sub>x</sub>	QSSA NO <sub>x</sub>	Hybrid Prop.	QSSA Prop.
NO	4.39E-05	2.3	5.9	0.5	1.3	2.3	6.9
NO <sub>2</sub>	4.55E-03	1.9	37.3	0.7	2.9	2.3	1.0
O <sub>3</sub>	4.22E-01	0.2	33.1	0.2	2.3	0.2	9.7
N <sub>2</sub> O <sub>5</sub>	2.68E-05	3.2	147.6	1.5	8.4	4.3	13.4
ISOP	3.55E-11	7.3	100.0	5.7	48.0	3.0	95.5
OH	5.42E-08	0.4	41.3	0.0	0.3	0.0	11.0
Total N	1.00E-01	0.5	49.8	0.0	0.0	0.0	0.0
Total C	2.05E+00	0.0	0.3	0.0	0.3	0.0	1.3

[1991] were used to calculate the emissions shown in Table 6. NO<sub>x</sub> emissions were introduced to make the ground level ROG/NO<sub>x</sub> emission ratio equal to 20:1. Keeping the same ROG emissions and increasing the NO<sub>x</sub> emissions, 9 more vertical levels were added so that the ROG/NO<sub>x</sub> ratio is decreased by 2 at each level, to an upper level ROG/NO<sub>x</sub> emission ratio of 2:1. This range of input parameters covers most ROG/NO<sub>x</sub> ratios encountered in urban atmospheres. To illustrate the stiffness and the range of conditions of the test problem, the O<sub>3</sub> concentration at noon is plotted, in Figure 3, for

TABLE 6. Test Case ROG Emissions.

Species	Emissions (ppm / min)
CO	2.908E-02
HCHO	4.996E-05
Higher aldehydes	5.662E-05
Alkanes	1.205E-03
Alkenes	2.308E-04
Aromatics	6.650E-05
Ethene	5.303E-05
Toluene	1.780E-04

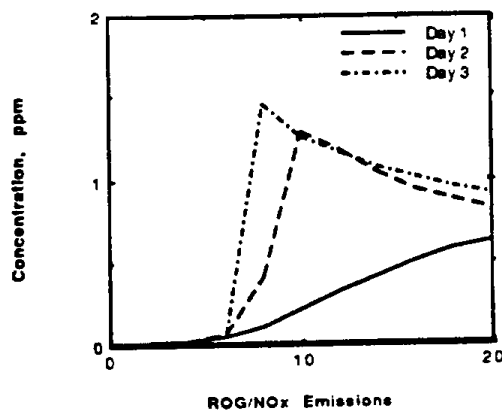


Fig. 3. Ozone concentrations at noon.

the three day simulation.

As mentioned before, if the time step taken by the QSSA scheme is too long, strong couplings between species in photochemical mechanisms may cause severe instability problems. In this test, the time step for the QSSA scheme is equal to 1 min for nighttime, 30 sec for daytime and 12 sec during sunrise and sunset (Shieh *et al.*, 198). An instability problem was encountered when the ROG/NO<sub>x</sub> emission ratio was 20:1. This led to an ROG/NO<sub>x</sub> ratio on the third day of about 300. Though this ratio is unlikely to occur in urban atmospheres, this finding is still interesting to emphasize potential limitations of the current algorithm. It was observed that, in the late afternoon of the first day of simulation, the coupling of NO<sub>2</sub> with NO, N<sub>2</sub>O<sub>5</sub>, HNO<sub>4</sub> and peroxy acetyl nitrate (PAN), and the coupling between N<sub>2</sub>O<sub>5</sub> and NO<sub>3</sub> were the major causes of instability. The nitrogen oxide lumping of section 2.3 breaks the first coupling. To break the second coupling, N<sub>2</sub>O<sub>5</sub> and NO<sub>3</sub> were lumped in a single variable and the concentration was calculated using Equation (6c). In the late afternoon of the second day of simulations, the coupling between HNO<sub>4</sub> and HO<sub>2</sub>, and finally, around the same time in the third day, the coupling between PAN and MCO<sub>3</sub> became equally strong and led to instabilities. Similar lumping techniques were used to break these couplings. It is also important to note that the proportional distribution operator is also very effective in breaking these couplings. When it is used with the QSSA scheme, no instabilities were observed. Another solution is, of course, to decrease the time step (e.g., to 15 sec).

An error analysis is performed on the hybrid and QSSA solutions using the LSODE solution as a reference. Root mean square (RMS) errors were calculated for different species at each level as

$$\text{rms error} = \sqrt{\frac{1}{N} \sum_{i=1}^N [c_i - c_i^L]^2} \quad (11)$$

where,  $c_i^L$  is the solution from LSODE and  $N$  is the number of sampling points. For each solution, sampling was performed at 6 hrs intervals, thus  $N$  is equal to 12. Over a wide range of ROG/NO<sub>x</sub> emission ratios, it is observed that the hybrid scheme showed little improvement in accuracy when mass conservation was enforced. The QSSA scheme on the other hand performs the best when NO<sub>x</sub> lumping is used. For most species, the RMS errors for QSSA with NO<sub>x</sub> lumping

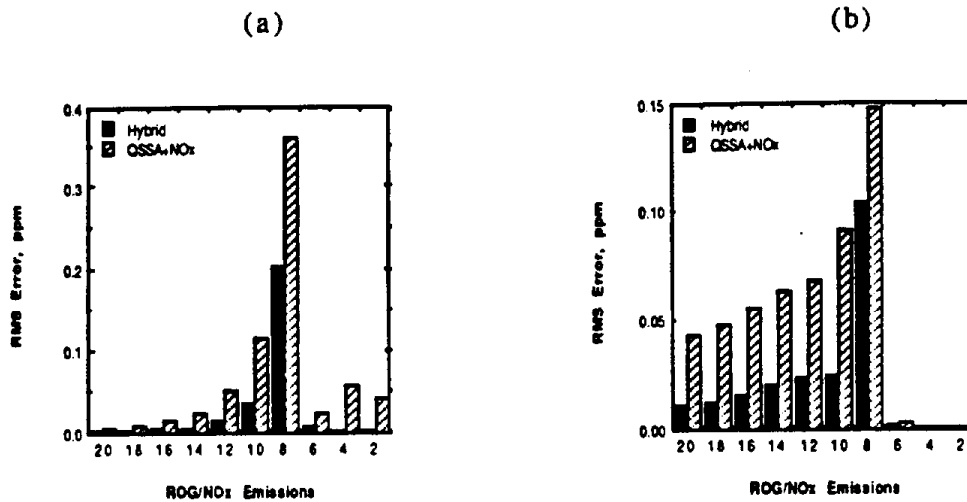


Fig. 4. RMS errors produced by hybrid and QSSA with NO<sub>x</sub> lumping schemes at various ROG/NO<sub>x</sub> emissions ratios: a) NO<sub>x</sub>, b) O<sub>3</sub>.

were approximately twice as large as those for the hybrid scheme. The RMS errors in predicting NO<sub>x</sub> and O<sub>3</sub> using various solvers at different levels are shown in Figure 4. These errors were found to be highest at the level where the ROG/NO<sub>x</sub> emissions ratio is 8:1, which is near that found for many urban areas. The NO<sub>x</sub> and O<sub>3</sub> solutions from the hybrid and QSSA with NO<sub>x</sub> lumping schemes are compared to LSODE solutions at this level in Figure 5. Deviations are not always as large at other ROG/NO<sub>x</sub> emissions ratios where the slopes of the concentration curves are not changing as rapidly.

To get an idea of what kind of speed-up can be expected from the vectorization of these fast solvers, run time tests were conducted on a CRAY YMP computer, using the flowtracing facility. CPU times are shown in Table 7. These values are averaged over several measurements. In scalar mode, 50 - 55% of the total CPU time is spent in calculating the production and loss rates.

Unfortunately, this process is not readily vectorizable. The scheme that requires fewer updates of these rates will apparently run much faster in either mode. During the simulations, QSSA called the production and loss updating routine approximately 4 times less than the hybrid scheme. Simply for this reason, QSSA is about 4 times faster than the hybrid scheme. It is more interesting to note the vector speedups of the integration parts. Integration in the hybrid scheme improved approximately by a factor of 3 in vector mode while the same portion of QSSA ran about twice faster. The number of species in the mechanism determines how many times the innermost loops are executed. For both mechanisms, this number (~30) was far from the number of vector memory banks of the CRAY YMP computer which is 128. In other words it is possible to obtain better vector speedups if the mechanism had more species, or if more vertical cells are computed

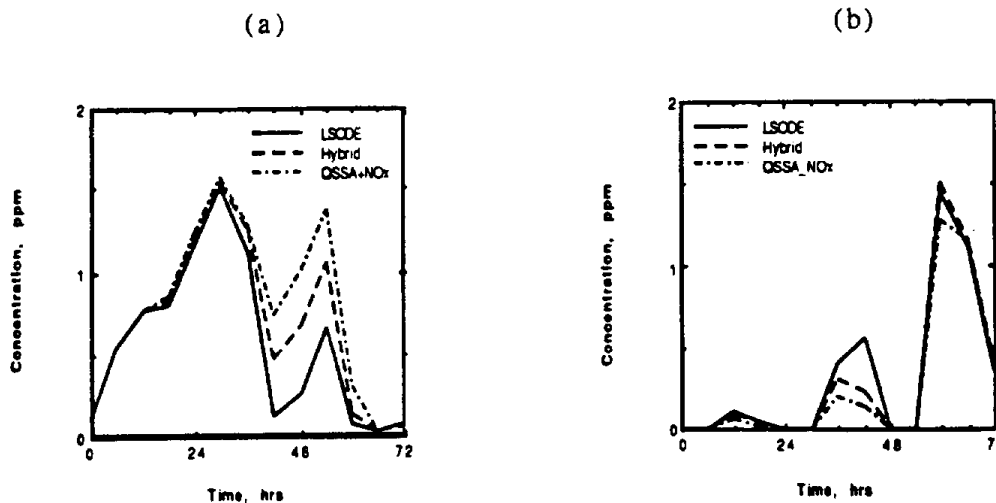


Fig. 5. Predictions of hybrid and QSSA with NO<sub>x</sub> lumping schemes compared to LSODE solution at an ROG/NO<sub>x</sub> emission ratio of 8:1 : a) NO<sub>x</sub>, b) O<sub>3</sub>.

TABLE 7. CPU Times (sec)

	Hybrid		QSSA-NO <sub>x</sub>	
	Scalar	Vector	Scalar	Vector
Computing Rates	15.9	14.5	3.3	3.0
Integrating	13.6	4.7	2.8	1.3
Lumping	-	-	0.5	0.5
Total	29.9	19.6	7.0	5.2

simultaneously (as is often the case).

#### 4. SUMMARY AND CONCLUSIONS

The treatment of nonlinear chemical kinetics requires special attention in air quality models because most of the computer time is spent in solving the equations describing the chemistry. Two fast solvers, the hybrid and QSSA schemes were compared to the Gear method for accuracy. The conservation errors in the QSSA scheme are significant, therefore, it should be used with a mass conservative linear transformation technique. The NO<sub>x</sub> lumping technique yields better accuracy than the proportional distribution of errors among all nitrogen containing species. The hybrid scheme, even without lumping, is about two times more accurate than the QSSA. The latter can be made more accurate by decreasing the predetermined time step, but the resulting scheme is usually less efficient than the hybrid scheme.

Simple test problems may be misleading in efficiency considerations. A moderate-sized test problem with varying photolysis rates and ROG/NO<sub>x</sub> emission ratios was designed specifically to measure the performances in vector processing mode. This problem, spanning a three day period, approximates real simulation situations better than test problems with constant rates. Both schemes displayed the largest errors around an ROG/NO<sub>x</sub> emission ratio of 8:1, which is similar to the observed value in many urban areas. The QSSA scheme with NO<sub>x</sub> lumping used about 4 times less computer time in solving this problem. Both schemes spend about 50% of their CPU times in computing the production and loss rates. This process is not readily vectorizable and restricts the overall gain for both schemes. In vector processing mode, the integrating part of the hybrid scheme experienced approximately 50% larger speed-up than the QSSA.

These results show that there is a trade-off between the accuracy and efficiency of fast chemical kinetic solvers considered here. When the suggested time steps are used, the QSSA scheme is faster than the hybrid scheme, though less accurate. In multi-day simulations, instability problems were encountered. Depending on the stiffness of the problem, special techniques may be required to obtain stable solutions. These techniques may be different for different chemical mechanisms and, different atmospheric conditions may require new techniques. On the other hand, the hybrid scheme gives stable solutions of better accuracy and is not restrictive computationally. Since the hybrid scheme displays better vector speed-ups, the CPU time differences between the two become smaller in vector processing mode. Thus the hybrid scheme is numerically more robust, though usually slower.

**Acknowledgements** - The support for this project was provided by the U.S. Environmental Protection Agency, Division of University Grants, Coordinating Research Council, the Pittsburgh Supercomputer Center and the California Air Resources Board. This support is greatly appreciated.

#### REFERENCES

- Carmichael G.R., Peters L.K. and Kitada T. (1986), "A second generation model for regional-scale transport/chemistry/deposition," *Atmos. Environ.*, **20**, 173-188.
- Chang J.S., Brost R.A., Isaksen I.S.A., Madronich S., Middleton P., Stockwell W.R. and Walcek C.J. (1987), *J. Geophys. Res.*, **92**, 14,681-14,700.
- Dodge M. C. (1989), "A comparison of three photochemical oxidant mechanisms," *J. Geophys. Res.*, **94**, 5121-5136.
- Gery M.W., Whitten G.Z., Killus J.P. and Dodge M.C. (1989), "A photochemical kinetics mechanism for urban and regional scale computer modeling," *J. Geophys. Res.*, **94**, 12,925-12,956.
- Hesstvedt E., Hov Ø. and Isaksen I.S.A. (1978), "Quasi-steady-state approximations in air pollution modeling," *Int. J. Chem. Kinetics*, **10**, 971-994.
- Hindmarsh A.C. (1980), "LSODE and LSODI, Two new initial value ordinary differential equation solvers," *ACM-SIGNAL Newsletter*, **15**, No. 4, 10-11.
- Hogo H. and Gery M. W. (1988), "User's guide for executing OZIPM-4 with CBM-IV or optional mechanisms," *Rep. EPA/600/8-88/082*, U.S. Environ. Prot. Agency, Research Triangle Park, N.C.
- Lamb R.G. (1983), "A regional scale (1000 km) model of photochemical air pollution: part 1, theoretical formulation," *Rep. EPA/600/3-83/025*, U.S. Environ. Prot. Agency, Research Triangle Park, N.C.
- Lurmann F.W., Carter W.P.L. and Coyner L.A. (1987), "A surrogate species chemical reaction mechanism for urban-scale air quality simulation models, Vol. II-Guidelines for using the mechanism," *Rep. EPA 68-02-4104*, U.S. Environ. Prot. Agency, Research Triangle Park, N.C.
- McRae G.J., Goodin W.R. and Seinfeld J.M. (1982), "Numerical solutions of the atmospheric diffusion equation for chemically reacting flows," *J. Comput. Physics*, **45**, 1-42.
- Milford J.B., Russell A.G. and McRae G.J. (1991), "Comparison of condensed chemical mechanisms for photochemical air pollution modeling," submitted.
- Morris R.E. and Myers T.C. (1990), "User's guide for the urban airshed model, Vol. 1: User's manual for UAM (CB-IV)," *Rep. EPA/450/4-90/007A*, U.S. Environ. Prot. Agency, Research Triangle Park, N.C.
- Pacific-Sierra Research Corp. (1989), "Efficient fortran techniques for parallel and vector processors," Los Angeles, CA.

- Russell A.G., McNair L., Odman M.T. (1991), "Airshed calculation of the sensitivity of pollutant formation to organic compound classes and oxygenates associated with alternative fuels," *JAWMA*, in press.
- Shieh, D. S., Chang Y., Carmichael G. R. (1988), "The evaluation of numerical techniques for solution of stiff ordinary differential equations arising from chemical kinetic problems," *Environ. Software*, 3, 28-38.
- Sillman S., Logan J. and Wofsy C. (1990), "A regional scale model for ozone in the United States with subgrid representation of urban and power plant plumes," *J. Geophys. Res.*, 95, 5,731-5,748.
- Yamartino R.J., Scire J.S., Hanna S.R., Carmichael G.R., Chang Y.S. (1989), "CALGRID: a mesoscale photochemical grid model," Report No. A049-1, California Air Resources Board, Sacramento, CA.
- Young T.R. and Boris J.P. (1977), "A numerical technique for solving stiff ordinary differential equations associated with the chemical kinetics of reactive flow problems," *J. Phys. Chem.*, 81, 2424-2427.

## **Appendix B**

### **Use of Sensitivity Analysis to Compare Chemical Mechanisms for Air Quality Modeling**

**Milford, J.B., Gao, D. Russell, A.G. and McRae, G.J., (1992)  
*Environmental Science and Technology*, 26 , 1179-1189**

## Use of Sensitivity Analysis To Compare Chemical Mechanisms for Air-Quality Modeling

Jana B. Milford,\* Dongfen Gao, Armistead G. Russell,<sup>†</sup> and Gregory J. McRae<sup>‡</sup>

Department of Civil Engineering, University of Connecticut, Storrs, Connecticut 06269

■ The LCC and CB4 mechanisms have been compared through a detailed sensitivity analysis. The formal method used provides an efficient means of comparing the influence of initial concentrations and reaction rate constants across mechanisms. The analysis identified discrepancies between the CB4 and LCC mechanisms that were overlooked in less formal tests. For the conditions studied, which approximate those of a smog chamber, the mechanisms generally show close agreement in predicted ozone concentrations, with larger differences for hydrogen peroxide and formaldehyde. The mechanisms differ in the sensitivity of peak O<sub>3</sub>, H<sub>2</sub>O<sub>2</sub>, and HCHO concentrations to the initial concentrations of key classes of organic compounds. These differences have important implications for use of the mechanisms in developing reactivity scales. Revisions to the CB4 mechanism that have been recommended based on recent studies of peroxy acetyl radical + NO and NO<sub>2</sub> reaction rates are shown to be significant.

### 1. Introduction

Over the past decade, rapid progress has been made in understanding the gas-phase chemical reactions that produce ozone and other secondary pollutants in urban atmospheres. Several "condensed" chemical mechanisms are currently in use to represent the most important of these reactions in a form tractable for mathematical air-quality modeling. The existence of alternative reaction schemes raises questions for those who use photochemical air-quality models: which mechanism ought to be used to estimate emissions reduction requirements, and what difference will it make if one is selected versus another? To answer these questions, mechanisms are tested against smog chamber experiments, and the results of simulations performed with alternative mechanisms are compared in detail.

Typically, mechanisms are analyzed and compared on the basis of predicted concentrations of key species. However, including sensitivity analysis as one component of a comparison can be extremely useful in helping to determine the significance of uncertainties or apparent differences between two mechanisms. Previous mechanism comparison studies have employed sensitivity analysis only informally, by repeating otherwise identical simulations with a change in the value of a selected parameter, such as a reaction rate constant or initial concentration (1-4).

This article demonstrates the application of a formal sensitivity analysis method, the direct decoupled method (DDM) (5, 6), to the task of comparing chemical mechanisms. The sensitivity coefficients calculated with the DDM are the partial derivatives of the model output concentrations with respect to the input parameters, including initial concentrations as well as reaction rate constants. Because the direct decoupled method calculates sensitivity coefficients for all species and rate parameters

simultaneously, a single DDM application can replace hundreds of simulations performed in conducting an informal sensitivity analysis. Previous applications of formal sensitivity analysis to gas-phase chemical mechanisms focused on understanding various aspects of a single mechanism (7, 8). The utility of formal sensitivity analysis for comparing mechanisms has not previously been illustrated.

A second problem of current interest to which the direct decoupled method is well-suited is the question of ranking organic compounds by their relative contributions to the formation of ozone or other secondary pollutants. Regulations are currently being developed that will use reactivity weighting in determining allowable emissions (9). A standard approach used to estimate organic compound reactivities in the past has been to look at how ozone concentrations change when computer simulations or smog chamber experiments are repeated, with small changes made in the initial concentration (and/or the simulated emissions rate) of the compound under investigation (10-12). In contrast, the sensitivities calculated with the DDM are numerically exact local sensitivities, as opposed to approximations based on two separate runs, each with possible numerical inaccuracies. Furthermore, with a single simulation the reactivities of all of the input compounds are given by the sensitivity coefficients calculated with the direct decoupled method. The application of the direct decoupled method to the problem of calculating reactivities is also demonstrated in this study.

The mechanisms to which the DDM is applied here are the CB4 mechanism (13, 14) and the LCC mechanism (15). Both are actively used in research and regulatory applications. In addition to the published version of CB4, a version with recently recommended modifications (16, 17) is included in this study. Dodge (4, 18) has previously compared the LCC mechanism with the 1988 version of CB4. Her comparisons were made by examining the outputs of numerous simulations covering a variety of conditions. Dodge's studies thus provide a useful basis for comparison with the formal sensitivity analysis approach adopted here.

The reader is referred to Dunker (5) for a detailed description of the direct decoupled method. The next section of this paper introduces the CB4 and LCC mechanisms and reviews the results of previous studies that have compared them. The simulation conditions used for the study are presented in Section 3. Section 4 presents the results of the sensitivity analysis, exploring the differences between the CB4 and LCC mechanisms and demonstrating the utility of the DDM. Section 5 compares the sensitivity coefficients calculated for this study with the "incremental reactivities" of Carter and Atkinson (12) and compares the results of the DDM-based comparison of CB4 and LCC with Dodge's (4, 18) findings. The conclusions of the study are given in Section 6.

### 2. Description of the CB4 and LCC Mechanisms

Listings of the CB4 and LCC mechanisms as they were implemented for this analysis are available from the authors. Table I summarizes the number of reactions and

\*Department of Mechanical Engineering, Carnegie Mellon University, Pittsburgh, PA 15213.

<sup>†</sup>Department of Chemical Engineering, Carnegie Mellon University, Pittsburgh, PA 15213.

**Table I. Summary Characteristics of the CB4 and LCC Mechanisms**

	mechanism	
	CB4	LCC
total species	33	50
primary ROG species	8	12
organic radicals	6	11
no. of reactions	81	131
photolysis reactions	11	17
references	13, 14	15
evaluation studies	13	19

**Table II. Modifications Recommended for CB4 (16, 17) and Incorporated into CB4.1**

reaction 82 has been added  
 $\text{XO}_2 + \text{HO}_2 \rightarrow (\text{no products})$  (82)  
 $k_{82} = 113.4 \exp(1300/T)$  ( $\text{ppm}^{-1} \text{min}^{-1}$ )  
 rates for the following CB4 reactions have been changed  
 $\text{C}_2\text{O}_3 + \text{NO} \rightarrow \text{HCHO} + \text{NO}_2 + \text{HO}_2 + \text{XO}_2$  (46)  
 $\text{C}_2\text{O}_3 + \text{NO}_2 \rightarrow \text{PAN}$  (47)  
 $\text{PAN} \rightarrow \text{C}_2\text{O}_3$  (48)

CB4  
 $k_{46} = 7.915 \times 10^3 \exp(250/T)$  ( $\text{ppm}^{-1} \text{min}^{-1}$ )  
 $k_{47} = 1.18 \times 10^{-4} \exp(5500/T)$  ( $\text{ppm}^{-1} \text{min}^{-1}$ )  
 $k_{48} = 5.616 \times 10^{18} \exp(-14000/T)$  ( $\text{min}^{-1}$ )

CB4.1  
 $k_{46} = 5.15 \times 10^4 \exp(-180/T)$  ( $\text{ppm}^{-1} \text{min}^{-1}$ )  
 $k_{47} = 3.84 \times 10^3 \exp(380/T)$  ( $\text{ppm}^{-1} \text{min}^{-1}$ )  
 $k_{48} = 1.2 \times 10^{18} \exp(-13500/T)$  ( $\text{min}^{-1}$ )

species in each mechanism and gives references to their documentation and experimental evaluations (13–15, 19). Mechanism development is an ongoing process, and modifications have been recommended for CB4 since it was published (16, 17). Accordingly, an updated version of CB4 that incorporates these modifications is also examined in this study. Hereafter, the modified version of CB4 will be referred to as CB4.1 and the published version as CB4. The modifications incorporated into CB4.1 are listed in Table II.

In order to develop computationally tractable mechanisms, highly condensed representations of the complex organic chemistry that occurs in polluted atmospheres are required. In the past, differences introduced in selecting and approximating organic reactions have led to substantial discrepancies in predicted product concentrations (1–3, 20, 21). In contrast to the reactions of the organics, among recently developed mechanisms there have been few differences in the inorganic reactions of primary importance under urban conditions. Key aspects of the treatment of organics in the CB4 and LCC mechanisms are described below.

Classes of organics in the CB4 mechanism are based on functional groups and include paraffinic and olefinic bonds, ethylene, isoprene, two aldehydes, and two aromatic classes. Key organic peroxy radicals include an acetyl peroxy radical and a generalized alkyl peroxy radical that produces  $\text{NO}_2$  upon reaction with  $\text{NO}$ . The other stable products produced from alkyl peroxy radical +  $\text{NO}$  reactions are included as products of the ROG oxidation reactions that would have produced distinct radicals in the first place. Acetyl peroxy radicals in CB4 react with  $\text{NO}$ ,  $\text{NO}_2$ , other acetyl peroxy radicals, and  $\text{HO}_2$ . Alkyl peroxy radicals in the published version of CB4 react with other alkyl peroxy radicals in addition to reacting with  $\text{NO}$ , but not with acetyl peroxy radicals or  $\text{HO}_2$ . As noted in Table II, a reaction between alkyl peroxy radicals and  $\text{HO}_2$  has been included in CB4.1.

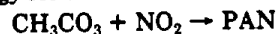
In the LCC mechanism, groups of stable organic species with similar reaction rates and products are represented

by surrogate species for which rate expressions and product yields have been preset based on an assumed mixture. Four primary carbonyl classes, two alkane classes, ethylene, two classes of higher alkenes, and three aromatics classes are included. The chemistry of the radical products of organic oxidation reactions has been condensed using a treatment similar to that used in the CB4 mechanism. However, a larger number of generalized radicals are used, each of which yields different products upon reaction with  $\text{NO}$ . In further contrast to CB4, in the LCC mechanism both alkyl and acetyl peroxy radicals react with each other as well as with other alkyl and acetyl peroxy radicals and with  $\text{HO}_2$ .

A thorough comparison of the LCC and CB4 mechanisms has been conducted by Dodge (4, 18). In these studies, differences between LCC and CB4 in aromatics chemistry, temperature dependence of PAN formation, and termination reactions for peroxy radicals were noted as particularly significant. Differences in the absorption cross sections used to calculate formaldehyde photolysis rates for the two mechanisms also produced significant differences in predicted concentrations of formaldehyde and hydrogen peroxide (18). For the present study, as discussed below, the formaldehyde photolysis rates given for LCC were adopted for CB4.

For ozone, as well as  $\text{H}_2\text{O}_2$  and PAN, comparisons of the predictions of different mechanisms and tests against smog chamber experiments have indicated that uncertainty about aromatic chemistry is a critical source of discrepancies among current mechanisms. Several recent studies have singled out uncertainties in aromatics mechanisms, including product yields and rate constants for secondary reactions, as having a significant impact on calculated ozone formation rates and maximum concentrations (3, 4, 18, 22–24).

The published version of CB4 includes a large, negative activation energy for the PAN formation reaction (13, 14)



$$k = 1.2 \times 10^{-4} \exp(5500/T) \text{ ppm}^{-1} \text{ min}^{-1}$$

compared to the reaction rate expression used in LCC (15)

$$k = 4.1 \times 10^3 \exp(180/T) \text{ ppm}^{-1} \text{ min}^{-1}$$

At low temperatures, this discrepancy leads to low ozone production with CB4 (4). As noted in Table II, the temperature dependence of reactions associated with PAN formation and decomposition have been altered in deriving CB4.1 from CB4. The new rate expressions used in CB4.1 are based on recent studies of the kinetics of PAN decomposition (25, 26) and of the relative rates of the reactions of acetyl peroxy radicals with  $\text{NO}$  versus  $\text{NO}_2$  (26, 27).

Finally, as described above, CB4 and LCC differ in their treatment of termination reactions for peroxy radicals. Dodge (4) showed that adding the reaction of alkyl peroxy radicals with  $\text{HO}_2$  reduced the peak  $\text{H}_2\text{O}_2$  concentrations predicted with CB4, bringing about better agreement with LCC. In addition, differences in formaldehyde concentrations in simulations conducted with high ROG to  $\text{NO}_2$  ratios and with acetaldehyde or alkenes as the only input organics were attributed to differences in the acetyl peroxy radical termination reactions included in LCC versus CB4.

### 3. Simulation Conditions

The ROG composition used in this study is listed in Tables III and IV. Intended to represent a typical morning composition for an urban area, the mixture listed in Table III is based on morning compositions reported by Grosjean and Fung (28) and Baugues (29). Grosjean

**Table III. Initial Reactive Organic Gas Composition (ppmv/ppm C)<sup>a</sup> Used in the Sensitivity Studies<sup>b</sup>**

ethane	0.019	propene	0.013
propane	0.012	<i>trans</i> -2-butene	0.011
butane	0.037	benzene	0.0061
pentane	0.019	toluene	0.014
hexane	0.010	xylylene	0.015
heptane	0.010	formaldehyde	0.030
octane	0.010	acetaldehyde	0.014
acetylene	0.019	propionaldehyde	0.010
ethylene	0.014		

<sup>a</sup> Concentration of the given compound (ppmv)/total concentration of organic compounds (ppm C). <sup>b</sup> Composition derived from the data of Grosjean and Fung (28) and Baugues (29).

**Table IV. Initial Reactive Organic Gas Composition (ppmv/ppm C) As Implemented for the LCC and CB4 Mechanisms<sup>a,b</sup>**

CB4		LCC	
PAR (1)	0.50	ALK4 (4.1)	0.063
		ALK7 (7)	0.030
ETH (2)	0.014	ETHE (2)	0.014
OLE (2)	0.013	PRPE (3)	0.013
		TBUT (4)	0.011
TOL (7)	0.014	TOLU (7)	0.014
XYL (8)	0.015	XYLE (8)	0.015
FORM (1)	0.030	HCHO (1)	0.030
ALD2 (2)	0.046	ALD2 (2)	0.014
		RCHO (3)	0.010
NR <sup>c</sup> (1)	0.098	NR (2.5)	0.048

<sup>a</sup> The species names correspond to those used in the original mechanisms. <sup>b</sup> The number of carbon atoms per molecule is given in parentheses for each species. <sup>c</sup> NR, nonreactive.

and Fung reported the average of measurements made over 23 days during the fall of 1981 at a downtown Los Angeles location. Baugues reported median morning compositions for the 1984 and 1985 summer seasons in approximately 20 cities. Table IV shows the splitting factors derived for the LCC and CB4 mechanisms, following the guidance provided by their developers.

Also reflecting typical urban conditions, an initial NO to NO<sub>2</sub> ratio of 3.0 and CO concentration of 1.5 ppm were used in all of the runs. Initial ROG and NO<sub>2</sub> concentrations for the three cases analyzed were case A: ROG = 1.8 ppm C, NO<sub>x</sub> = 0.15 ppm (ROG:NO<sub>x</sub> = 12:1); case B: ROG = 0.9 ppm C, NO<sub>x</sub> = 0.15 ppm (ROG:NO<sub>x</sub> = 6:1); case C: ROG = 1.8 ppm C, NO<sub>x</sub> = 0.075 ppm (ROG:NO<sub>x</sub> = 24:1). No smog chamber-dependent reactions were included in the simulations. Constant conditions, including a constant temperature of 298 K, relative humidity of 50%, no dilution, and constant photolysis rates, were assumed in order to facilitate interpretation of the sensitivities to the rate parameters. The photolysis rates approximated average values over the daylight hours in midsummer at a latitude of 40° N. Table V gives the photolysis rates used in each mechanism. Photolysis rates used with the LCC mechanism are those recommended by Lurmann et al. (15). With CB4, the recommendations of Gery et al. (13) were adopted, except for formaldehyde and other associated compounds. Following Dodge (18), the formaldehyde photolysis rates used in LCC were also adopted here for CB4. Photolysis rates for H<sub>2</sub>O<sub>2</sub>, MGLY (methylglyoxal), and OPEN (an aromatic ring fragment) are specified in the CB4 documentation as ratios to the formaldehyde photolysis rates and were adjusted accordingly.

The sensitivity calculations in this study were performed using a direct decoupled method code developed by

**Table V. Photolysis Rates Used in Each Mechanism**

photolytic reaction	rxn no.	rate, min <sup>-1</sup>
LCC Mechanism		
NO <sub>2</sub> → NO + O	(1)	0.300
NO <sub>3</sub> → NO	(13)	0.865
NO <sub>3</sub> → NO <sub>2</sub> + O	(14)	0.775 × 10 <sup>1</sup>
O <sub>3</sub> → O	(15)	0.196 × 10 <sup>-1</sup>
O <sub>3</sub> → OSD	(16)	0.352 × 10 <sup>-3</sup>
HONO → NO + OH	(20)	0.566 × 10 <sup>-1</sup>
H <sub>2</sub> O <sub>2</sub> → 2OH	(35)	0.182 × 10 <sup>-3</sup>
ROOH → HO <sub>2</sub> + OH	(42)	0.182 × 10 <sup>-3</sup>
HCHO → 2HO <sub>2</sub> + CO	(46)	0.677 × 10 <sup>-3</sup>
HCHO → CO	(47)	0.133 × 10 <sup>-2</sup>
ALD2 → CO + HCHO + HO <sub>2</sub> + RO <sub>2</sub> R + RO <sub>2</sub>	(52)	0.730 × 10 <sup>-4</sup>
RCHO → ALD2 + HO <sub>2</sub> + CO + RO <sub>2</sub> R + RO <sub>2</sub>	(61)	0.210 × 10 <sup>-3</sup>
ACET → MCO <sub>3</sub> + HCHO + RCO <sub>3</sub> + RO <sub>2</sub> R + RO <sub>2</sub>	(69)	0.202 × 10 <sup>-4</sup>
MEK → MCO <sub>3</sub> + ALD2 + RCO <sub>3</sub> + RO <sub>2</sub> R + RO <sub>2</sub>	(71)	0.291 × 10 <sup>-4</sup>
GLYX → 0.13HCHO + 1.87CO	(73)	0.271 × 10 <sup>-2</sup>
MGLY → MCO <sub>3</sub> + HO <sub>2</sub> + CO + RCO <sub>3</sub>	(82)	0.599 × 10 <sup>-2</sup>
DIAL → HO <sub>2</sub> + CO + MCO <sub>3</sub> + RCO <sub>3</sub>	(116)	0.155 × 10 <sup>-1</sup>
CB4 Mechanism		
NO <sub>2</sub> → NO + O	(1)	0.300
O <sub>3</sub> → O	(8)	0.159 × 10 <sup>-1</sup>
O <sub>3</sub> → O1D	(9)	0.409 × 10 <sup>-3</sup>
NO <sub>3</sub> → 0.89NO <sub>2</sub> + 0.89O + 0.11NO	(14)	0.102 × 10 <sup>2</sup>
HONO → NO + OH	(23)	0.593 × 10 <sup>-1</sup>
H <sub>2</sub> O <sub>2</sub> → 2OH	(34)	0.338 × 10 <sup>-3</sup>
FORM → 2HO <sub>2</sub> + CO	(38)	0.677 × 10 <sup>-3</sup>
FORM → CO	(39)	0.133 × 10 <sup>-2</sup>
ALD2 → FORM + 2HO <sub>2</sub> + CO + XO <sub>2</sub>	(45)	0.976 × 10 <sup>-4</sup>
OPEN → C <sub>2</sub> O <sub>3</sub> + HO <sub>2</sub> + CO	(69)	0.612 × 10 <sup>-2</sup>
MGLY → C <sub>2</sub> O <sub>3</sub> + HO <sub>2</sub> + CO	(74)	0.653 × 10 <sup>-2</sup>

McCroskey and McRae (6), which utilizes Gear's method (30) to numerically integrate both the rate and sensitivity equations. An error tolerance of 10<sup>-7</sup> was used for this work.

#### 4. Sensitivity Analysis Results

This section begins by examining time series for key species predicted with the CB4, CB4.1, and LCC mechanisms and then examines sensitivity analysis results for each mechanism. The analysis focuses on O<sub>3</sub>, HCHO, and H<sub>2</sub>O<sub>2</sub>. H<sub>2</sub>O<sub>2</sub> is an important sink for peroxy radicals in ROG-rich systems and is the principal aqueous-phase oxidant of sulfur dioxide. Formaldehyde is an important source of radicals, as well as having potential health impacts.

Figure 1 presents O<sub>3</sub>, NO, and NO<sub>2</sub> concentrations plotted over time for three combinations of initial ROG and NO<sub>x</sub> concentrations. For case A (ROG:NO<sub>x</sub> = 12:1), the predicted ozone concentrations after 12 h range from 0.336 with CB4 to 0.373 ppm with CB4.1. CB4.1 and LCC show close agreement. For case B (ROG:NO<sub>x</sub> = 6:1), the predicted final ozone concentrations range from 0.111 to 0.132 ppm. The results for case C (ROG:NO<sub>x</sub> = 24:1) range from 0.234 to 0.279 ppm ozone after 12 h. In cases B and C, ozone concentrations predicted with CB4.1 are intermediate to the relatively high prediction of LCC and the low prediction of CB4.

Figure 2 shows predicted concentrations of H<sub>2</sub>O<sub>2</sub> and HCHO for the three cases. Larger discrepancies between the mechanisms occur for hydrogen peroxide and formaldehyde than for ozone. In case B (6:1) the final H<sub>2</sub>O<sub>2</sub> concentration predicted with LCC exceeds that predicted with CB4 by more than a factor of 2, although the concentrations are very low. The reverse is true for case C

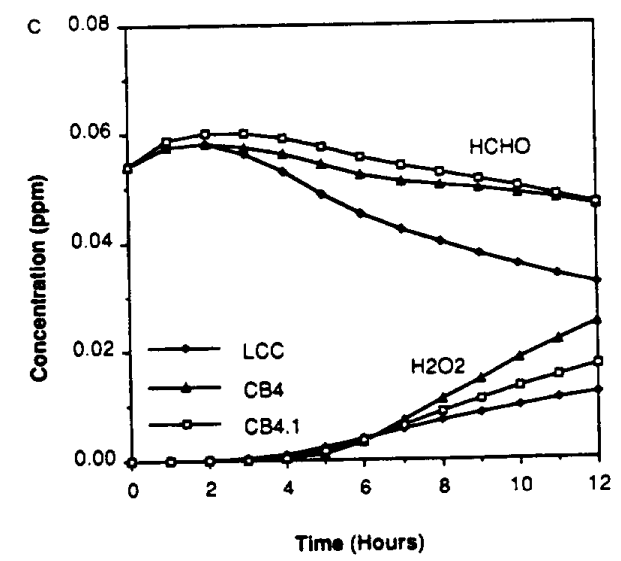
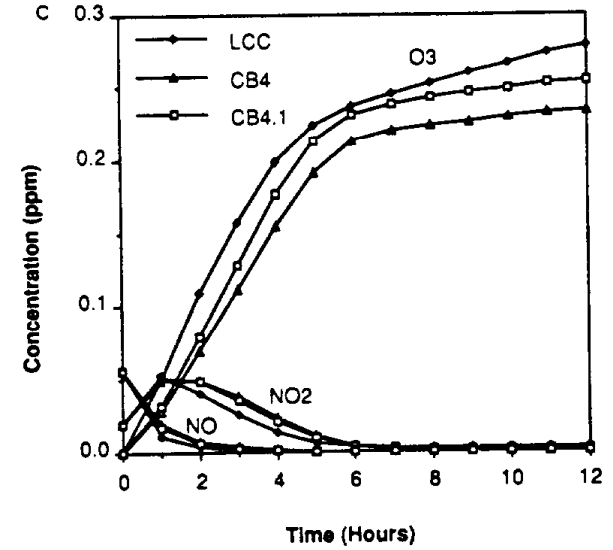
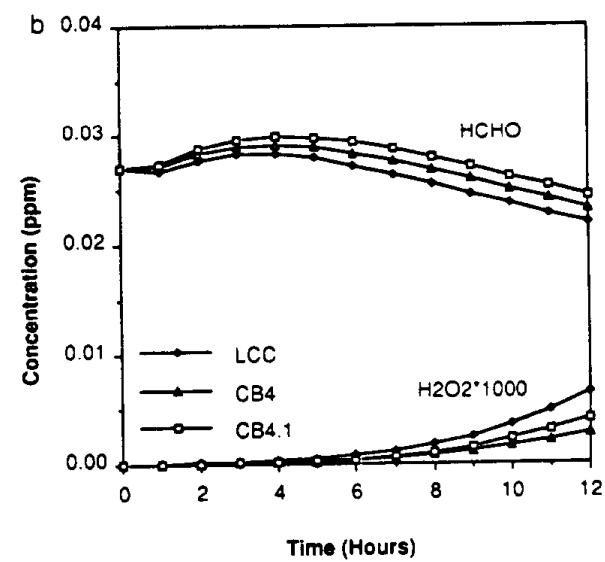
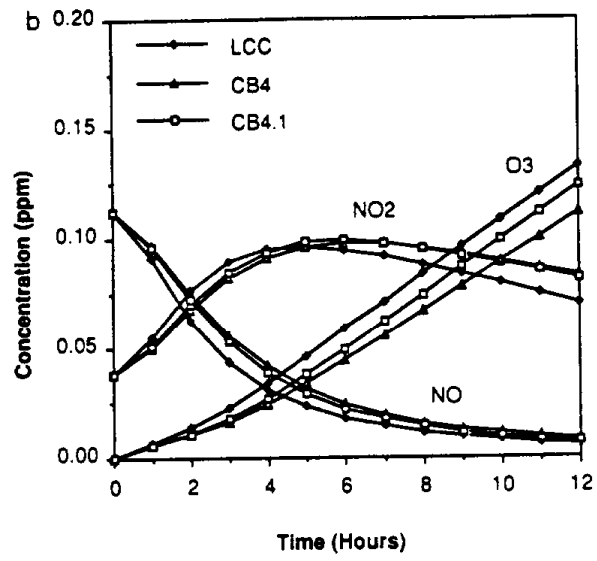
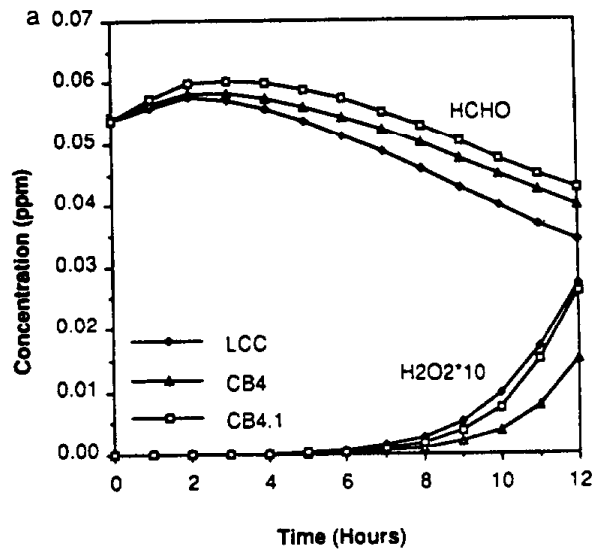
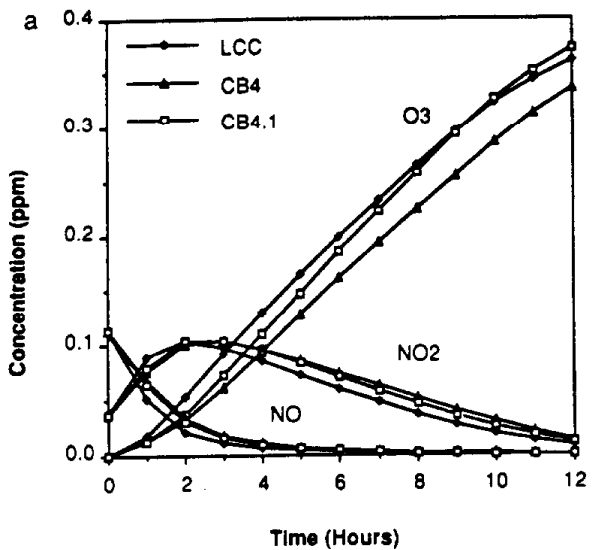
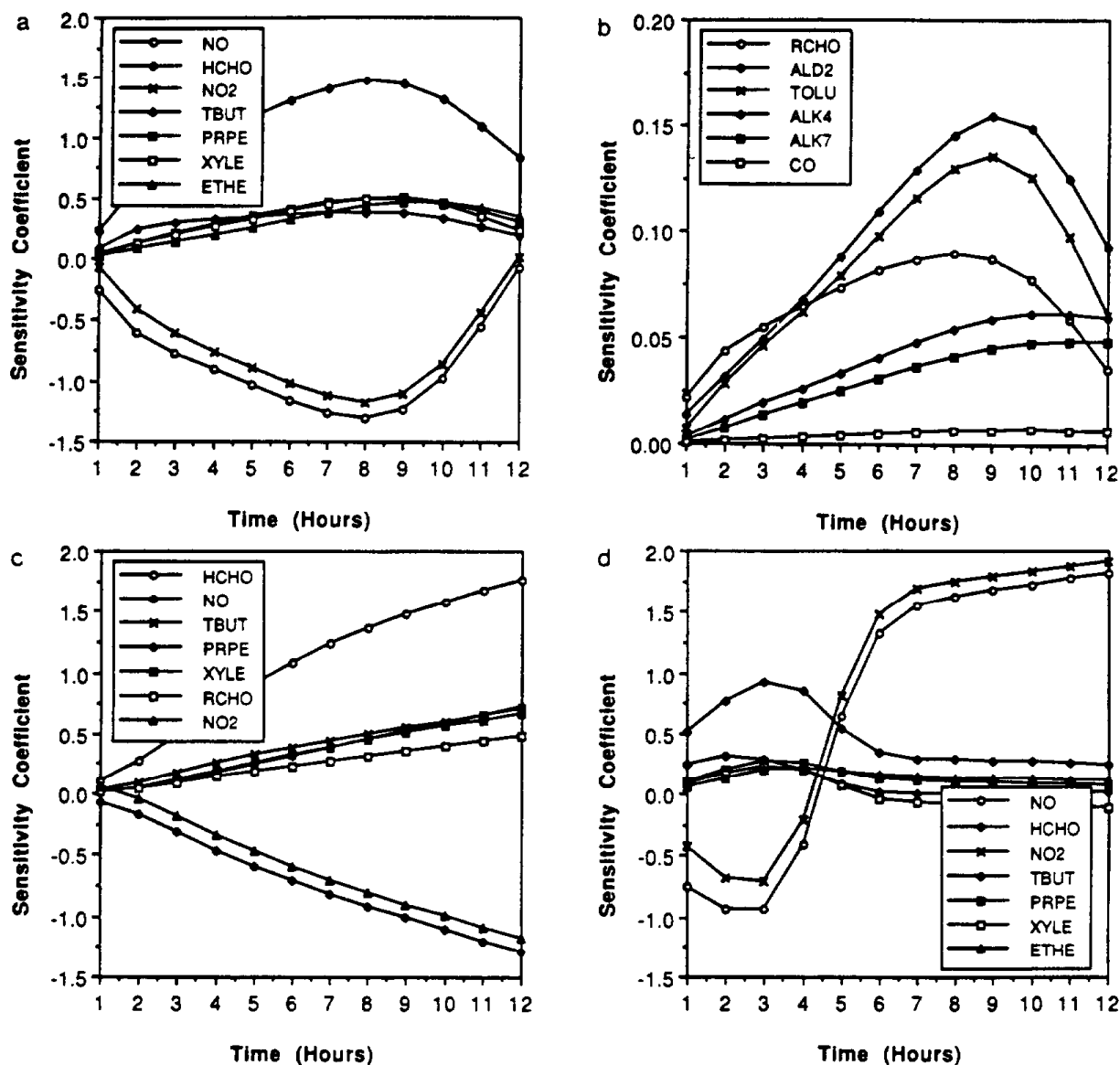


Figure 1. O<sub>3</sub>, NO, and NO<sub>2</sub> concentrations predicted with LCC, CB4, and CB4.1 for (a) case A, with initial concentrations of 1.8 ppm C ROG and 0.15 ppm NO<sub>2</sub>; (b) case B, with initial concentrations of 0.9 ppm C ROG and 0.15 ppm NO<sub>2</sub>; and (c) case C, with initial concentrations of 1.8 ppm C ROG and 0.075 ppm NO<sub>2</sub>.

Figure 2. H<sub>2</sub>O<sub>2</sub> and HCHO concentrations predicted with LCC, CB4, and CB4.1 for (a) case A (initial ROG:NO<sub>x</sub> = 12:1); (b) case B (6:1); and (c) case C (24:1).



**Figure 3.** Sensitivity of ozone to initial  $\text{NO}_x$  and ROG concentrations predicted with the LCC mechanism for (a and b) case A (initial  $\text{ROG}:\text{NO}_x = 12:1$ ); (c) case B (8:1); and (d) case C (24:1). The sensitivity coefficients are given in units of  $\text{ppm O}_3$  per  $\text{ppm NO}_x$  or  $\text{ppm O}_3$  per  $\text{ppm C}$  ROG. For cases B and C, coefficients are shown only for the five ROG classes to which ozone shows the greatest sensitivity.

(24:1) in which the  $\text{H}_2\text{O}_2$  concentration predicted with CB4 is more than twice as high as that predicted with LCC. In all three cases CB4.1 gives intermediate  $\text{H}_2\text{O}_2$  concentrations compared to CB4 and LCC. For HCHO, however, the concentrations predicted with CB4 fall between those of CB4.1 and LCC. Thus the modifications incorporated in CB4.1 increased the discrepancy in the formaldehyde predictions of the different mechanisms.

Table VI shows final concentrations of key species predicted in cases A-C. Relatively close agreement is apparent between CB4, CB4.1, and LCC for nitric acid and peroxyacetyl nitrate, especially in cases A and C. However, when PAN analogues represented in the LCC mechanism are considered, "total PAN" concentrations are distinctly higher with LCC than with CB4 and CB4.1.

In order to further explore the differences between the mechanisms, the direct decoupled method has been used to calculate the sensitivity of the predicted concentrations of key species to initial conditions and reaction rate constants. As an illustration, Figure 3 shows results for the sensitivity of ozone to the initial concentrations of  $\text{NO}_x$

and ROG species calculated for the LCC mechanism. Time-dependent sensitivity coefficients

$$s_{ij}(t) = \partial y_i(t) / \partial p_j$$

are shown, with  $p_j$  representing an element of the initial concentration vector  $y_0$ . For the organic species, the units of  $p_j$  are  $\text{ppm C}$ , i.e., the sensitivity coefficients are given on a per-carbon basis. Although not shown, the sensitivity results for CB4 and CB4.1 are generally similar to those for LCC, with a few important differences discussed below.

For LCC, in cases A and B, the sensitivity of ozone to the initial  $\text{NO}$  and  $\text{NO}_2$  concentrations is negative throughout the simulations. In contrast, after the first 4 h in case C, the sensitivity coefficients for  $\text{NO}$  and  $\text{NO}_2$  are positive. The sensitivity of ozone to  $\text{NO}_x$  reflects the balance between  $\text{NO}_x$  and ROG (and hence peroxy radical production) in the system. This balance determines whether the result of adding  $\text{NO}_x$  is decreased levels of ozone and radicals as they are scavenged by  $\text{NO}$  and  $\text{NO}_2$  or enhanced concentrations as more  $\text{NO}_2$  is available to be photolyzed and more  $\text{NO}$  is available to cycle radicals.

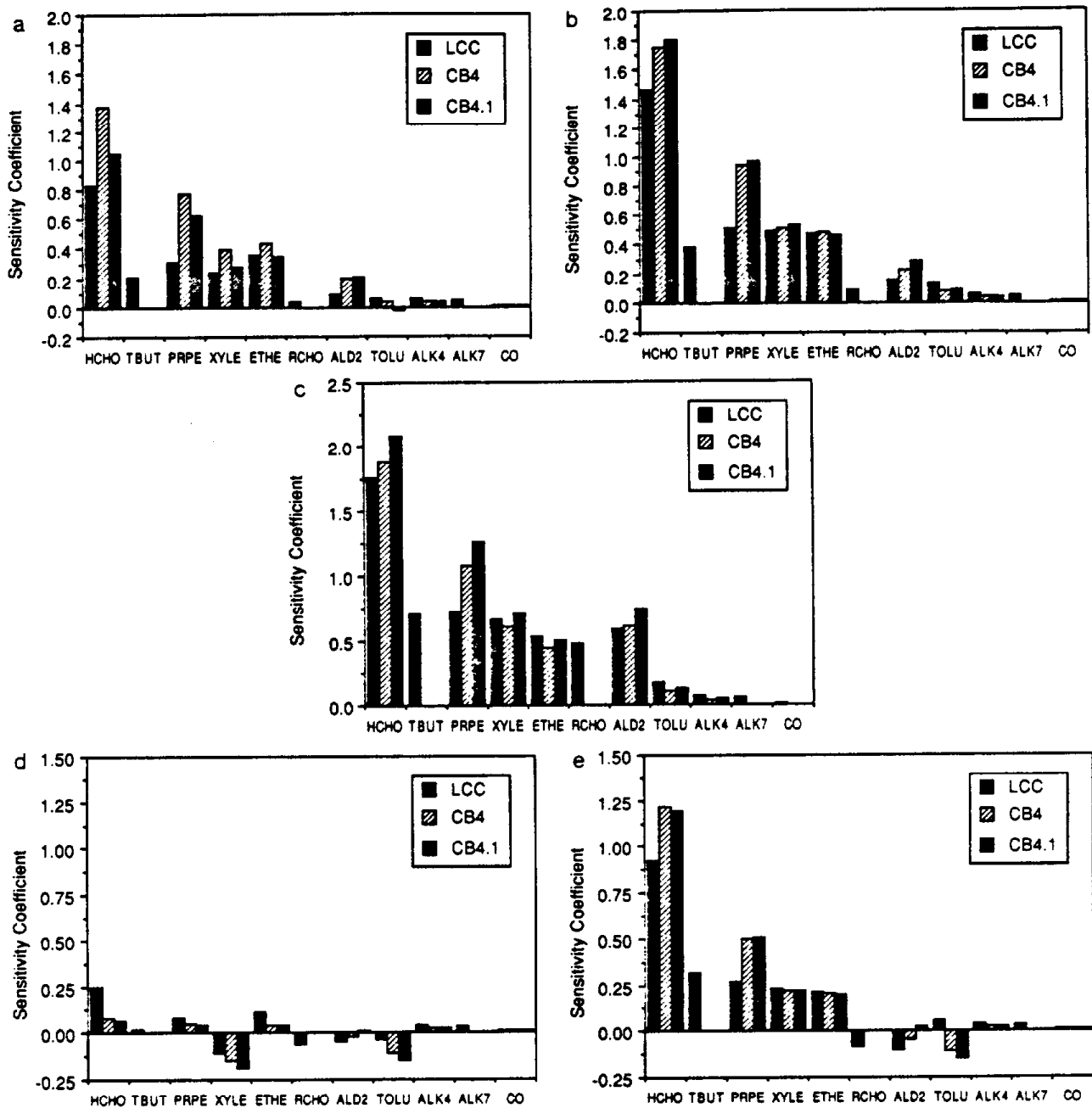


**Figure 4.** (a, c, and d) Sensitivity of peak ozone to initial concentrations and (b, c, and e) maximum sensitivity of ozone to the initial concentration for each ROG class. (a and b) Case A (Initial ROG:NO<sub>x</sub> = 12:1); (c) case B (6:1); (d and e) case C (24:1). For case B, the maximum sensitivities and sensitivities of peak ozone coincide, so only one graph (c) is shown. Sensitivity coefficients are given in units of ppm O<sub>3</sub> per ppm C. LCC classes were used for labeling the graph, so the CB4 and CB4.1 OLE class is shown as 'PRPE' and the PAR class as 'ALK4'.

The sensitivity of the O<sub>3</sub> concentration to the initial concentrations of the organic classes reflects both the demand for radicals in the system and the supply provided by each class. In cases A and B, the sensitivity of ozone to the initial concentrations of the ROG species remains positive throughout the simulation. However, in case C, with a 24:1 ratio of ROG to NO<sub>x</sub>, sensitivity coefficients for the xylene and toluene (not shown) classes in LCC switch sign from positive to negative after about 5 h, and coefficients for the acetaldehyde and propionaldehyde (RCHO) classes are always negative (also not shown). Similar results occur with CB4 and CB4.1.

For purposes of comparing the mechanisms, Figure 4 presents instantaneous sensitivity coefficients for each of

the organic classes in CB4, CB4.1, and LCC. The sensitivity coefficients depend strongly on time, so two sets of instantaneous coefficients are shown. The first set of coefficients (Figure 4, panels a, c, and d) are evaluated at the time at which the peak ozone concentration is produced, i.e., the end of the 12-h simulation period for each of the three cases included in this study. The instantaneous sensitivity coefficient at the time of the peak is equivalent to the "incremental reactivity" (IR) defined by Carter and Atkinson (12)

$$IR = \lim_{\Delta HC_j \rightarrow 0} \left[ \frac{R(HC_j + \Delta HC_j) - R(HC_j)}{\Delta HC_j} \right] \quad (1)$$

**Table VI. Predicted Concentrations (ppm) of Key Species after 12 h**

species	mechanism	ROG/NO <sub>x</sub>		
		12:1	6:1	24:1
O <sub>3</sub>	LCC	0.361	0.132	0.279
	CB4	0.336	0.111	0.234
	CB4.1	0.373	0.124	0.255
HNO <sub>3</sub>	LCC	0.0696	0.0578	0.0260
	CB4	0.0655	0.0452	0.0266
	CB4.1	0.0702	0.0483	0.0283
H <sub>2</sub> O <sub>2</sub>	LCC	0.00270	6.5 × 10 <sup>-6</sup>	0.0120
	CB4	0.00154	2.8 × 10 <sup>-6</sup>	0.0249
	CB4.1	0.00258	4.0 × 10 <sup>-6</sup>	0.0170
HCHO	LCC	0.0340	0.0219	0.0324
	CB4	0.0398	0.0232	0.0466
	CB4.1	0.0426	0.0244	0.0468
PAN	LCC	0.0456	0.0087	0.0278
	CB4	0.0489	0.0075	0.0279
	CB4.1	0.0450	0.0062	0.0253
PPN	LCC	0.0108	0.00177	0.00643
GPN	LCC	0.173 × 10 <sup>-3</sup>	0.247 × 10 <sup>-4</sup>	0.870 × 10 <sup>-4</sup>
total PAN	LCC	0.0566	0.0105	0.0343

where  $R(\text{HC}_i)$  is the maximum value of  $[\text{O}_3] - [\text{NO}]$  calculated in a base case simulation and  $R(\text{HC}_i + \Delta\text{HC}_i)$  is the maximum value of  $[\text{O}_3] - [\text{NO}]$  calculated in a simulation with  $\Delta\text{HC}_i$  added to the inputs from the base case. (Except in NO<sub>x</sub>-rich cases,  $[\text{NO}]$  can be neglected at the time when  $[\text{O}_3] - [\text{NO}]$  reaches its maximum value.) The second set of sensitivity coefficients in Figure 4 (panels b, c, and e) show the maximum sensitivity of ozone to the initial concentration of each organic, irrespective of the hour at which the maximum value occurs. [For example, referring back to Figure 3a and b, the maximum sensitivity of ozone to the initial formaldehyde concentration occurs at 8 h, whereas the maximum sensitivity to the higher alkanes class (ALK7) occurs at the end of the simulation.] In case B, all of the maximum sensitivities as well as the peak ozone concentrations occur at the end of the simulation, so the two sets of coefficients coincide (Figure 4c).

Figure 4 shows that formaldehyde is uniformly the most reactive of the organic classes per molecule of carbon. The alkenes and xylene generally follow. The sensitivity of ozone to compounds that react comparatively slowly, such as the alkanes, increases late in the simulations relative to the sensitivity to the more rapidly reacting compounds (see Figure 3a and b). Thus maximum reactivity values show more spread across compounds than do the reactivities at the time of the ozone peaks. In the high ROG:NO<sub>x</sub> case, the xylene, toluene, acetaldehyde and propionaldehyde classes ultimately inhibit ozone formation. This means that a small reduction in the input concentration of one of these compounds would increase the final ozone concentration.

Of special interest is the degree of consistency in the sensitivity coefficients from one mechanism to another. One factor that influences this is the time at which the coefficients are evaluated. For example, for CB4 and CB4.1, the maximum sensitivity coefficients in case A suggest better agreement than the sensitivities at the time of the ozone peak. However, the times at which the maximum sensitivities occur are different; for formaldehyde, the aromatics, and the alkenes, the maximum sensitivity coefficients occur 1 h earlier with CB4.1 than with CB4. The uniformly higher sensitivity coefficients with CB4.1 than with CB4 in the low-ROG:NO<sub>x</sub> case, and the higher and earlier maximum coefficients with CB4.1 than with CB4 in case A, indicate that CB4.1 is more reactive in terms of radical production. As ROG to NO<sub>x</sub> ratios increase beyond about 10:1, the demand for radicals

declines, accompanied by a trend toward lower sensitivity to input organic concentrations. The generally higher sensitivity coefficients with CB4 than CB4.1 in the 24:1 case reflect the overall higher rates of radical production in CB4.1, which results in less "demand" for radicals for ozone formation.

Comparing LCC with the carbon bond mechanisms, the reactivities of the alkanes classes in LCC are consistently higher than the reactivities of the PAR class in CB4 and CB4.1. To understand the source of this difference, the oxidation reactions of the products of the ALK4 + OH and PAR + OH reactions can be traced, and the peroxy radicals that would ultimately be produced in these reactions counted. Assuming the oxidation reactions go to completion, more peroxy radicals are produced per carbon with the ALK4 class in LCC than with PAR in CB4 and CB4.1.

The reactivity of the toluene class in LCC is also consistently high compared to the toluene class in CB4 and CB4.1. Dodge (18) previously found the same result in comparing LCC to CB4. She suggested that in CB4 the radical intermediate produced in the reaction of TOL + OH is assumed either to react with NO to produce NO<sub>2</sub> and a dicarbonyl or to rearrange, producing a cresol. The cresol species is significantly less reactive than the dicarbonyl species. In LCC, only the reaction with NO occurs.

In contrast to the cases of the alkanes and toluene, CB4 and CB4.1 generally display higher reactivity for the aldehydes and propene classes than LCC. As explained below, the difference is partly due to differences in reaction rates used for the acetyl peroxy radical + NO and NO<sub>2</sub> reactions in the three mechanisms. Another notable discrepancy between the mechanisms is seen in comparing the sensitivity coefficients for the *trans*-2-butene class in LCC and the acetaldehyde classes in CB4 and CB4.1, which represent *trans*-2-butene in those mechanisms. At high ROG to NO<sub>x</sub> ratios, the maximum sensitivity to the LCC *trans*-2-butene class is much greater than the sensitivity to the CB4.1 acetaldehyde class, and for CB4, the maximum sensitivity in magnitude is negative in sign.

In the same manner as for ozone, the sensitivity of formaldehyde, hydrogen peroxide, and other secondary pollutants to input concentrations can be calculated and interpreted as reactivities. Figure 5 shows instantaneous sensitivity coefficients for formaldehyde, on a per molecule of carbon basis, for case A. Again, coefficients are shown for the time that the peak formaldehyde concentration occurs with each mechanism, i.e., at the end of the second hour for CB4 and LCC and at the end of the third hour for CB4.1 (Figure 5a), and maximum coefficients are shown for each organic class irrespective of the time at which they occur (Figure 5b). After formaldehyde itself, the ethylene and propene classes are the most reactive in terms of formaldehyde production. The sensitivity coefficients for CB4.1 are generally slightly higher than those for CB4. The three mechanisms show fairly close agreement for the maximum sensitivities to ethylene and acetaldehyde. As with ozone, the sensitivity of formaldehyde to propene is higher with CB4 and CB4.1 than with LCC.

Finally, Figure 6 shows instantaneous sensitivity coefficients for hydrogen peroxide, for the 12:1 case, in which final H<sub>2</sub>O<sub>2</sub> concentrations ranged from 0.00154 ppm with CB4 to 0.00270 ppm with LCC. The sensitivity coefficients for H<sub>2</sub>O<sub>2</sub> are shown for the end of the simulations, the time of both the peak H<sub>2</sub>O<sub>2</sub> concentrations and the maximum sensitivities. For H<sub>2</sub>O<sub>2</sub>, sensitivity coefficients were uniformly higher for CB4.1 than for CB4, corresponding to higher H<sub>2</sub>O<sub>2</sub> production with CB4.1. H<sub>2</sub>O<sub>2</sub>

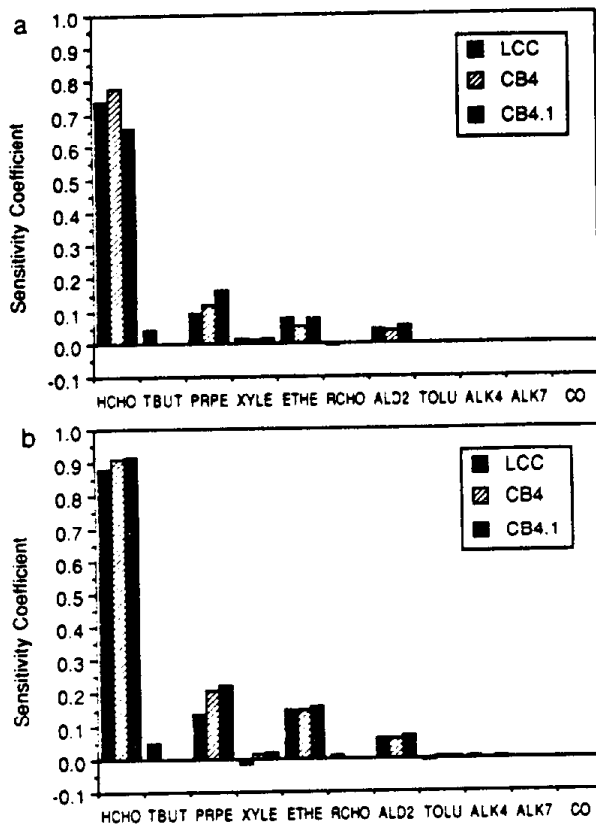


Figure 5. (a) Sensitivity of peak formaldehyde to the initial concentrations for each ROG class and (b) maximum sensitivity of formaldehyde to initial concentrations for case A (Initial ROG:NO<sub>x</sub> = 12:1). Sensitivity coefficients are given in units of ppm HCHO per ppm C.

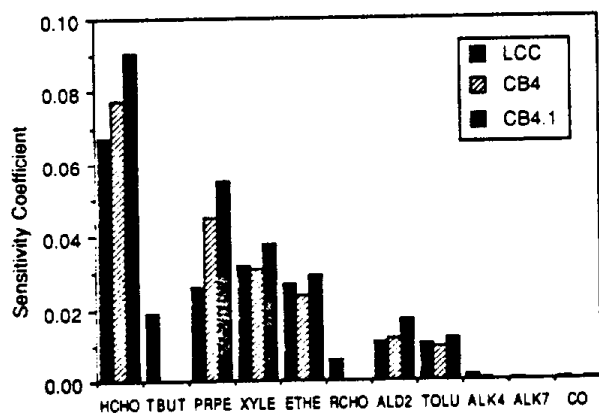


Figure 6. Sensitivity of peak hydrogen peroxide to the initial concentration for each ROG class for case A (Initial ROG:NO<sub>x</sub> = 12:1). Sensitivity coefficients are given in units of ppm H<sub>2</sub>O<sub>2</sub> per ppm C.

sensitivity coefficients were also higher for CB4.1 than for LCC, for all species except for CO and the alkanes. Sensitivity coefficients for CB4 were higher than those of LCC for propene, formaldehyde, and acetaldehyde.

Given the few modifications made to CB4 to derive CB4.1, a straightforward way to understand how the differences affect the results of these two mechanisms is to conduct a few additional simulations, making the modifications one at a time. Thus, the first diagnostic test performed (test 1) was to add reaction 82 to CB4 but to retain the original rate expressions for reactions 46–48 (see Table II). Test 2 changed the rate expressions but left out reaction 82. The results of these tests are shown in Table VII, for comparison with the original results shown in

Table VII. Predicted Concentrations (ppm) of Key Species after 12 h

species	test case	ROG/NO <sub>x</sub>		
		12:1	6:1	24:1
O <sub>3</sub>	CB4 test 1	0.333	0.111	0.232
	CB4 test 2	0.376	0.124	0.252
	LCC test 3	0.358	0.132	0.267
HNO <sub>3</sub>	CB4 test 1	0.0654	0.0452	0.0265
	CB4 test 2	0.0703	0.0483	0.0284
	LCC test 3	0.0696	0.0579	0.0260
H <sub>2</sub> O <sub>2</sub>	CB4 test 1	0.00136	2.8 × 10 <sup>-6</sup>	0.0152
	CB4 test 2	0.00314	4.0 × 10 <sup>-6</sup>	0.0276
	LCC test 3	0.00303	6.6 × 10 <sup>-6</sup>	0.0151
HCHO	CB4 test 1	0.0399	0.0232	0.0451
	CB4 test 2	0.0423	0.0244	0.0480
	LCC test 3	0.0385	0.0220	0.0425
PAN	CB4 test 1	0.0483	0.0075	0.0284
	CB4 test 2	0.0459	0.00616	0.0249
	LCC test 3	0.0459	0.00873	0.0279

Table VI. Adding reaction 82 (test 1) has little effect, with the exception of the final H<sub>2</sub>O<sub>2</sub> concentration in case C. In this case the H<sub>2</sub>O<sub>2</sub> concentration is significantly reduced and thus matches more closely the concentrations produced with CB4.1 and LCC.

Concentrations of ozone and formaldehyde are affected more by the changes made to the rates of reactions 46–48 than by the addition of reaction 82. In particular, compared to the rates used in CB4, the rates used at 298 K in CB4.1 and test 2 tend to favor reaction 46 over reaction 47, and thus increase O<sub>3</sub> and HCHO concentrations. The result of altering the rates for reactions 46–48 could have been anticipated by examining the sensitivity results for CB4. For LCC, CB4, and CB4.1, Table VIII shows the reactions with the rate constants to which ozone has the highest sensitivity in case A. The table also shows the sensitivity of the ozone concentration to each rate constant, evaluated at the end of the simulation. Seminormalized sensitivity coefficients

$$s_{ij}' = p_j(\partial y_i / \partial p_j)$$

(in ppm) are shown, where  $p_j$  represents the rate constant of reaction  $j$ . CB4 reactions 46–48 are included in the top eight. Assuming that the changes in the rate constants are small enough for the combined response to them to be linear, the expected response is a 0.05 ppm increase in peak ozone over the concentration produced with the original CB4 mechanism. The results for test 2 show that the simulated response is a 0.04 ppm increase.

As in the comparison of CB4.1 with CB4, the relative rates of the acetyl peroxy radical + NO reaction versus the PAN formation reaction in CB4.1 are more favorable to O<sub>3</sub> and HCHO production than the relative rates of these reactions in LCC. The newly updated rates used in CB4.1 are in better agreement with recent studies (26, 27) than those used in LCC. Acetyl peroxy radicals are produced via the reactions of acetaldehyde + OH and propene + OH, suggesting that the acetyl peroxy radical + NO<sub>x</sub> reaction rates partially account for the enhanced reactivity of the acetaldehyde and propene classes in CB4.1 compared to LCC. In addition, the acetaldehyde photolysis rate used in CB4.1 and CB4 is higher than that used in LCC.

Coefficients for the sensitivity of formaldehyde to reaction rate constants in the 24:1 case identify a major reason for the discrepancy between the formaldehyde concentrations predicted with LCC versus those predicted with CB4.1. Table IX shows the reactions with the rate constants to which formaldehyde has the highest sensitivity in case C. Reactions involving the acetyl peroxy

**Table VIII. Sensitivity of Peak Ozone to Reaction Rate Constants in Case A (12:1)**

reaction	rxn no.	rate constant at 298 K, ppm <sup>-n</sup> min <sup>-1</sup> <sup>a</sup>	sensitivity coeff, ppm O <sub>3</sub>
LCC Mechanism			
NO <sub>2</sub> + hν → NO + O	(1)	0.3	0.144
NO + O <sub>3</sub> → NO <sub>2</sub> + O <sub>2</sub>	(5)	0.268 × 10 <sup>2</sup>	-0.133
NO <sub>2</sub> + OH → HNO <sub>3</sub>	(22)	0.168 × 10 <sup>5</sup>	-0.0943
MCO <sub>3</sub> + NO <sub>2</sub> → PAN	(55)	0.757 × 10 <sup>4</sup>	-0.0745
MCO <sub>3</sub> + NO → HCHO + NO <sub>2</sub> + RO <sub>2</sub> R + RO <sub>2</sub>	(54)	0.114 × 10 <sup>5</sup>	0.0742
PAN → MCO <sub>3</sub> + NO <sub>2</sub> + RCO <sub>3</sub>	(59)	0.221 × 10 <sup>-1</sup>	0.0647
HCHO + hν → 2HO <sub>2</sub> + CO	(46)	0.677 × 10 <sup>-3</sup>	0.0634
NO + HO <sub>2</sub> → NO <sub>2</sub> + OH	(26)	0.122 × 10 <sup>5</sup>	0.0249
CB4 Mechanism			
NO <sub>2</sub> + hν → NO + O	(1)	0.3	0.143
NO + O <sub>3</sub> → NO <sub>2</sub> + O <sub>2</sub>	(3)	0.267 × 10 <sup>2</sup>	-0.133
HCHO + hν → 2HO <sub>2</sub> + CO	(38)	0.677 × 10 <sup>-3</sup>	0.118
NO <sub>2</sub> + OH → HNO <sub>3</sub>	(26)	0.168 × 10 <sup>5</sup>	-0.115
C <sub>2</sub> O <sub>3</sub> + NO <sub>2</sub> → PAN	(47)	0.121 × 10 <sup>5</sup>	-0.0981
C <sub>2</sub> O <sub>3</sub> + NO → HCHO + NO <sub>2</sub> + HO <sub>2</sub> + XO <sub>2</sub>	(46)	0.183 × 10 <sup>5</sup>	0.0977
PAN → C <sub>2</sub> O <sub>3</sub> + NO <sub>2</sub>	(48)	0.228 × 10 <sup>-1</sup>	0.0847
XYLE + OH → 0.7HO <sub>2</sub> + 0.5XO <sub>2</sub> + 0.2CREG + 0.8MGLY + 0.3TO <sub>2</sub> + 1.1PAR	(72)	0.362 × 10 <sup>5</sup>	0.0534
CB4.1 Mechanism			
NO <sub>2</sub> + hν → NO + O	(1)	0.3	0.156
NO + O <sub>3</sub> → NO <sub>2</sub> + O <sub>2</sub>	(3)	0.267 × 10 <sup>2</sup>	-0.143
NO <sub>2</sub> + OH → HNO <sub>3</sub>	(26)	0.168 × 10 <sup>5</sup>	-0.116
C <sub>2</sub> O <sub>3</sub> + NO <sub>2</sub> → PAN	(47)	0.137 × 10 <sup>5</sup>	-0.0937
C <sub>2</sub> O <sub>3</sub> + NO → HCHO + NO <sub>2</sub> + HO <sub>2</sub> + XO <sub>2</sub>	(46)	0.282 × 10 <sup>5</sup>	0.0932
HCHO + hν → 2HO <sub>2</sub> + CO	(38)	0.677 × 10 <sup>-3</sup>	0.0887
PAN → C <sub>2</sub> O <sub>3</sub> + NO <sub>2</sub>	(48)	0.260 × 10 <sup>-1</sup>	0.0832
XYLE + OH → 0.7HO <sub>2</sub> + 0.5XO <sub>2</sub> + 0.2CREG + 0.8MGLY + 0.3TO <sub>2</sub> + 1.1PAR	(72)	0.362 × 10 <sup>5</sup>	0.0419

<sup>a</sup>The units of the rate constants depend on the order of the reactions.

radical are clearly important. For LCC, however, the third-ranked reaction is that of HCHO + HO<sub>2</sub>, which is not included in the CB4 mechanism. Recent evaluation of this reaction indicates that the LCC mechanism is in error (31). Reaction 50 is largely ineffective because the peroxy radical produced rapidly decomposes back into the reactants. Because the back-decomposition reaction was not included in LCC, a spurious effect was introduced. The results of omitting reaction 50 from LCC are shown as test 3 in Table VII. The change has marked effects on H<sub>2</sub>O<sub>2</sub> and HCHO concentrations in cases A and C, resulting in closer agreement between CB4.1 and LCC.

To summarize, ozone concentrations predicted with CB4, CB4.1, and LCC showed close agreement, but larger disparity occurred for hydrogen peroxide and formaldehyde concentrations. Moreover, some discrepancies were noted in the sensitivity coefficients of individual organic classes in the three mechanisms. In particular, the reactivities of the alkanes and toluene classes in LCC tend to be high relative to the reactivities of the respective classes in CB4 and CB4.1; and the reactivities of the aldehydes and propene classes in CB4 and CB4.1 tend to be higher than those in LCC. Overall, for the cases simulated, the HCHO + HO<sub>2</sub> reaction in LCC and the revised acetyl peroxy radical reaction rates in CB4.1 appear to contribute most significantly to the differences in the predictions of the CB4, CB4.1, and LCC mechanisms.

**Table IX. Sensitivity of Final HCHO to Reaction Rate Constants in Case C (24:1)**

reaction	rxn no.	rate constant at 298 K, ppm <sup>-n</sup> min <sup>-1</sup> <sup>a</sup>	sensitivity coeff, ppm HCHO
LCC Mechanism			
HCHO + hν → CO	(47)	0.133 × 10 <sup>-2</sup>	-0.0145
HCHO + hν → 2HO <sub>2</sub> + CO	(46)	0.677 × 10 <sup>-3</sup>	-0.00888
HCHO + HO <sub>2</sub> → RO <sub>2</sub> R + RO <sub>2</sub>	(50)	0.148 × 10 <sup>2</sup>	-0.00760
HCHO + OH → HO <sub>2</sub> + CO	(48)	0.133 × 10 <sup>5</sup>	-0.00703
NO <sub>2</sub> + hν → NO + O	(1)	0.3	0.00538
PAN → MCO <sub>3</sub> + NO <sub>2</sub> + RCO <sub>3</sub>	(59)	0.221 × 10 <sup>-1</sup>	0.00519
ALD2 + OH → MCO <sub>3</sub> + RCO <sub>3</sub>	(51)	0.236 × 10 <sup>5</sup>	0.00477
MCO <sub>3</sub> + NO <sub>2</sub> → PAN	(55)	0.757 × 10 <sup>4</sup>	-0.00458
CB4.1 Mechanism			
HCHO + hν → CO	(39)	0.133 × 10 <sup>-2</sup>	-0.0232
HCHO + OH → HO <sub>2</sub> + CO	(37)	0.150 × 10 <sup>5</sup>	-0.0131
HCHO + hν → 2HO <sub>2</sub> + CO	(38)	0.677 × 10 <sup>-3</sup>	-0.00984
ALD2 + OH → C <sub>2</sub> O <sub>3</sub>	(43)	0.240 × 10 <sup>5</sup>	0.00793
NO <sub>2</sub> + hν → NO + O	(1)	0.3	0.00745
C <sub>2</sub> O <sub>3</sub> + NO <sub>2</sub> → PAN	(47)	0.137 × 10 <sup>5</sup>	-0.00665
PAN → C <sub>2</sub> O <sub>3</sub> + NO <sub>2</sub>	(48)	0.260 × 10 <sup>-1</sup>	0.00702
NO + O <sub>3</sub> → NO <sub>2</sub> + O <sub>2</sub>	(3)	0.267 × 10 <sup>2</sup>	-0.00526

<sup>a</sup>The units of the rate constants depend on the order of the reactions.

However, for initial ROG mixtures that are especially rich in alkanes or toluene, the differences between the LCC and CB4/CB4.1 mechanisms in the reactivities of these classes will also be important.

### 5. Discussion

The sensitivity coefficients shown in Figure 4 are consistent in both magnitude and ranking among classes with the incremental reactivities calculated by Carter and Atkinson (12) for similar cases, despite the use in the present study of simplifying assumptions such as constant photolysis rates. Carter and Atkinson also found HCHO, alkenes, and xylene to be the most reactive species in terms of ozone production and noted negative reactivities for toluene, xylene, and acetaldehyde in some cases. It is also notable that Carter's (32) maximum incremental reactivities and Russell et al.'s (33) reactivities usually fall within the range of sensitivities determined in this study for ROG to NO<sub>2</sub> ratios of 6:1 and 12:1. The results of the DDM analysis also underscore Carter and Atkinson's conclusion that absolute reactivities are extremely sensitive to initial ROG to NO<sub>2</sub> ratios and the duration of the simulations. In addition to these factors, this study shows that differences between mechanisms can also lead to significant differences in estimates of organic reactivities, even if the mechanisms show close agreement for predicted ozone concentrations.

When the differences between the organic reactivities predicted with LCC, CB4, and CB4.1 are highlighted, the results of this analysis have important implications for current discussions concerning regulatory use of organic reactivity scales for comparing emissions from variously fueled vehicles, including alternative fuels and reformulated gasoline. First, sensitivities of ozone to the same compounds in CB4 and CB4.1 differed by 10-20% in some cases. Thus for reactivity calculations, the modifications to CB4 that were recommended by Gery (16) appear to be important. Second, the sensitivities given by LCC and CB4.1 were often within about 20%, but in certain cases they differed by over a factor of 2. Of special significance with respect to motor vehicles, the sensitivities to the toluene classes in the two mechanisms differed substantially. Because toluene is a major component of automobile

exhaust, this suggests that airshed model-based calculations of the reactivity of automobile exhaust may differ depending on which mechanism is used.

The direct decoupled method offers two key advantages over previous approaches used to estimate incremental reactivities. First, earlier modeling studies and experimental investigations have been constrained to approaching the limit in eq 1 using changes in initial concentrations or modeled emissions on the order of a few percent (10–12). In contrast, the sensitivity coefficients calculated with the direct decoupled method are evaluated at the limit as the change in the parameter value approaches zero. Second, previous investigators have had to estimate reactivities for each compound class one class at a time, with some studies using hundreds of simulations (32), whereas with the DDM the sensitivity of all of the output species to all of the input species and reaction rates can be calculated simultaneously.

Comparing the results of this study with previous studies undertaken to compare CB4 and LCC illustrates additional advantages of the formal sensitivity analysis approach taken here. In earlier comparisons of CB4 and LCC, Dodge (4, 18) used hundreds of simulations, including a variety of mixtures of organics and a range of temperatures, to explore the differences between the mechanisms. Clearly, additional simulations would have been needed in this study to examine the temperature dependence of CB4 and LCC predictions. Otherwise, the conclusions of the comparisons made by using the DDM generally support and in some instances elaborate upon Dodge's findings. A good example of the utility of the formal sensitivity analysis is the fact that it highlighted the HCHO + HO<sub>2</sub> reaction as a key discrepancy between CB4/CB4.1 and LCC. This difference was overlooked in the earlier comparisons of the two mechanisms (4, 18).

Overall, Dodge (18) found good agreement for formaldehyde and ozone production with CB4 and LCC when typical urban mixtures of organics were studied. However, differences were noted when isolated organic compounds were used as inputs instead of a mixture. These conclusions are supported by the DDM analysis. For H<sub>2</sub>O<sub>2</sub> concentrations, Dodge (4) found that agreement between CB4 and LCC at high ROG to NO<sub>x</sub> ratios was significantly improved when the HO<sub>2</sub> + XO<sub>2</sub> reaction was added to CB4. Even with this reaction and at a 9:1 ROG to NO<sub>x</sub> ratio, Dodge (18) found higher H<sub>2</sub>O<sub>2</sub> yields with CB4 than with LCC for simulations in which propene and acetaldehyde were studied individually. The results of the current analysis are also consistent with these findings for H<sub>2</sub>O<sub>2</sub>.

Of the individual organic compound classes, the aromatics are of special note because the chemistry of the aromatics is considered highly uncertain. Dodge found that the toluene class in LCC was more reactive than that in CB4. The sensitivity analysis supports this finding for toluene. Also consistent with Dodge's results (18), but in contrast to previous findings of discrepancies between mechanisms in xylene chemistry, the sensitivities of O<sub>3</sub>, HCHO, and H<sub>2</sub>O<sub>2</sub> to the initial xylene concentrations in CB4.1 and LCC calculated in this study show fairly good agreement.

One case in which the DDM results do not agree with those of Dodge highlights the fact that the comparative performance of alternative mechanisms can depend on the ROG composition used. Dodge (18) found that CB4 gave relatively high formaldehyde and ozone concentrations in a simulation with a 9:1 ROG to NO<sub>x</sub> ratio in which *trans*-2-butene was studied alone. This discrepancy was

attributed to the use of acetaldehyde to represent *trans*-2-butene in CB4. In contrast to Dodge's results, application of the DDM indicated that ozone and formaldehyde sensitivities to acetaldehyde in CB4 and CB4.1 were similar to or lower than the sensitivities to *trans*-2-butene in LCC.

## 6. Conclusions

The results of this study generally support the conclusions of earlier comparisons of CB4 and LCC. However, the formal sensitivity analysis method brought out important characteristics of their comparative behavior that were not apparent in previous studies. And, because it calculates sensitivity coefficients for all species and rate parameters simultaneously, a single DDM application can replace numerous kinetic simulations performed in informal sensitivity analysis. The direct decoupled method thus provides a highly efficient tool for comparing competing mechanisms. Kinetic simulation results can be used to compare the predictions of different mechanisms but are difficult to interpret in terms of what gives rise to disagreements. Detailed examination of mechanism listings is useful for identifying potential sources of disagreement, but less helpful in determining which are the key discrepancies. The sensitivity analysis method thus fills a critical gap by providing a means of determining which discrepancies are most significant. Because chemical mechanisms developed for use in air-quality models are frequently revised and often need to be reevaluated, the efficiency and guidance afforded by the DDM approach are major benefits.

For the conditions studied, which approximate those of a smog chamber with a multicomponent mixture of input organics, ozone concentrations predicted with CB4, CB4.1, and LCC showed close agreement, but larger disparity occurred for hydrogen peroxide and formaldehyde concentrations. Sensitivity analysis of the three mechanisms indicated that the reactivities of the alkanes and toluene classes in LCC tend to be high relative to the reactivities of the respective classes in CB4 and CB4.1; and the reactivities of the aldehydes and propene classes in CB4 and CB4.1 tend to be high compared to those in LCC. Furthermore, the sensitivity analysis indicates that the incorrect treatment of the HCHO + HO<sub>2</sub> reaction in LCC and the differences between the acetyl peroxy radical reaction rates of LCC, CB4 and CB4.1 are key factors contributing to the differences in the predictions. In particular, recommended changes (16) to the rates of the acetyl peroxy radical + NO and PAN formation and decomposition reactions, which were incorporated into CB4.1, contribute to the relatively high "reactivity" of acetaldehyde and propene in that mechanism.

The direct decoupled method is also well-suited to the problem of quantitatively ranking organic compounds by their relative contributions to the formation of ozone or other secondary pollutants of concern. Use of the direct decoupled method offers two key advantages over reactivity estimation approaches that have been used previously. Sensitivity coefficients calculated with the direct decoupled method are exact reactivities, in that they are evaluated at the limit as the change in the input concentration of the organic under study approaches zero. And, with the DDM the sensitivity of all of the output species to all of the input species can be calculated at once rather than one at a time. Direct decoupled method sensitivity results were consistent with previous calculations of incremental reactivities, indicating HCHO, alkenes, and xylene to be the most reactive species in terms of ozone production. Carter and Atkinson (12) have previously emphasized the dependence of reactivity estimates on

simulation conditions. The current study has also shown that even for mechanisms giving peak ozone concentrations in close agreement the underlying reactivities they show for specific classes of organics can differ substantially.

#### Acknowledgments

Computer time, facilities, and assistance were provided by the Pittsburgh Super Computing Center and Cray Research, Inc. We greatly appreciate comments given by Marcia Dodge and William Stockwell.

Registry No. O<sub>3</sub>, 10028-15-6; NO<sub>x</sub>, 11104-93-1; HCHO, 50-00-0; H<sub>2</sub>O<sub>2</sub>, 7722-84-1.

#### Literature Cited

- (1) Dunker, A. M.; Kumar, S.; Berzins, P. H. *Atmos. Environ.* 1984, 18, 311-321.
- (2) Shafer, T. B.; Seinfeld, J. H. *Atmos. Environ.* 1986, 20, 487-499.
- (3) Hough, A. M. *J. Geophys. Res.* 1988, 93, 3789-3812.
- (4) Dodge, M. C. *J. Geophys. Res.* 1989, 94, 5121-5136.
- (5) Dunker, A. M. *J. Chem. Phys.* 1984, 81, 2385-2393.
- (6) McCroskey, P. S.; McRae, G. J. *Documentation for the Direct Decoupled Sensitivity Analysis Method—DDM*; Department of Chemical Engineering Report, Carnegie Mellon University: Pittsburgh, PA, 1987.
- (7) Falls, A. H.; McRae, G. J.; Seinfeld, J. H. *Int. J. Chem. Kin.* 1979, 11, 1137-1162.
- (8) Stockwell, W. R. Presented at XVII Informal Conference on Photochemistry, University of Colorado, Boulder, CO, June 1986.
- (9) *Low-Emission Vehicles/Clean Fuels—Technical Support Document*; California Air Resources Board: Sacramento, CA, 1990.
- (10) Dodge, M. C. *Atmos. Environ.* 1984, 18, 1657-1665.
- (11) Carter, W. P. L.; Atkinson, R. *Environ. Sci. Technol.* 1987, 21, 670-679.
- (12) Carter, W. P. L.; Atkinson, R. *Environ. Sci. Technol.* 1989, 23, 864-880.
- (13) Gery, M. W.; Whitten, G. Z.; Killus, J. P. *Development and Testing of the CBM-IV for Urban and Regional Modeling*; EPA/600/3-88/012; U.S. Environmental Protection Agency: Research Triangle Park, NC, 1988.
- (14) Gery, M. W.; Whitten, G. Z.; Killus, J. P.; Dodge, M. C. *J. Geophys. Res.* 1989, 94, 12925-12956.
- (15) Lurmann, F. W.; Carter, W. P. L.; Coyner, L. A. *A Surrogate Species Chemical Reaction Mechanism for Urban-Scale Air Quality Simulation Models*; EPA/600/3-87-014; U.S. Environmental Protection Agency: Research Triangle Park, NC, 1987.
- (16) Gery, M. W. Atmospheric Research Associates, Inc., personal communication to Marcia Dodge, Nov 1990.
- (17) Dodge, M. C. U.S. Environmental Protection Agency, personal communication, Mar 1991.
- (18) Dodge, M. C. *J. Geophys. Res.* 1990, 95, 3635-3648.
- (19) Carter, W. P. L.; Lurmann, F. W.; Atkinson, R.; Lloyd, A. C. *Development and Testing of a Surrogate Species Chemical Reaction Mechanism, Volumes 1 and 2*; EPA/600/3-86-031; U.S. Environmental Protection Agency: Research Triangle Park, NC, Aug 1986.
- (20) Jeffries, H. E.; Sexton, K. G.; Salmi, C. N. *The Effects of Chemistry and Meteorology on Ozone Control Calculations Using Simple Trajectory Models and the EKMA Procedure*; EPA-450/4-81-034; U.S. Environmental Protection Agency: Research Triangle Park, NC, 1981.
- (21) Leone, J. A.; Seinfeld, J. H. *Atmos. Environ.* 1985, 19, 437-464.
- (22) Milford, J. B. Ph.D. Dissertation, Carnegie Mellon University, 1988.
- (23) Carter, W. P. L.; Lurmann, F. W. *Evaluation of the RADM Gas-Phase Chemical Mechanism*; EPA/600/3-90/001; U.S. Environmental Protection Agency: Research Triangle Park, NC, 1990.
- (24) Stockwell, W. R.; Lurmann, F. W. *Intercomparison of the ADOM and RADM Gas Phase Chemical Mechanisms*; Electric Power Research Institute: Palo Alto, CA, 1990.
- (25) Bridier, I.; Caralp, F.; Loirat, H.; Lesclaux, R.; Veyret, B.; Becker, K. H.; Reimer, A.; Zabel, F. *J. Phys. Chem.* 1991, 95, 3594-3600.
- (26) Tuazon, E. C.; Carter, W. P. L.; Atkinson, R. *J. Phys. Chem.* 1991, 95, 2434-2437.
- (27) Kirchner, F.; Zabel, F.; Becker, K. H. *Ber. Bunsenges. Phys. Chem.* 1990, 94, 1379-1382.
- (28) Grosjean, F.; Fung, K. *JAPCA* 1984, 34, 537-543.
- (29) Baugues, K. *A Review of NMOC, NO<sub>x</sub> and NMOC/NO<sub>x</sub> Ratios Measured in 1984 and 1985*; EPA-450/4-86-015; U.S. Environmental Protection Agency: Research Triangle Park, NC, 1986.
- (30) Gear, C. W. *Numerical Initial Value Problems in Ordinary Differential Equations*; Prentice-Hall: Englewood Cliffs, NJ, 1971; pp 209-228.
- (31) Atkinson, R. *Atmos. Environ.* 1990, 24A, 1-41.
- (32) Carter, W. P. L. *Development of Ozone Reactivity Scales for Volatile Organic Compounds*; Draft Final Report to the U.S. Environmental Protection Agency on Contract No. CR-814396-01-0; Statewide Air Pollution Research Center, University of California: Riverside, CA, Nov 1990.
- (33) Russell, A. G.; McNair, L.; Odman, M. T. Airshed Calculation of the Sensitivity of Pollutant Formation to Organic Compound Classes and Oxygenates Associated with Alternative Fuels. *J. Air Waste Manage. Assoc.* 1992, 42, 174-178.

Received for review June 12, 1991. Revised manuscript received December 30, 1991. Accepted February 17, 1992. Early phases of this work were supported by the National Science Foundation under a Presidential Young Investigator Award CEE000659 to G.J.M. and by the PRECP program under Grant B-K5877-A-E from Battelle Pacific Northwest Laboratories.



# REPORT DOCUMENTATION PAGE

1. AGENCY USE ONLY <i>(Leave Blank)</i>  <b>PB94214558</b>		2. REPORT DATE  May 1993	3. REPORT TYPE AND DATES COVERED  Final Report	
4. TITLE AND SUBTITLE  An Investigation of Error Propagation in the California Air Resources Board Air Quality Model			5. FUNDING NUMBERS  C - A932-091	
6. AUTHOR(S)  M. Talat Odman, Menner A. Tatang, Naresh Kumar, Laurie A. McNair, Gregory J. McRae, and Armistead G. Russell				
7. PERFORMING ORGANIZATION NAME(S) AND ADDRESS(ES)  Carnegie Mellon University Pittsburgh, PA 15213-3890			8. PERFORMING ORGANIZATION REPORT NUMBER	
9. SPONSORING/MONITORING AGENCY NAME(S) AND ADDRESS(ES)  California Air Resources Board Research Division 2020 L Street Sacramento, CA 95814			10. SPONSORING/MONITORING AGENCY REPORT NUMBER  ARB/R-94/507	
<p><b>LIBRARY</b> <b>CALIFORNIA AIR RESOURCES BOARD</b> <b>P.O. BOX 2815</b> <b>SACRAMENTO, CA 95812</b></p>				
11. SUPPLEMENTARY NOTES				
12a. DISTRIBUTION/AVAILABILITY STATEMENT  Release unlimited. Available from National Technical Information Service. 5285 Port Royal Road Springfield, VA 22161			12b. DISTRIBUTION CODE	
13. ABSTRACT <i>(Maximum 200 Words)</i>  This study investigated the initiation and propagation of errors in the California Air Resources Board's airshed model (CalGrid) as a means of understanding the inherent precision and accuracy of photochemical model calculations. The most significant finding of the study is that the horizontal transport algorithm used by CalGrid is a source of significant error when concentration gradients are high (as is often observed in ozone episodes). This was tested in three ways: 1) the rotating puff test; 2) a rotating puff test with a parabolic tangential velocity profile; and 3) application of the Southern California Air Quality Study database. Each test suggested that the error in the horizontal advection algorithm is on the order of 20 to 40%. CalGrid's chemical mechanism solver was shown to have less error than the horizontal transport solver. The ability of the Chapeau function scheme to adapt to the non-linear aspects of the chemistry was evaluated with a simplified chemical mechanism and the rotating puff test. The test showed no additional errors due to any mismatch of CalGrid's horizontal transport and chemical solution schemes. This study also introduced some new computational procedures that make use of stochastic finite elements for assessing error propagation. Using CalGrid's vertical transport code, it was found that vertical diffusivity errors and uncertainties were more significant than dry deposition and chemical conversion errors.				
14. SUBJECT TERMS  error propagation, photochemical airshed model, CalGrid Chapeau function, horizontal transport rotating puff test, chemical mechanism solver stochastic finite elements, Southern California Air Quality Study			15. NUMBER OF PAGES  172	
			16. PRICE CODE	
17. SECURITY CLASSIFICATION OF REPORT  Unclassified	18. SECURITY CLASSIFICATION OF THIS PAGE  Unclassified	19. SECURITY CLASSIFICATION OF ABSTRACT  Unclassified	20. LIMITATION OF ABSTRACT  Unlimited	

